Chem Soc Rev

REVIEW ARTICLE

View Article Online
View Journal | View Issue

Cite this: *Chem. Soc. Rev.*, 2024, **53**, 3167

Strategies to address key challenges of metallacycle/metallacage-based supramolecular coordination complexes in biomedical applications

Dongdong Xu,[a] Yang Li,*[a] Shouchun Yin *[a] and Feihe Huang *[bc]

Owing to their capacity for dynamically linking two or more functional molecules, supramolecular coordination complexes (SCCs), exemplified by two-dimensional (2D) metallacycles and three-dimensional (3D) metallacages, have gained increasing significance in biomedical applications. However, their inherent hydrophobicity and self-assembly driven by heavy metal ions present common challenges in their applications. These challenges can be overcome by enhancing the aqueous solubility and *in vivo* circulation stability of SCCs, alongside minimizing their side effects during treatment. Addressing these challenges is crucial for advancing the fundamental research of SCCs and their subsequent clinical translation. In this review, drawing on extensive contemporary research, we offer a thorough and systematic analysis of the strategies employed by SCCs to surmount these prevalent yet pivotal obstacles. Additionally, we explore further potential challenges and prospects for the broader application of SCCs in the biomedical field.

Received 28th November 2023

DOI: 10.1039/d3cs00926b

rsc.li/chem-soc-rev

1. Introduction

Synthesizing therapeutic systems that involve strong covalent bonds is complex and cumbersome, often leading to challenges in achieving precise drug release and preserving drug activity due to their highly stable structures. These issues also complicate clinical translation.[1–5] Consequently, the simple and flexible supramolecular self-assembly approach, leveraging interactions such as van der Waals,[6] π–π stacking,[7] hydrophobic,[8] electrostatic,[9] metal-coordination,[10] hydrogen bonding,[11] and host–guest interactions,[12] has garnered

[a] *Key Laboratory of Organosilicon Chemistry and Materials Technology of Ministry of Education, College of Materials, Chemistry and Chemical Engineering, Hangzhou Normal University, Hangzhou 311121, P. R. China. E-mail: liyang@hznu.edu.cn, yinsc@hznu.edu.cn*
[b] *Stoddart Institute of Molecular Science, Department of Chemistry, Zhejiang University, Hangzhou 310058, P. R. China. E-mail: fhuang@zju.edu.cn*
[c] *Zhejiang-Israel Joint Laboratory of Self-Assembling Functional Materials, ZJU-Hangzhou Global Scientific and Technological Innovation Center, Zhejiang University, Hangzhou, 311215, P. R. China*

Dongdong Xu

Dongdong Xu was born in Henan, China, in 1991. He received his PhD degree from Max Planck Institute for Polymer Research in 2020 under the direction of Prof. Katharina Landfester and Prof. Seraphine Wegner. He is currently a lecturer at Hangzhou Normal University. His research interests are focused on the construction of functional supramolecular coordination complexes and protein modified biomaterials.

Yang Li

Yang Li was born in Hubei, China, in 1989. She received her PhD degree from Zhejiang University for Chemistry Research in 2018 under the direction of Prof. Guping Tang. She is currently an Associate Professor at Hangzhou Normal University. Her research interests are mainly in the synthesis of functional supramolecular coordination complexes and exploration of their applications in bio-imaging and cancer therapy.

significant interest in the biomedical field. Specifically, supramolecular systems assembled through weak non-covalent bonds (such as hydrophobic, hydrogen, and electrostatic interactions) often exhibit unstable structures. This instability can lead to disassembly in the complex *in vivo* microenvironments, resulting in diminished drug efficacy and potential harm to normal cells.[13] Conversely, supramolecular self-assembled systems driven by metal-coordination bonds, possessing a strength intermediate between strong covalent and weak non-covalent bonds, offer relative stability and dynamic flexibility.[14,15] Supramolecular coordination complexes (SCCs) developed by Verkade,[16] Fujita,[17,18] Stang,[19,20] Nitschke,[21–23] Therrien,[24] Newkome,[25] Raymond,[26,27] and Mirkin[28,29] have been intensively researched in the fields of functional polymers, molecular imaging, catalysis, biomedicine, sensing, and more.[30–37]

SCCs typically comprise two-dimensional (2D) metallacycles and three-dimensional (3D) metallacages. These structures can exhibit customized shapes, sizes, topologies, and physicochemical properties by adjusting the chemical structures of the metal-based acceptors and organic donors, alongside the coordination angles.[38–42] Over the past two decades, the chemotherapeutic function of metal ions in the coordination center, such as platinum (Pt),[43] ruthenium (Ru),[44] palladium (Pd),[45] and iridium (Ir),[46] combined with advancements in functional ligand design, has positioned SCCs as pivotal in linking multiple distinct functional molecules through metal–nitrogen (N) coordination bonds (*e.g.*, Pt(II)–N and Ru(II)–N). This capability plays a significant role in enhancing therapeutic modalities, overcoming the limitations of traditional therapeutic methods, and advancing theranostics, among other biomedical applications.[30–32] For instance, to enhance the generation of reactive oxygen species (ROS), SCCs can be assembled using Pt(II)–N or Ru(II)–N coordination bonds. These bonds leverage the heavy atom effect to facilitate intersystem crossing relaxation, increasing the yield of ROS in photodynamic therapy (PDT).[47] Additionally, to address the challenges of poor PDT efficacy in the hypoxic microenvironments of tumor tissues and the inhibition of photothermal therapy (PTT) due to heat shock protein expression in tumor cells, SCCs can be employed to develop a synergistic PDT/PTT model.[48] To tackle the limitations of short excitation wavelength and low tissue penetration depth in traditional phototherapy, BODIPY (fluoroboron dipyrrole) derivatives, featuring high quantum yields and stable chemical/photophysical properties,[49–51] or organic ligands with a donor–acceptor–donor (D–A–D) structure[52] can be employed for incorporation into SCCs. This approach extends the π-conjugation planes and enhances the push–pull electronic effect across the molecules, red-shifting the emission wavelength of the ligand and enabling phototherapy in the second near-infrared (NIR-II) region. Furthermore, to meet the dual requirements of diagnosis and treatment and to overcome the aggregation-induced quenching (ACQ) of fluorophores and the heavy atom effect on fluorescence imaging, aggregation-induced emission (AIE) units like tetraphenylethylene (TPE),[53–57] triphenylamine,[58,59] and other molecules can be integrated into the SCC system. This integration aids in constructing a theranostic platform.[60] These strategic approaches address specific challenges across various domains, significantly broadening and deepening the biomedical applications of SCCs. Numerous reviews have focused on aspects such as molecular structure design, PDT/PTT applications, and theranostics in the near-infrared/infrared region.[30,42,47,48,52] However, the path to clinical application of SCCs remains extensive. Beyond the aforementioned specific issues, SCCs also encounter several general but critical obstacles, including water solubility, biosafety, biocompatibility, potential toxicity, and biodistribution, which must be overcome before their real-

Shouchun Yin

Shouchun Yin received his PhD degree from the University of Science and Technology of China under the guidance of Prof. Wenfang Shi and Prof. Hongyao Xu in 2005. He worked in Prof. Xi Zhang's group at the University of Tsinghua from 2006 to 2007, Prof. Win Dehaen's group at Katholieke Universiteit Leuven from 2008 to 2010, and Prof. Peter J. Stang's group at the University of Utah from 2016 to 2017, as a postdoctor, respectively. He is currently a Professor at Hangzhou Normal University. His research interests are supramolecular coordination complexes, supramolecular polymers, opto-electric functional materials, fluorescent probes, and dyes.

Feihe Huang

Feihe Huang is a Changjiang Scholar Chair Professor of Zhejiang University. His current research is focused on supramolecular polymers and nonporous adaptive crystals (NACs). Awards and honours he has received include the Chinese Chemical Society AkzoNobel Chemical Sciences Award, The Cram Lehn Pedersen Prize in Supramolecular Chemistry, the Royal Society of Chemistry Polymer Chemistry Lectureship Award, and the Bruno Werdelmann Lectureship Award. His publications have been cited more than 32 476 times. His h-index is 98. He sits/sat on the Advisory Boards of JACS, Chem. Soc. Rev., ChemCommun, Macromolecules, ACS Macro Lett., and Polym. Chem. He is an Editorial Board Member of Mater. Chem. Front.

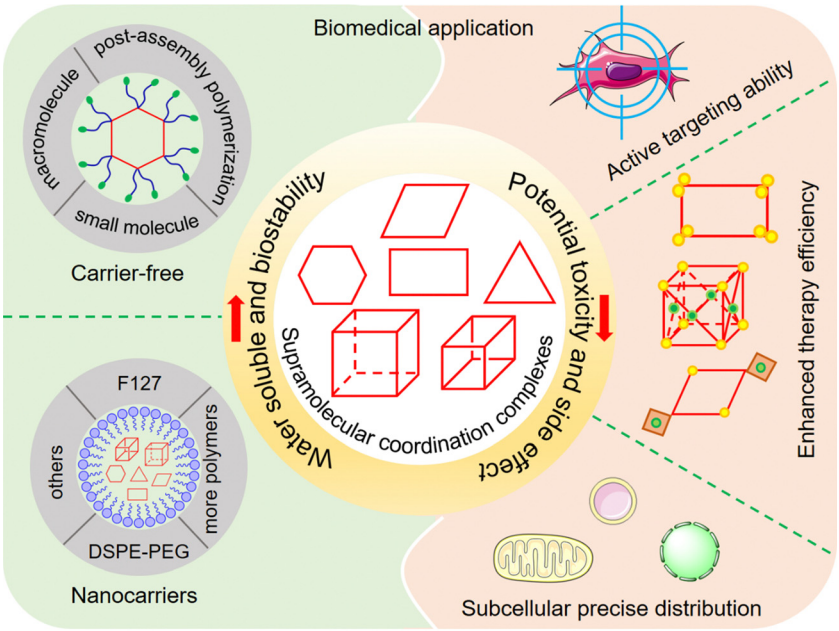

Fig. 1 Schematic representation of general strategies employed by supramolecular coordination complexes (SCCs) to enhance water solubility and biostability and reduce potential toxicity and side effects for biomedical applications.

world implementation. Despite considerable progress in these areas, comprehensive and up-to-date reviews addressing these advancements are lacking.

We emphasize the significant strategies employed by SCCs to address key challenges in biomedical applications. Our focus includes methods to impart appropriate water solubility to hydrophobic SCCs, enhancing their biocompatibility, strategies to improve cellular selectivity and reduce potential toxicity for increased biosafety, and techniques for precise drug distribution within cells to analyze active sites and mechanisms (Fig. 1). Finally, we summarize the current state-of-the-art research, discuss additional challenges for future applications, and propose potential research directions to tackle these issues.

2. Strategies to improve the water solubility and biostability of SCCs

The preparation process of SCCs typically progresses from synthesizing simple small-molecule components to assembling metallacycles/metallacages, predominantly conducted in organic solvents. Most chemotherapeutic drugs (such as doxorubicin (DOX) and paclitaxel (PTX)), phototherapeutic agents (like BODIPY), and AIE molecules, including TPE, possess hydrophobic conjugate groups. Consequently, the multifunctional SCCs constructed in this manner are typically hydrophobic and rigid structures. The hydrophobic nature of SCCs facilitates their rapid and firm binding to the lipophilic cell membrane surfaces,[61] enhancing their cellular uptake efficiency. However, this hydrophobicity leads to their rapid aggregation and precipitation in the aqueous environment of living organisms, posing challenges in maintaining their *in vivo* stability and biocompatibility. Consequently, enhancing water solubility is crucial for the further biomedical application of SCCs. Presently, two primary strategies are employed to improve their water solubility (Fig. 2). One involves encapsulating hydrophobic SCCs within nanocarriers featuring hydrophilic surfaces.[62–64] The other strategy is to chemically modify SCCs with hydrophilic groups or long chains, conferring a degree of water solubility (carrier-free).[65–67]

2.1. Encapsulate SCCs with nanocarriers

Nanocarrier encapsulation strategies typically involve creating nanoparticles or vesicles that encapsulate SCCs within a hydrophilic exterior. The therapeutic efficacy of these nanocarriers is influenced by factors such as their surface charge, size, and chemical composition.[68] Given that cell membranes are usually negatively charged, positively charged nanocarriers can facilitate enhanced cell adhesion and promote rapid endocytosis. However, a positive surface charge on nanocarriers may result in increased nonspecific protein adsorption in the bloodstream and heightened nonspecific phagocytosis by cells of the reticuloendothelial system.[69] Therefore, nanocarriers with negatively or neutrally charged surfaces are also favored to mitigate these issues.[70] Regarding their size, while the diameter range of drug delivery systems (DDS) is defined as 1–1000 nm,[71] practical applications typically employ nanocarriers with diameters of 10–200 nm. This size range prevents early elimination by glomerular filtration due to the small carrier size (below 10 nm)[72] and mitigates phagocytosis and destruction by the reticuloendothelial system for large-sized carriers. Consequently, this size range facilitates selective extravasation from the blood vessels and passive targeting to tumor tissues, leveraging the enhanced permeability and retention (EPR) effect.[73–75] Data suggest that an appropriate nanocarrier size

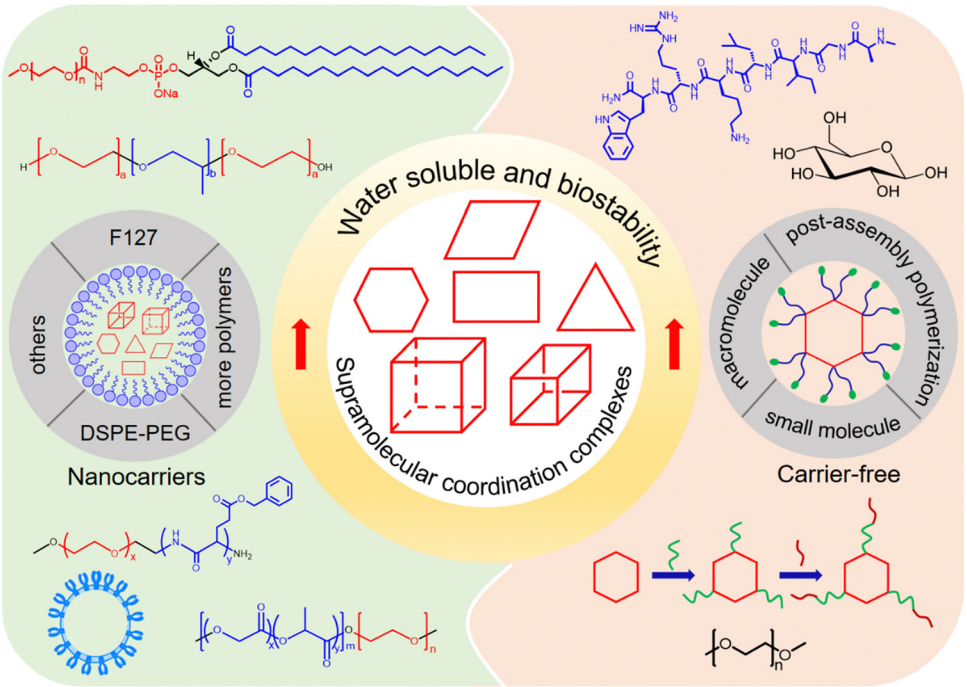

Fig. 2 Schematic representation of general strategies of supramolecular coordination complexes (SCCs) to enhance water solubility and biostability for biomedical applications.

can maximize the benefits of the EPR effect, increasing drug concentration in tumor tissue by up to 10–100 times compared to healthy tissue.[76] This can lead to more effective therapies at lower doses. However, there is still no definitive consensus on the precise size that ensures nanocarriers effectively overcome physiological barriers, while simultaneously exhibiting potent anticancer activity and minimal side effects.[77] Indeed, the nanocarrier size is not static during blood circulation but typically decreases over time. Therefore, our subsequent discussion will consider both nanocarrier size and structure. In this context, liposomes prepared using DSPE–PEG (distearoyl phosphatidylethanolamine–polyethylene glycol) and block copolymers, exemplified by Pluronics, are two commonly utilized materials in nanocarrier fabrication. The key characteristics of this strategy are outlined in Table 1.

2.1.1. Encapsulate SCCs with nanocarriers prepared using DSPE–PEG-like liposomes. Liposomes, frequently utilized in DDSs as carriers, are primarily composed of phospholipids and various additives. Phospholipids consist of a hydrophilic head, including a phosphate group and a quaternary ammonium group, and a lipophilic tail comprising two long hydrocarbon chains. They can be either natural or synthetic. Natural phospholipids are predominantly lecithin (phosphatidylcholine, PC), whereas synthetic ones are varied, encompassing compounds like DPPC (dipalmitoyl phosphatidylcholine), DPPE (dipalmitoyl phosphatidylethanolamine), DSPE, and DSPC (distearoyl phosphatidylcholine). Among these, the DSPE–PEG amphiphilic polymer created by attaching PEG to the hydrophilic group of DSPE (Fig. 3a) is a crucial material for sustained-release drug carriers such as liposomes, vesicles, and nanoparticles in the current DDSs.[78–80] Adding PEG enhances the flexibility and hydrophilicity of DSPE liposomes. In blood circulation, DSPE–PEG resists phagocytosis by the monocyte–macrophage system, which reduces interactions between the liposome's lipid membrane and plasma proteins,[81,82] prolonging the circulation time. This property makes it suitable for long-circulating liposomes, enhancing long-term absorption into tissues or organs. Due to these numerous advantages, the strategy of using DSPE–PEG in nanocarrier construction has become widely adopted to improve the aqueous solubility and circulatory stability of SCCs under physiological conditions.

As illustrated in Fig. 3b, hexagonal[83] (chemical **1**) and triangular[84,85] (chemicals **2** and **3**) metallacycles were encapsulated using DSPE–PEG derivatives (DSPE–mPEG: DSPE-methoxy PEG; DSPE–PEG–MAL: DSPE-maleimide PEG), forming water-soluble nanoparticles. Our findings and those of our colleagues demonstrate that the size of these nanoparticles is influenced by the molecular structure and morphology of metallacycles. For instance, hexagonal metallacycles (chemical **1**) possess a larger spatial structure compared to triangular metallacycles (chemical **2**), leading to the formation of larger nanoparticles (145 nm *vs.* 49 nm). Furthermore, the final nanoparticle size is influenced by factors, including the type and molecular weight of PEG, the operational method, the size of the filter used, the ratio of SCCs to DSPE–PEG, and the stacking arrangement of nanoparticles. Consequently, predicting the size of nanoparticles is challenging, even when metallacycles of similar structures are synthesized using the same nanoprecipitation technique. However, these nanoparticles generally exhibit robust stability in aqueous solutions or physiological

Table 1 Features of encapsulated supramolecular coordination complexes (SCCs) with nanocarriers to improve water solubility and biostability. The particle size is determined by dynamic light scattering (DLS)

Topological structures	Nanocarriers used	Particle size (nm)	Biostability test	Aqueous solution	Load efficiency	Ref.
 Chemical **1**	DSPE–mPEG$_{2000}$	145	2 days	PBS	—	83
 Chemical **2**	DSPE–PEG$_{2000}$–MAL	49	7 days	H_2O	—	84
 Chemical **3**	DSPE–mPEG$_{5000}$	32	20 h	PBS + 10% FBS	—	85
 Chemical **4**	DSPE–PEG$_{5000}$	220	7 days	PBS/PBS + 10% FBS/blood	—	86
 Chemical **5**	DSPE–mPEG$_{5000}$	240	7 days	PBS + 10% FBS	—	87
 Chemical **6**	F127	150	21 days	H_2O	10%	101
 Chemical **7**	F127	130	4 days	H_2O	4.98%	103
 Chemical **8**	F127	110	7 days	PBS/FBS/H_2O	—	104
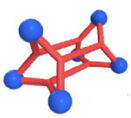 Chemical **9**	mPEG-*b*-PLGA	65	7 days	PBS/H_2O	—	105
 Chemical **10**	mPEG-*b*-PBLG	134 ± 13.7	—	—	6.1%	106
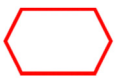 Chemical **11**	Heavy chain ferritin	13.32	1 day	PBS/PBS + 10% FBS	—	107
 Chemical **12**	PEG/melanin dots	100	7 days	PBS + 10% FBS	—	108

environments (such as phosphate-buffered saline (PBS) and fetal bovine serum (FBS)), maintaining consistent particle size and spectroscopic properties for durations ranging from 20 h to one week. After DSPE–PEG encapsulated nanoparticles are internalized by cells through fusion with the cell membrane phospholipid bilayer or endocytosis, the acidic lysosomal environment cleaves the Pt(II)–N coordination bond. This process releases the smaller components of SCCs, facilitating a synergistic chemotherapeutic effect with the heavy metals. Consequently, DSPE–PEG encapsulation ensures SCC stability during transport and preserves its therapeutic efficacy. This dual functionality substantially enhances the potential of hydrophobic SCCs to be utilized in physiological environments.

Compared to those formed through Pt(II)–N coordination, SCCs created using Ru(II)–N coordination exhibit slightly higher water solubility and can be directly utilized in PBS or FBS for *in vitro* experiments. Sun *et al.*[86] synthesized a tetragonal metallacycle based on Ru-pyridine coordination (Fig. 3c, chemical **4**), demonstrating effective PDT and PTT in the NIR-II region. These metallacycles show potential as antitumor phototherapeutic agents. However, for *in vivo* applications, encapsulating SCCs with DSPE–PEG remains essential to ensure prolonged circulation time and passive tumor targeting. The nanoparticles resulting from this encapsulation exhibit stable size and optical properties across various environments (PBS, FBS, whole blood) for up to one week (Fig. 3d). Moreover, a gradual increase in fluorescence intensity at the tumor site was observed, peaking 24 h post-injection, with the signal persisting for up to 5 d and exhibiting a high signal-to-background ratio (Fig. 3e). This suggests that DSPE–PEG encapsulated nanoparticles possess effective tumor accumulation capabilities. Additionally, they engineered and assembled different tetragonal Ru metallacycles[87] utilizing a D–A–D structure (Fig. 3c, chemical **5**). The nanoparticles produced following encapsulation with DSPE–mPEG$_{5000}$ demonstrated efficacy in treating bacteria-infected wounds. These outcomes further underscore that DSPE–PEG encapsulation significantly enhances the applicability of SCCs in biomedical contexts.

2.1.2. Encapsulate SCCs with nanocarriers prepared using block copolymers. Block copolymers represent another nanocarrier type. These are amphiphilic polymers that covalently link hydrophilic and hydrophobic chains in varying ratios to form diblocks or triblocks. Typically, due to the rigid structure and the challenges in modifying the two long alkyl chains in the lipophilic part of DSPE, liposomes typified by DSPE–PEG often undergo modifications in the molecular weight (*e.g.*, DSPE–PEG$_{2000}$, DSPE–PEG$_{5000}$) or the terminal group (*e.g.*, DSPE–mPEG, DSPE–PEG–MAL) of the hydrophilic PEG segment. However, it is challenging to adjust their affinity and loading capacity for SCCs by altering these terminal long alkyl chains. Contrastingly, block copolymers offer the flexibility to easily adjust the lengths and molecular weights of hydrophilic and hydrophobic chains, catering to diverse requirements. Pluronics, a prominent example of block copolymers utilized in DDSs, are typically non-ionic surfactants with a triblock structure, comprising hydrophilic PEO and hydrophobic polypropylene oxide (PPO).[88–92] Varying the length ratio between hydrophilic and hydrophobic blocks can alter the physicochemical properties of Pluronics. This modulation significantly influences their *in vitro* and *in vivo* performance, alongside their interactions with cells and cell membranes.[93] For instance, augmenting the hydrophilic portion of these block copolymers promotes prolonged circulation, whereas increasing the hydrophobic content enhances their drug-loading capacity. Pluronic F127 (Fig. 4a), an FDA (U.S. Food and Drug Administration) approved commercial nanocarrier, is extensively utilized in DDSs owing to its biocompatibility and biodegradability.[94–97] In the designation F127, the letter F signifies the physical state as a flake solid. The first two digits, 12, multiplied by 300, indicate the approximate molecular weight of the PPO component in each F127 molecule, approximately 3600 g mol^{-1}. The last digit, 7, multiplied by 10, represents the weight fraction of PEO in each F127 molecule, approximately 70%.[88,98] Other members of the Pluronic series include Pluronic F68[99] and Pluronic F108,[100] each corresponding to different molecular weights of PPO and varying PEO contents. Pluronics offer simple synthesis, controllable performance, and easily adjustable structures. These features render them increasingly important in the biomedical field, evolving from basic surfactants to key components in the design of sophisticated and intelligent DDSs.

Compared to the hydrophobicity conferred by DSPE–PEG, which comprises only two alkyl chains with 18 saturated carbon atoms each, the hydrophobicity imparted by F127 with its PPO component of up to 3600 g mol^{-1} is markedly stronger. Consequently, F127 is frequently utilized for encapsulating certain highly hydrophobic SCCs or SCCs combined with hydrophobic small molecule drugs. Accordingly, we selected F127 for encapsulating BODIPY-based rhomboidal metallacycles (Fig. 4b, chemical **6**)[101] and various polydentate complexes.[102] Both cases resulted in the formation of stable nanoparticles. Additionally, F127 has been utilized to encapsulate rhomboidal metallacycles composed of the highly hydrophobic AIE moiety triphenylamine and the dicyano group (Fig. 4c, chemical **7**).[103] Conversely, Kim *et al.*[104] employed F127 to encapsulate hexagonal metal macrocycles (Fig. 4d, chemical **8**) and hydrophobic NIR-II fluorescent molecules, achieving a stable particle size for up to one week in FBS, PBS, and water. These examples underscore the vital role of F127 in enhancing the compatibility of SCCs for various applications.

Beyond F127, various block copolymers have been explored for encapsulating SCCs. These copolymers typically feature mPEG as the hydrophilic group, while the hydrophobic chain's structure is modified to achieve specific encapsulation effects. Principally, for the purpose of improving the encapsulation efficiency, more flexible chains can be designed for the ligands or acceptors of SCCs, which facilitate the encapsulation of SCCs by polymers such as DSPE–PEG, F127, or other polymers through the entanglement with the flexible chains. However, if SCCs themselves have a large π-plane that does not contain any flexible chains, amphiphilic block polymers containing aromatic rings are a better choice to encapsulate

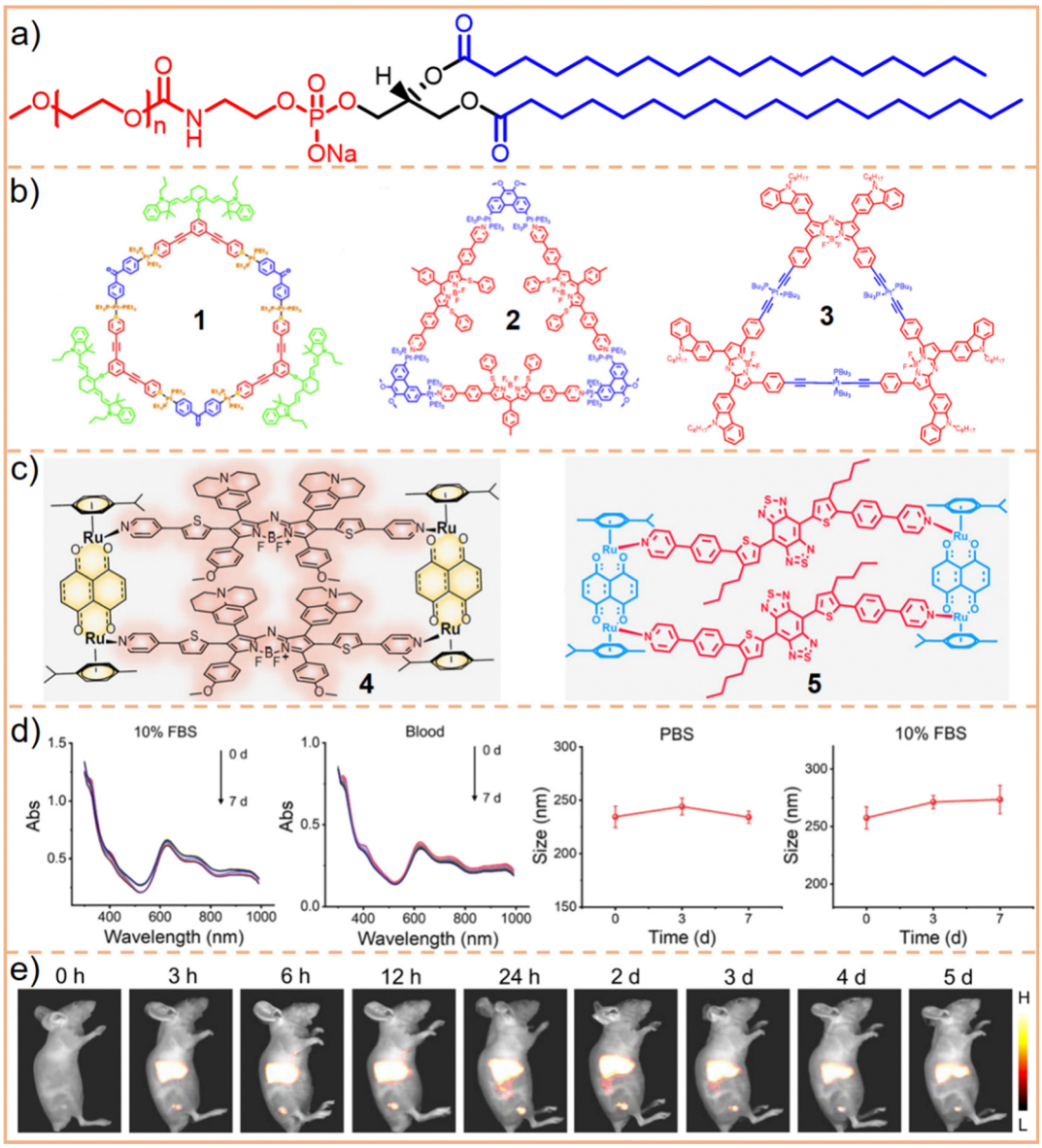

Fig. 3 (a) Chemical structure of DSPE–PEG, where the hydrophobic chains are depicted in blue and the hydrophilic motif in red. Typically, *n* represents the chain length or molecular weight of PEG, such as DSPE–PEG_{2000} (*n* = 45) and DSPE–PEG_{5000} (*n* = 113). (b) Chemical structures of SCCs **1**, **2**, and **3**, and (c) SCCs **4** and **5**. (d) SCC **4** nanoparticles (encapsulated by DSPE–PEG_{5000}), showing their hydrodynamic diameter when incubated in 10% FBS and whole blood and changes after incubation with PBS and 10% FBS over time. (e) Fluorescence images of tumor models post-injection with SCC **4** nanoparticles. This figure is adapted from ref. 86 with permission from Springer Nature, Copyright 2022.

metallacycles/metallacages by planar stacking between the carriers and SCCs. For instance, Wang *et al.*[105] synthesized an amphiphilic polymer, mPEG-*b*-PLGA, by covalently linking hydrophobic polylactic acid (PLGA) with mPEG. This polymer successfully encapsulated a 3D metallacage (Fig. 4e, chemical **9**) constructed *via* Pt(II)–N coordination, maintaining stability for one week in PBS and water. We[106] substituted PLGA with poly(γ-benzyl-L-glutamate) (PBLG) to encapsulate a metallacage composed of anthracene, porphyrin, and a Pt(II) acceptor (Fig. 4f, chemical **10**). The resulting nanoparticles enhanced the water solubility of the metallacage, and the increased hydrophobicity provided by PBLG helped maintain its integrity. In summary, compared to F127, mPEG-*b*-PLGA (Fig. 4g) possesses two modifiable hydrophobic chains, while mPEG-*b*-PBLG (Fig. 4h) incorporates an aromatic ring, rendering it more suitable for encapsulating compounds with highly hydrophobic and large rigid structures. Therefore, given that SCC **10** not only features a larger conjugation structure but lacks a flexible chain, unlike SCC **9**, conventional amphiphilic block polymers (F127, mPEG-*b*-PLGA) may not yield effective encapsulation. Contrastingly, using amphiphilic block polymers containing aromatic rings facilitates metallacage encapsulation by leveraging the stacking interactions between the benzene rings and the rigid planes of SCCs. This tailored design of block

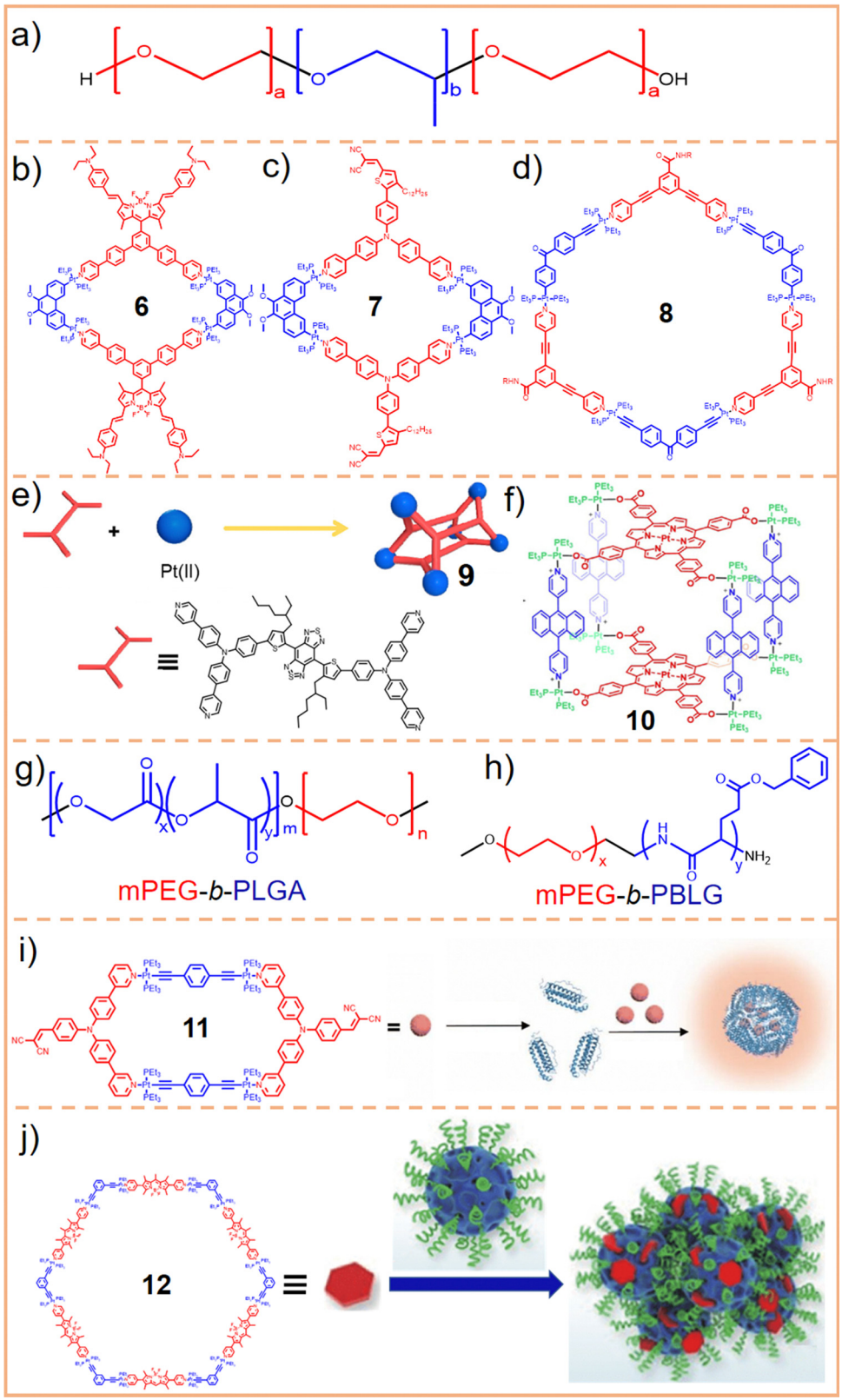

Fig. 4 (a) Chemical structure of Pluronic F127, with the hydrophobic chain (PPO) depicted in blue and the hydrophilic motif (PEO) represented in red. Typically, a = 101 and b = 56 for F127. Chemical structures of SCCs **6** (b), **7** (c), and **8** (d). Chemical structures of SCC **9** (e), SCC **10** (f), mPEG-*b*-PLGA (g), and mPEG-*b*-PBLG (h). (i) Chemical structure of SCC **11** and the following assembly process of nanoparticles. Figure adapted from ref. 107 with permission from the Royal Society of Chemistry, Copyright 2023. (j) Chemical structure of SCC **12** and the following assembly process of nanoparticles. Figure adapted from ref. 108 with permission from Science China Press and Springer-Verlag, Copyright 2021.

copolymers efficiently addresses the requirements for adaptability and biostability in the complex SCC systems within *in vivo* environments.

2.1.3. Encapsulate SCCs with nanocarriers prepared using other materials. Liposomes typified by DSPE–PEG and block copolymers exemplified by F127 are the most prevalent materials for designing nanocarriers for SCCs. However, to develop more effective carriers, research into alternative materials should also be considered. For instance, Liu *et al.*[107] employed human heavy chain ferritin as a nanocarrier for encapsulating a tetragonal metallacycle, assembled from 180° Pt(II) and 120° triphenylamine-based pyridine (Fig. 4i, chemical **11**). Human heavy chain ferritin consists of 24 subunits that self-assemble into a nanocage, featuring a hydrophobic interior and a hydrophilic exterior. In this study, ferritin was initially disassembled in 8 M urea at pH 5.0. Subsequently, it was reassembled with SCC **11** through a controlled reassembly process, gradually reducing the urea concentration from 8 M to 0 M in PBS. The resulting nanoparticles, featuring hydrophobic **11** within and hydrophilic human heavy chain ferritin externally, were relatively small in size (13.32 nm). They demonstrated the ability to specifically target tumor cells with high expression of the transferrin receptor. Moreover, these nanoparticles exhibited relative stability in a solution of PBS with 10% FBS, leading to effective PDT outcomes in cell-based and mouse experiments. Yang *et al.*[108] employed PEG-modified melanin dots, which were then π–π stacked with hexagonal metallacycles (Fig. 4j, chemical **12**). Incorporating metallacycles into the system enhanced its hydrophobicity, leading to the aggregation and formation of nanoparticles with an approximate size of 100 nm in an aqueous solution. This aggregation endowed metallacycles with a passive EPR effect. Such unique and valuable studies are instrumental in developing encapsulation strategies for SCCs, expanding the scope of SCC research within the biomedical field.

2.2. Carrier-free SCCs prepared by functional motif modification

For a DDS, drug loading capacity (DL = $m_1/(m_1 + m_2)$, where m_1 = mass of the drug and m_2 = mass of the carrier) is a crucial metric that directly influences the dosage required for clinical application. Typically, a higher DL is preferable as it more readily meets clinical requirements. However, approaches utilizing nanocarriers to encapsulate SCCs often lead to a low DL,[109,110] indicating that a substantial proportion of the material introduced into the body serves no therapeutic function but merely acts as a transport medium. This necessitates additional *in vivo* degradation, potentially impacting liver function and biliary excretion, posing short- or long-term toxicity risks to the human body.[111,112] Consequently, despite the significant role that carriers play in DDS research, only a few, such as Pluronics and PEG, have received approval from the FDA. Moreover, using materials like Pluronics, which are relatively non-toxic in animal models, is subject to stringent limitations. For instance, the maximum permissible daily exposure for intramuscular injection of the inactive ingredient Pluronic F68 is limited to 4 mg;[88] an intradermal injection of 137.5 mg kg^{-1} Pluronic F127 can lead to significant increases in cholesterol and triglycerides. Similarly, intraperitoneal injection of Pluronic F127 at dosages of 0.5–1 g kg^{-1} induces a hyperlipidemic effect.[113,114] While nanocarriers can be employed to encapsulate SCCs to enhance their water solubility and biological stability, challenges such as low DL capacity and the excessive use of carrier materials must also be considered. Presently, the typical encapsulation techniques for SCCs, including nanoprecipitation,[115–117] nanoemulsification,[118–120] and thin-film hydration,[121–123] face difficulties in addressing these specific challenges. In this context, a carrier-free self-delivery system can be developed by modifying SCCs to have an amphiphilic structure. In this system, SCCs themselves are an integral part of the carrier, eliminating the need for additional materials. This strategy effectively mitigates the toxicity issues associated with the degradation of excess carriers. Simultaneously, it ensures a degree of water solubility for SCCs, effectively resulting in a DL capacity of 100%.[124] Unlike direct amphiphilic macromolecule encapsulation, this approach typically involves modifying hydrophobic donors or acceptors with hydrophilic small molecules[125,126] or polymer chains.[66,127] These modified components are then assembled into SCCs, which subsequently self-assemble into nanoparticles or vesicles due to their amphiphilic nature. These hydrophilic segments can reduce the adhesion of proteins and cells to the material and shield the hydrophobic components of SCCs from hydrolysis and enzymatic degradation. This enhances the circulation stability of SCCs in the bloodstream and facilitates the long-term sustained release of the materials. However, this carrier-free approach might require using small amounts of organic solvents, such as methanol, for nanoparticle formation. Additionally, maintaining long-term size stability under physiological conditions often presents challenges compared to the first method, highlighting an area that needs further exploration and improvement. Overall, developing carrier-free SCCs remains a promising strategy to enhance their water solubility. The characteristics of this approach are detailed in Table 2.

2.2.1. Carrier-free SCCs prepared by hydrophilic small molecule modification. Nanocarriers designed for encapsulating SCCs are typically amphiphilic polymers. These polymers leverage their hydrophobic segments to π–π stack with the rigid structures of SCCs, subsequently forming nanoparticles or vesicles. These structures are stabilized in aqueous solutions by the hydrophilic segments of polymers. Based on this mechanism, one strategy involves covalently attaching hydrophilic small molecules (such as glycosyl groups[128] and peptides[129]) around the rigid, hydrophobic core of metallacycles/metallacages. This approach creates amphiphilic SCCs that can self-assemble into nanoparticles or micelles in an aqueous environment. This method effectively fulfills the function of nanocarriers without the need for adding additional polymeric materials.

We engineered a hydrophilic glycosyl group onto the 120° pyridine ligand and combined it with a 60° Pt(II) acceptor to construct a rhomboidal supramolecular metallacycle (chemical **13**, Fig. 5a) exhibiting amphiphilic characteristics.[128] At low concentrations, these rhomboidal SCCs can self-assemble into

Table 2 Features of carrier-free SCCs with improved water solubility and biostability. The particle size is determined by dynamic light scattering (DLS)

Topological structures	Hydrophilic units used	Particle size (nm)	Biostability test	Aqueous solution	Ref.
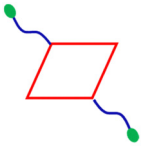 Chemical **13**	Glycosyl group	80	—	H_2O + 5% CH_3OH	128
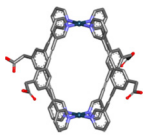 Chemical **14**	Peptide-$(PEG)_2$	—	1 day	H_2O	129
 Chemical **15**		145 (chemical **15**)			
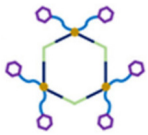 Chemical **16**	Glycosyl group	210 (chemical **16**)	—	H_2O + 50% CH_3OH	130
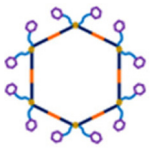 Chemical **17**		1008 (chemical **17**)			
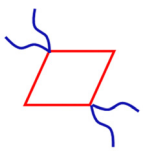 Chemical **18**, **19**, **20**	$(PEG)_6$	78 (chemical **18**), 77 (chemical **19**), 69 (chemical **20**)	—	H_2O + 6% CH_3OH	131
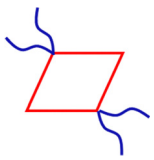 Chemical **21**	$(PEG)_3$	110	1 day	PBS + 10% FBS	65
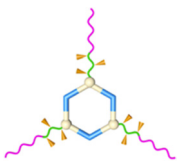 Chemical **22**	PBEMA-*b*-POEGMA on SCCs	80–120	2 days	PBS + 10% FBS	133

Table 2 (*continued*)

Topological structures	Hydrophilic units used	Particle size (nm)	Biostability test	Aqueous solution	Ref.
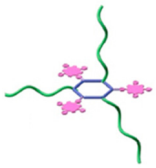 Chemical **23**	POEGMA on SCCs	130	—	H_2O	134

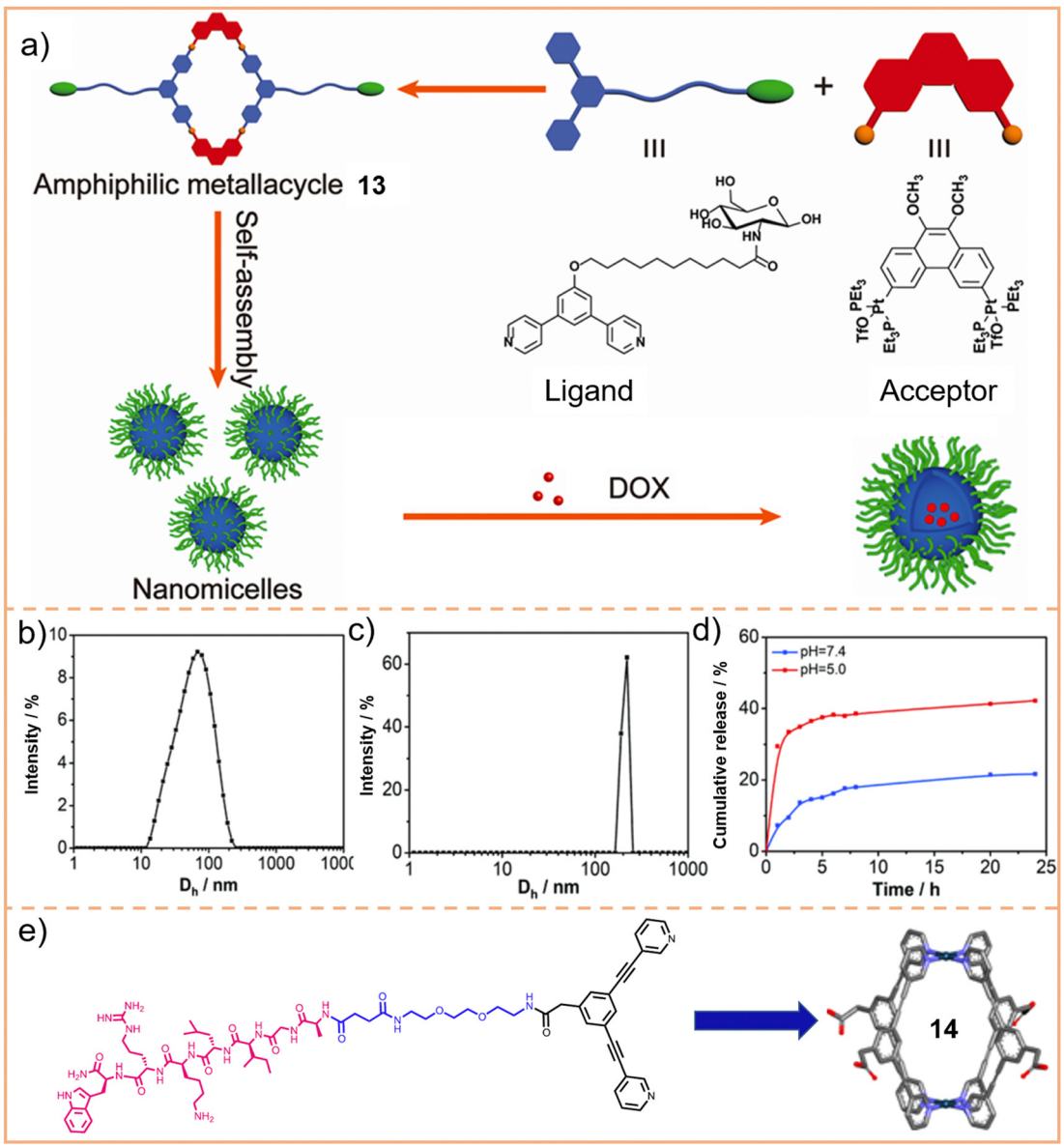

Fig. 5 (a) Chemical structure of the amphiphilic rhomboidal metallacycle **13** and schematic illustration of the formation of nanomicelles, and applications in the encapsulation of DOX. Dynamic light scattering (DLS) spectrum of nanomicelles before (b) and after (c) encapsulation of DOX. (d) Drug release curves of the metallacycle within DOX at pH = 7.5 and 5.0. Figure adapted from ref. 128 with permission from American Chemical Society, Copyright 2020. (e) PepH3 functionalized pyridine ligand and the formed metallacage **14**. Figure adapted from ref. 129 with permission from American Chemical Society, Copyright 2021.

80 nm nanovesicles in an aqueous environment (Fig. 5b). These nanovesicles are capable of acting as carriers for the hydrophobic anticancer drug DOX (Fig. 5c). The encapsulated DOX demonstrates prolonged release under neutral conditions and accelerated release in acidic environments, where the increased protonation of DOX enhances its solubility and leads to SCC disassembly. This release behavior is facilitated by the stabilizing effect of the glycosyl groups in an aqueous environment and the encapsulation within the amphiphilic SCCs (Fig. 5d). These findings demonstrate that amphiphilic SCCs can effectively serve as carriers in DDSs. Casini *et al.*[129] modified a pyridine ligand with PepH3, a peptide that can translocate across the blood–brain barrier. This modification resulted in the formation of a water-soluble homoleptic metallacage upon the addition of coordination Pd^{2+} ions. Furthermore, this metallacage (chemical **14**, Fig. 5e) was utilized as a targeted delivery system to encapsulate a radiotherapy agent. Chen *et al.*[130] compared the structures of amphiphilic metallacycles, assembled in various ratios using different angular Pt(II) receptors on 120° pyridine ligands modified with galactoside. They also examined the sizes of nanoparticles or vesicles that are formed by their aggregation. Transmission electron microscopy (TEM) analysis revealed the diverse morphologies of nanoparticles and vesicles formed through the self-assembly of a galactoside-modified pyridine ligand with different acceptors. Specifically, after [2 + 2] self-assembly with the acceptor, resulting in a rhomboidal metallacycle (chemical **15**), nanoparticles with an average size of 145 nm were observed (Fig. 6a). In the case of [3 + 3] self-assembly, which formed a hexagonal metallacycle (chemical **16**), the structures manifested as 210 nm nanovesicles (Fig. 6b). Furthermore, [6 + 6] self-assembly, forming a larger hexagonal metallacycle (chemical **17**), produced micrometer-sized microvesicles of 1.08 μm (Fig. 6c). These findings suggest a linear correlation between the size of the metallacycle and the resultant nanoparticle size for a given structural framework. The micrometer-sized vesicles formed by the [6 + 6] self-assembly exhibited potent biofilm inhibition properties against *Staphylococcus aureus*. Furthermore, they were effective in alleviating pneumonia in mice caused by this bacterium, demonstrating their potential therapeutic applications.

2.2.2. Carrier-free SCCs prepared by hydrophilic macromolecule modification. Another strategy to create amphiphilic metallacycles/metallacages involves covalently linking hydrophilic macromolecules, such as PEG, which then undergo hydrophilic/hydrophobic self-assembly to form stable nanoparticles or vesicles in an aqueous environment. Compared to small molecules, incorporating PEG into SCCs imparts more flexible and dynamically tunable properties. Alterations in the ligand structure do not significantly impact the size and biostability of the resulting nanoparticles, highlighting the versatility of this approach. To illustrate this concept, we modified a Pt(II) receptor with PEG and varied the linkage between the aniline core and the pyridine of the ligand.[131] This modification allowed us to synthesize rhombic metallacycles with single, double, and triple bonds (chemicals **18**, **19**, and **20**, depicted in Fig. 7a–c). Leveraging both hydrophilic and hydrophobic interactions, these SCCs spontaneously self-aggregated into nanomicelles, negating the need for additional amphiphilic macromolecules. Utilizing TEM and DLS, it was verified that the various nanomicelles had similar sizes, all approximately 75 nm in diameter. This uniformity demonstrates that

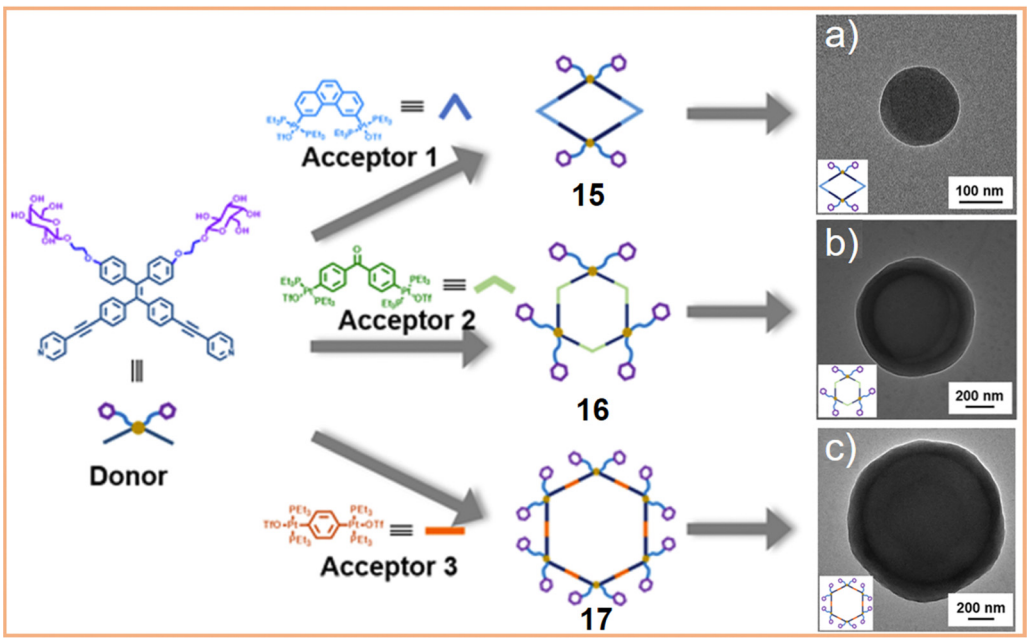

Fig. 6 Schematic representation of the formation and hierarchical self-assembly morphologies of amphiphilic metallacycles and transmission electron microscopy (TEM) images of (a) [2 + 2] chemical **15**, (b) [3 + 3] chemical **16**, and (c) [6 + 6] chemical **17**. Figure adapted from ref. 130 with permission from American Chemical Society, Copyright 2020.

alterations in the ligand structure do not substantially impact the hierarchical self-assembly of PEG-modified metallacycles. Furthermore, Stang *et al.*[65] employed PEG to modify Pt(II) acceptors and melanin nanoparticles. After assembling the former into a rhombic metallacycle (Fig. 7d, chemical **21**), 110 nm nanoparticles were formed in an aqueous environment through π–π bonding between metallacycles and melanin. These particles were able to maintain their stability for 24 h in a physiological environment. To solve the problem of poor stability and solubility in water of multicomponent lanthanide organic assemblies, which significantly limit their biomedical applications, Sun *et al.*[132] also functionalized bis-tridentate tetrazolate ligands with PEG, which facilitate a good water solubility, and then assembled with a series of lanthanide metals (such as Eu^{III} and Gd^{III}). The prepared water-soluble anionic polyhedral complexes were suitable for luminescence and magnetic resonance dual-modal imaging. This result not only provides a new design route toward water-stable multinuclear lanthanide organic assemblies but also offers potential candidates for supramolecular edifices for bioimaging and drug delivery. Collectively, these results indicate that modifying SCCs with hydrophilic macromolecules like PEG can ensure good dispersion and stability while preserving the dynamically adjustable structures of the ligands and acceptors.

2.2.3. Carrier-free SCCs prepared by post-assembly block polymerization. Beyond employing glycosyl groups and PEG as hydrophilic segments for crafting amphiphilic SCCs, more intricate approaches have been developed. For instance, we[133] synthesized amphiphilic supramolecular block copolymers by combining coordination-driven self-assembly with post-assembly reversible addition–fragmentation chain-transfer (RAFT) polymerization. Initially, we modified a 120° pyridine donor with a trithioester group, a conventional RAFT chain transfer agent. This modified donor was then involved in a [3 + 3] self-assembly process with a 120° Pt(II) acceptor, forming a hexagonal metallacycle. The metallacycle–PBEMA polymer was then polymerized with [2-((((4-(4,4,5,5-tetramethyl-1,3,2-dioxaborolan-2-yl)benzyl)-oxy)carbonyl)oxy) ethyl methacrylate] (BEMA), leveraging the trithioester group on the metallacycle. Subsequently, in a similar manner, the metallacycle–PBEMA polymer underwent polymerization with poly(ethylene glycol) methacrylate (POEGMA), yielding a PBEMA-*b*-POEGMA copolymer (Fig. 8b) attached to the metallacycle (Fig. 8a, chemical **22**). In this unique system, the metallacycle functions as a cross-linker and stabilizer for the amphiphilic polymer. Consequently, this metallacycle-based amphiphilic copolymer can act as a nanocarrier, aggregating into nanoparticles in an aqueous environment. Moreover, it can be loaded with DOX and palmitoyl ascorbate, utilizing hydrophilic/hydrophobic interactions and π–π stacking, to facilitate synergistic therapeutic applications. Zhang *et al.*[134] employed the RAFT method to directly polymerize POEGMA onto a metallacycle modified with a porphyrin photosensitizer. This process led to the formation of amphiphilic SCCs (Fig. 8c, chemical **23**), which self-assembled into nanoparticles approximately 130 nm in size in an aqueous environment. These polymers were further combined with gold nanorods, leveraging their photothermal properties. This combination facilitated a synergistic treatment approach, integrating PDT, PTT, and chemotherapy within a single system, demonstrating the

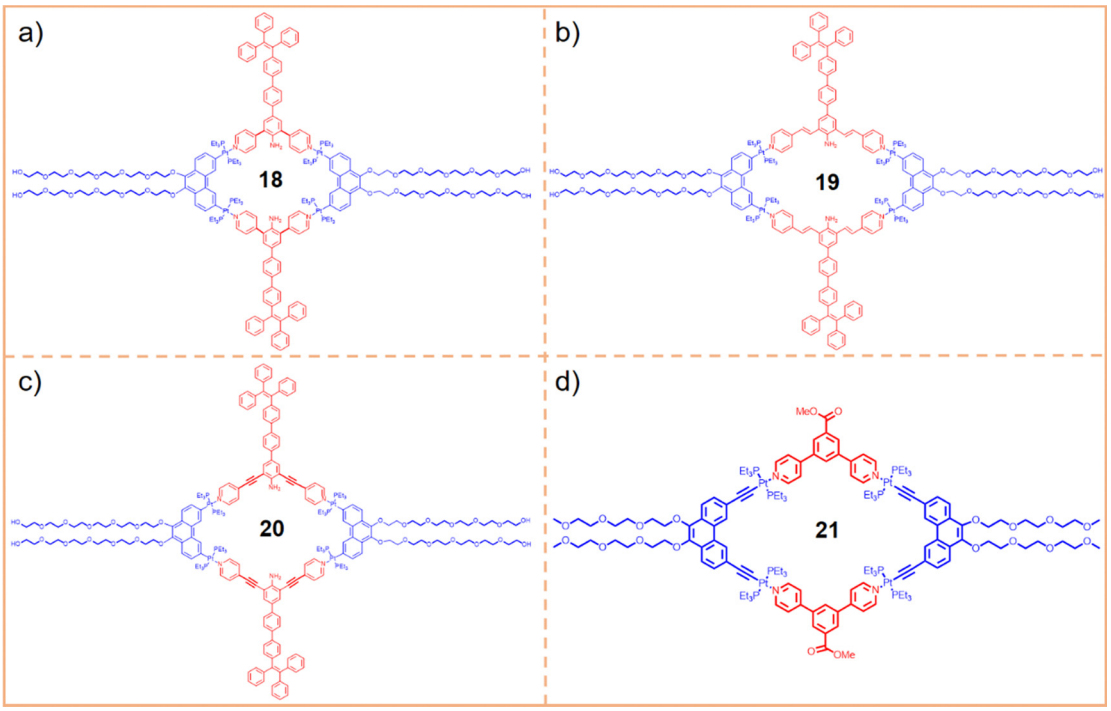

Fig. 7 Structures of metallacycles **18** (a), **19** (b), **20** (c), and **21** (d).

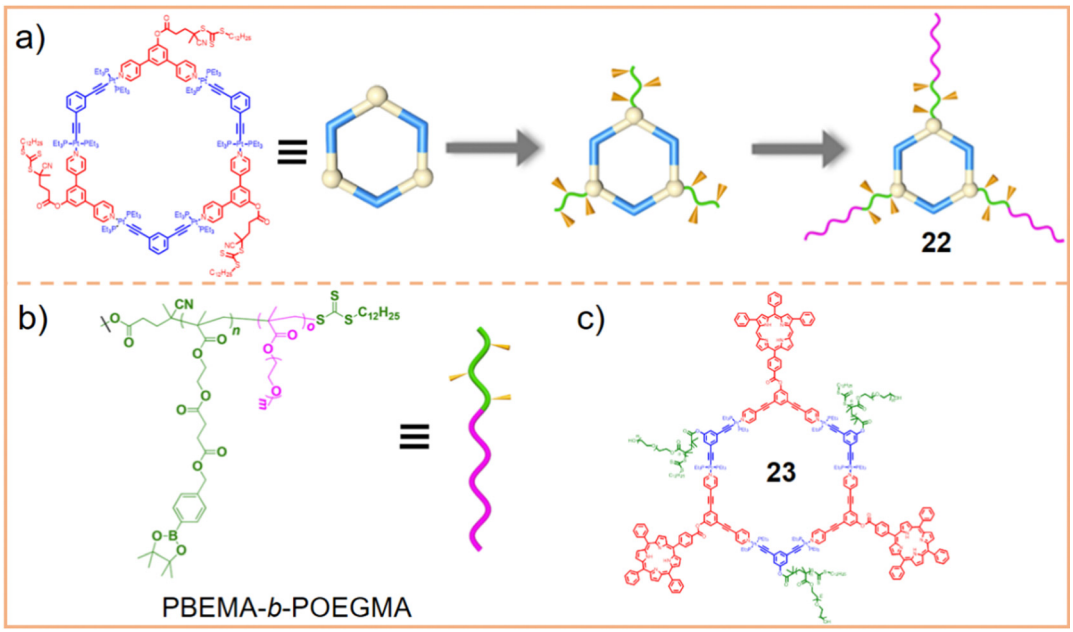

Fig. 8 (a) Schematic representation of the preparation of a metallacycle with a supramolecular block copolymer (chemical **22**) and (b) the chemical structure of PBEMA-*b*-POEGMA. Figure adapted from ref. 133 with permission from American Chemical Society, Copyright 2020. (c) Chemical structure of metallacycle **23**.

potential for multifaceted therapeutic strategies. It is evident that directly attaching hydrophilic small molecules or macromolecular segments to SCCs can enhance their water solubility and biocompatibility and enable the design of more complex systems for applications in the biomedical field. Additionally, the formation of nanoparticles or vesicles, coupled with the repulsion and obstruction of proteins in the bloodstream by the hydrophilic components, enables this approach to, to some extent, protect SCCs from degradation by the *in vivo* microenvironment during the delivery process. These findings demonstrate that post-assembly polymerization offers the flexibility to manipulate the architecture of supramolecular ensembles, leading to a higher level of structural complexity and diverse functionalities. This versatility is particularly advantageous for the development of biomedical SCCs, potentially expanding their applicability in various medical and therapeutic areas.

3. Strategies to reduce the potential toxicity and side effects of SCCs

As with any therapeutic intervention, potential toxicities and side effects must be thoroughly considered when administering drugs. Some of these adverse effects arise from the inherent chemical activity of the drug. For instance, the ROS generated by the interaction between DOX and iron can inflict damage on the myocardium,[135,136] leading to myofibrillar loss and cytoplasmic vesiculation. Others are related to the method of administration. For example, the FDA-approved drug DOXIL (DOX encapsulated in PEG liposomes) exhibits a high tendency to aggregate at the skin due to its PEG coating. During administration, minute quantities of the drug may seep out of capillaries into the palms and soles, causing redness, swelling, tenderness, discomfort and even pain due to skin peeling. This condition is known as palmar-plantar erythrodysesthesia or hand-foot syndrome.[137–139] Additionally, certain side effects may result from the treatment modality, such as chemotherapy-induced hepatitis B.[140–142] As SCCs progress toward clinical trials, these medical challenges must be addressed to align with the principles of precision medicine. As illustrated in Fig. 9, critical issues for SCCs at the cellular level include: (1) cell selectivity: the ability to differentiate and target diseased cells while sparing normal cells is essential for minimizing collateral damage and enhancing treatment efficacy; (2) heavy metals: the risk of heavy metal leakage from SCCs during transport poses a significant safety concern. Ensuring the containment and stability of these complexes is crucial to prevent unintended systemic exposure. On the other hand, the therapeutic index can be optimized by using dual metal coordination centers; and (3) intracellular distribution: understanding the specific action sites and mechanisms of SCCs within cells is vital for predicting their therapeutic impact and potential side effects. Each of these factors plays a fundamental role in the successful development and application of SCCs in clinical settings. Addressing these challenges is paramount to harnessing the full potential of SCCs in precision medicine.

3.1. Reduce the potential toxicity and side effects of SCCs by active cell selectivity

The non-selective drug action on diseased and healthy cells *in vivo* is a primary contributor to its toxic side effects. Enhancing the cell selectivity of SCCs to effectively distinguish

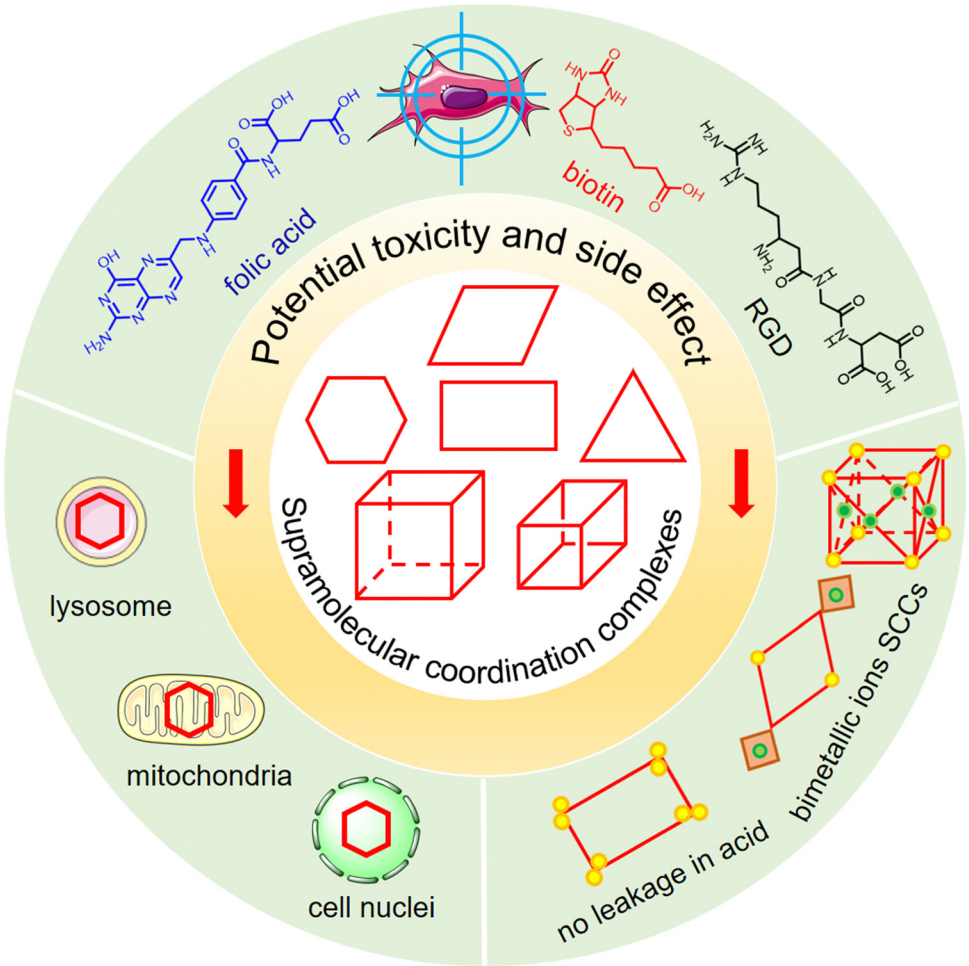

Fig. 9 Schematic representation of general strategies of SCCs to reduce the potential toxicity and side effects for biomedical applications.

between these two cell states is critical for minimizing these adverse effects. Although SCCs, as currently assembled, generally demonstrate improved cell uptake and, to a certain extent, better selectivity between diseased and healthy cells compared to their small-molecule counterparts, their performance in this regard is not yet optimal. This relative selectivity may be attributed to SCCs possessing multiple positive charges, a certain degree of lipophilicity, and unique ring tension.[42,143–149] However, further improvements are necessary to achieve satisfactory selectivity for clinical applications. Various strategies have been employed to encapsulate SCCs into nanoparticles or vesicles to enhance their water solubility and biostability while conferring a passive EPR effect. This effect is intended to augment SCC accumulation in tumor tissues. However, the effectiveness of the EPR effect is subject to ongoing scrutiny due to several factors:[150–161] (1) heterogeneity of the vascular system: there is considerable variability in the vascular systems across species and tumor types, which can significantly impact the distribution and effectiveness of nanomedicines; (2) tumor microenvironment variability: the diverse characteristics of tumor microenvironments, such as pH, interstitial pressure, and extracellular matrix composition, can influence the action and efficacy of nanomedicines; and (3) low delivery efficiency to solid tumors: studies indicate that only 0.7% of systematically administered nanomedicines reach solid tumors. The significant attrition rate in the efficacy of nanomedicines, primarily due to insufficient accumulation of nanoparticles in tumors and suboptimal pharmacokinetics, has led to skepticism about their effectiveness. This situation suggests that an excessive emphasis on the EPR effect might be misleading in the design of nanomedicines.[162,163] In this scenario, modifying SCCs with tumor-targeting moieties, such as folic acid (FA),[164] biotin,[165] Arg–Gly–Asp (RGD)[166–168] sequence, and other peptides,[169] offers a promising strategy. This approach aims to selectively concentrate the drugs in tumor tissues and cells through active recognition and binding of these targeting moieties to specific molecules and proteins present at tumor sites. Consequently, this endows SCCs with active cellular selectivity. For a more comprehensive understanding, the general pathway of SCCs equipped with targeting units is depicted in Fig. 10. Additionally, the characteristics of SCCs with active cell selectivity are outlined in Table 3.

3.1.1. Active cell selectivity realized by functional small molecule modification. Advancements in molecular biology

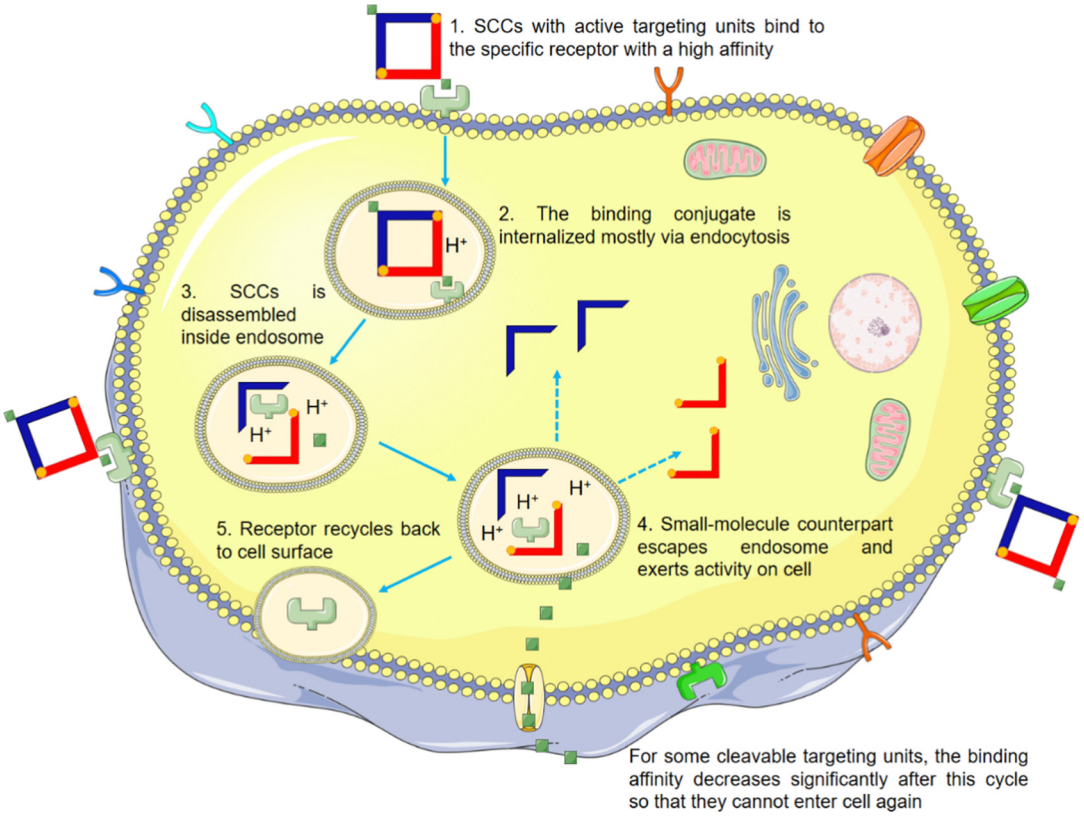

Fig. 10 Schematic representation of tumor cellular uptake of SCCs modified with targeting motifs (*e.g.*, FA, biotin, cRGDfk, *etc.*). Typically, a receptor binds to these modified SCCs with high affinity, facilitating endocytosis and internalization. Inside the lysosome/endosome, SCCs disassemble, allowing the small-molecule counterparts to escape and exert their activity within the cell. Subsequently, the vesicle, with receptors, returns to the cell plasma membrane. For certain cleavable targeting units, the binding affinity significantly decreases after this cycle, preventing further cellular entry.

Table 3 Features of SCCs with active cell selectivity. Targeting and therapy outcomes are determined by comparison to SCCs without target unit modification. Cell lines that are not marked as receptor-negative are receptor-positive by default

Target units used	Targeting receptors	Cell lines	Targeting outcomes	Therapy outcomes	Ref.
FA	FR		Higher intracellular Pt concentration	Lower IC_{50}	164
		DU145	1.6-fold	49%; with 1.4-fold higher level of apoptosis and necrosis	
		HeLa	2.3-fold	20%	
		A549	1.9-fold	56%	
		HCT116	2.8-fold	40%	
		HEK293 (FR-negative)	1.1-fold	84%	
Biotin	BR		Fluorescence image	Lower IC_{50}	165
		4T1	Brighter	20%	
		HepG2	Brighter	19%	
		HCT116 (BR-negative)	No difference	92%	
cRGDfk	$\alpha_v\beta_3$ integrin	U87MG	2.5-fold higher fluorescence intensity; 2.1-fold higher intracellular Pt concentration	Pretreatment with free cRGDfK resulted in diminished cytotoxicity	207
cRGDfk	$\alpha_v\beta_3$ integrin	A2780	Pretreatment with free cRGDfK resulted in diminished internalization	3.8-fold higher IC_{50} after pretreatment with free cRGDfK	210
(Tyr^3)-octreotate peptide	sst2R	CHO_{sst2}	—	—	169

and molecular pathology have uncovered that certain receptors are highly expressed on the surface of various tumor cells, whereas their expression is negligible or significantly lower in normal tissues. FA and biotin, as quintessential examples of active targeting agents, exhibit high affinity for their respective receptors under physiological conditions. This characteristic makes them highly effective for cancer labelling and targeted delivery of anticancer drugs.[170–175] Combining SCCs with FA or

biotin is a viable strategy to confer active cellular recognition capabilities to these complexes.

FA and its receptor, the folate receptor (FR), a glycosylated phosphatidylinositol-linked membrane glycoprotein, exhibit a very high affinity under physiological conditions. When FA is conjugated with a carrier, this complex can enter cells expressing the FR *via* the same pathway as free FA.[176–178] Utilizing this characteristic, Stang *et al.*[164] employed an FA-modified PEG-PLGA block copolymer (Fig. 11a) to encapsulate a square metallacycle. This metallacycle (3-NF-FA) was composed of a

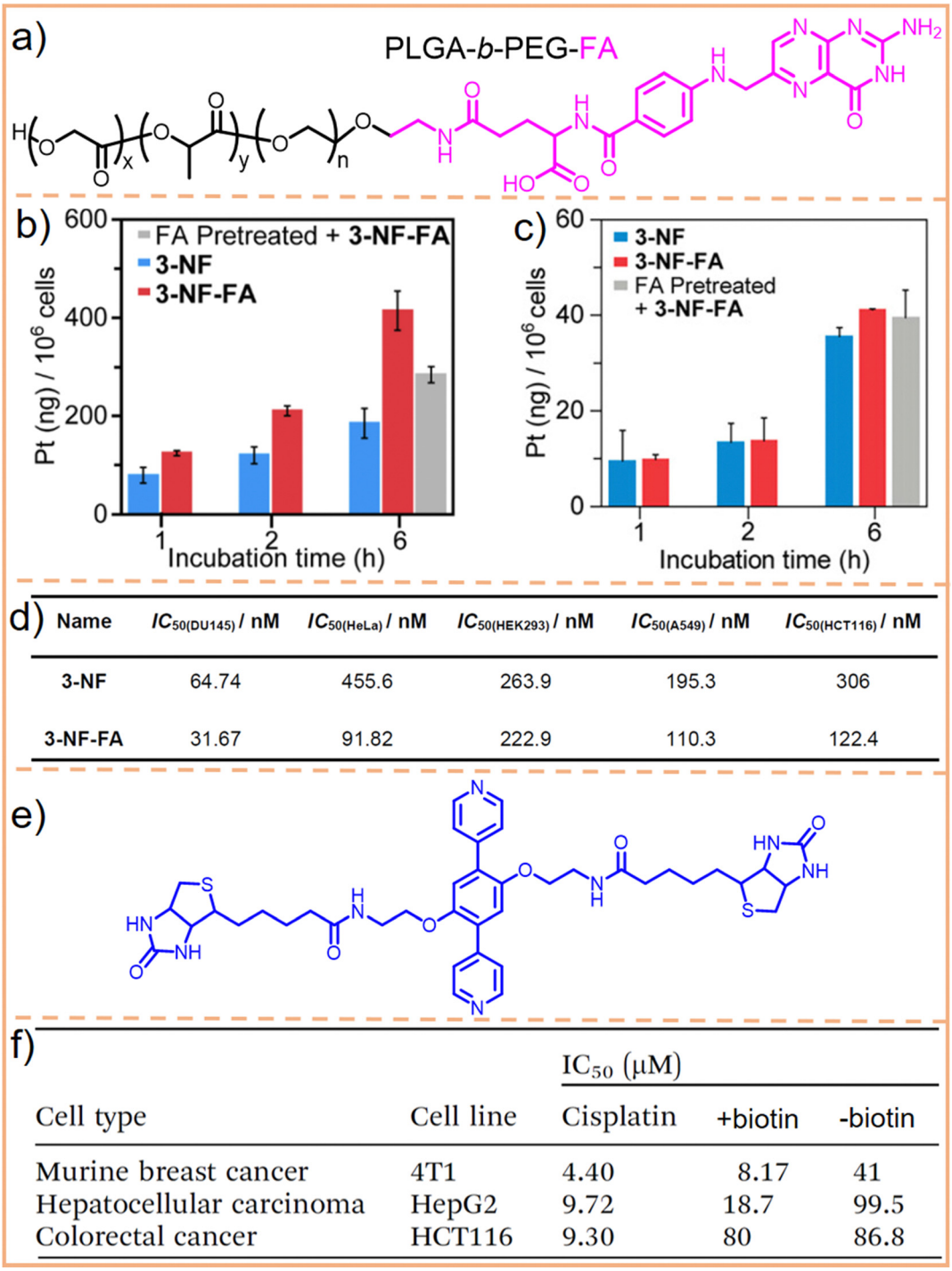

d)

Name	$IC_{50(DU145)}$ / nM	$IC_{50(HeLa)}$ / nM	$IC_{50(HEK293)}$ / nM	$IC_{50(A549)}$ / nM	$IC_{50(HCT116)}$ / nM
3-NF	64.74	455.6	263.9	195.3	306
3-NF-FA	31.67	91.82	222.9	110.3	122.4

e)

f)

		IC_{50} (μM)		
Cell type	Cell line	Cisplatin	+biotin	-biotin
Murine breast cancer	4T1	4.40	8.17	41
Hepatocellular carcinoma	HepG2	9.72	18.7	99.5
Colorectal cancer	HCT116	9.30	80	86.8

Fig. 11 (a) Chemical structure of PLGA-*b*-PEG-FA. Cell uptake analysis of 3-NF-FA and 3-NF in FR-positive HeLa cells (b), and FR-negative HEK293 cells (c), with or without preincubation with 1 mM free FA for 2 h. (d) Cytotoxicity analysis of 3-NF and 3-NF-FA on various cell lines. Figure adapted from ref. 164 with permission from American Chemical Society, Copyright 2022. (e) Chemical structure of the biotin-modified pyridine ligand and (f) IC_{50} values of the metallacage with or without biotin modification and cisplatin towards HepG2, 4T1, and HCT116 cells. Figure adapted from ref. 165 with permission from the Royal Society of Chemistry, Copyright 2020.

camptothecin-modified pyridine ligand and a combretastatin A-4-modified Pt(II) acceptor. Cell uptake analysis revealed that 3-NF-FA achieved a higher intracellular Pt concentration compared to its non-modified counterpart, 3-NF, in FR-positive HeLa cell lines (Fig. 11b). This increased uptake was not observed in FR-negative HEK293 cells (Fig. 11c). Further experiments showed that when FR-positive cells were pre-treated with free FA, 3-NF-FA uptake significantly decreased. Conversely, pre-treating HEK293 cells, which lack FR, with free FA had negligible effects on the endocytosis of 3-NF-FA, highlighting its potential for selective delivery in cells overexpressing FR. Consequently, 3-NF-FA demonstrated a greater cytotoxicity than 3-NF (Fig. 11d). Moreover, apoptosis analysis revealed that treatment with 3-NF-FA induced a higher level of apoptosis and necrosis, totaling 50.14%, whereas a lower proportion of apoptotic and necrotic cells was observed in cells treated with 3-NF (34.93%). These results confirmed that the introduction of FA enhances cellular uptake in cancer cells through FR-mediated endocytosis. This leads to higher drug concentrations within the cancer cells, effectively achieving targeted cell selectivity.

Compared to FA, biotin exhibits a relatively low molecular weight and simple chemical structure. It also has low toxicity (biotin is one kind of B vitamin, also known as vitamin H, vitamin B7, and coenzyme R, which is indispensable for the normal metabolism of fats and proteins) and a highly specific tumor-targeting capability due to its interaction with the biotin receptor (BR, a glycoprotein overexpressed in tumor cells, exhibits a high affinity for biotin and its derivatives).[179–181] We utilized biotin to modify DSPE–PEG macromolecules and encapsulated 3D metallacages within them.[182] This modification endowed metallacages with excellent biostability and conferred them with targeted delivery capabilities through receptor-mediated endocytosis. Recently, Zhang *et al.*[165] utilized biotin to modify a pyridine ligand (Fig. 11e), assembling it into a 3D supramolecular metallacage. This modification aimed at differentiating between BR-positive hepatocellular carcinoma cells (HepG2) and murine breast cancer cells (4T1), and BR-negative colorectal cancer cells (HCT116). The findings revealed that HepG2 and 4T1 cells incubated with the biotin-modified metallacages exhibited high fluorescence brightness. Additionally, the half maximal inhibitory concentration (IC_{50}) of metallacages for 4T1 and HepG2 cells was merely 20% and 19%, respectively, of that observed for metallacages without biotin modification. Conversely, IC_{50} of metallacages for HCT116 cells did not significantly differ (Fig. 11f). These results demonstrate the efficacy of biotin in enhancing the tumor-targeting capabilities of SCCs.

3.1.2. Active cell selectivity realized by functional peptide modification. Peptides, functional fragments composed of several to dozens of amino acids linked by amide bonds in a specific sequence, play specialized roles in physiological processes. They can be absorbed by the body and actively participate in cellular metabolism. In the realm of developing new anti-tumor drugs, diagnostic probes, and targeted delivery systems, peptides have emerged as a significant area of focus due to their minimal adverse effects and potent targeting capabilities.[183–187] Similar to small molecules like FA and biotin, certain peptides are highly expressed on the surfaces of tumor cells. These include receptors such as insulin-like growth factor 1 (IGF-1) receptor,[188–190] integrins,[191–195] and epidermal growth factor receptor (EGFR).[196–199] Integrins stand out as a crucial class of cell surface receptors within cell adhesion molecules. They are highly expressed in both tumor cells and genetically stable tumor vascular endothelial cells. RGD peptides, naturally present in the extracellular matrix of many organisms, can specifically bind to integrin $\alpha_v\beta_3$ receptors.[200–205] This specific binding property makes RGD peptides particularly effective for modifying SCCs to actively target tumor cells. However, considering the presence of peptide exonucleases/endonucleases in most tissues, which can degrade peptides, RGD is often cyclized or chemically modified to reduce the likelihood of degradation. One common approach involves using cRGDfk (cyclic Arg–Gly–Asp–D-Phe–Lys sequences). This modification significantly enhances the stability of the peptide, making it more resilient to enzymatic breakdown and thus more effective in biological settings.[206]

In our previous work, we utilized cRGDfk to modify the amphiphilic block polymer PEG-*b*-PEBP (poly(2-ethylbutoxy phospholane)) (Fig. 12a). This modified polymer was then employed to encapsulate 3D metallacages, assembled from porphyrin, organoplatinum(II), and disodium terephthalate.[207] The effectiveness of this approach was evaluated using confocal laser scanning microscopy (CLSM) and inductively coupled plasma mass spectrometry (ICP-MS). The results from these analyses demonstrated that integrin $\alpha_v\beta_3$ receptor-mediated endocytosis significantly enhanced the tumor cell targeting capability of metallacages. As depicted in Fig. 12b, the fluorescence intensity of cRGDfk-modified nanoparticles significantly increased over time. After 4 h of incubation, the fluorescence intensity of these cRGDfk-modified nanoparticles was 2.5 times higher than that of nanoparticles without cRGDfk modification. This observation indicates enhanced cellular uptake due to the specific interaction of the cRGDfk modification with integrin receptors. Furthermore, when cells were pre-treated with free cRGDfk before introducing nanoparticles, the fluorescence intensity considerably decreased. This reduction suggested that the presence of free cRGDfk competes with the cRGDfk-modified nanoparticles for integrin binding, inhibiting their internalization. Likewise, pre-treatment with cRGDfk resulted in a reduction in the intracellular Pt content (Fig. 12c). These experiments proved that the binding of cRGDfk to integrin receptors enhances the cellular uptake and internalization of metallacages. Chen *et al.*[208] and Zheng *et al.*[209] employed a similar strategy to encapsulate 3D metallacages with varying structures. This methodology effectively endowed SCCs with the capability of actively recognizing tumor cells, leveraging the targeting potential of the cRGDfk peptides. Building upon this concept, Mao *et al.*[210] further leveraged the integrin-mediated endocytosis and the elevated concentration of reduced glutathione (GSH) found in tumor cells. They accomplished this by modifying poly(ethylene glycol)

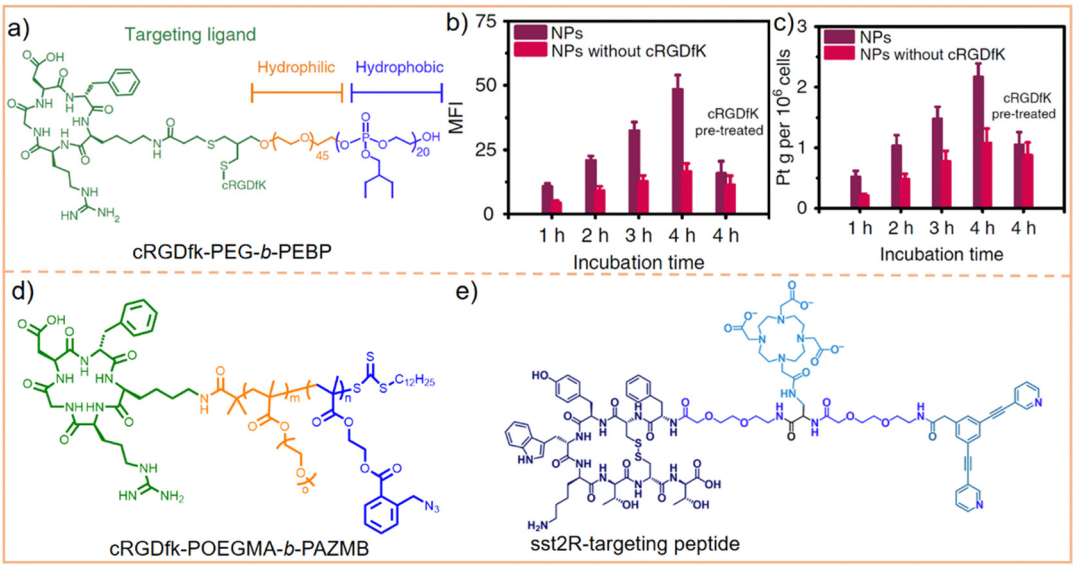

Fig. 12 (a) Chemical structure of cRGD-PEG-*b*-PEBP. (b) Mean fluorescence intensity (MFI) and (c) intracellular Pt amounts of tumor cells after treatment with nanoparticles with or without cRGDfK for different incubation times. Figure adapted from ref. 207 with permission from Springer Nature, Copyright 2018. (d) Chemical structure of cRGD-POEGMA-*b*-PAZMB and (e) chemical structure of the sst2R-targeting peptide functionalized pyridine ligand.

methacrylate (POEGMA)–poly(2-azidomethyl benzoyl glycerol methacrylate) (PAZMB) with cRGDfk (Fig. 12d). These modified copolymers were then used to encapsulate hexagonal metallacycles. The hydrophilic nature of POEGMA ensures prolonged circulation time of nanoparticles in the bloodstream. PAZMB enhances the loading capacity of metallacycles through π–π stacking and enables GSH-responsive drug release. This responsive release mechanism is triggered by a reduction-induced cascade elimination reaction of the azidomethyl benzoyl group. Incorporating cRGDfk into the system enhanced the active selectivity of metallacycles toward tumor cells. This was demonstrated by the marked decrease in the fluorescence intensity of metallacycles in tumor cells, along with a significant increase in their IC_{50} value against tumor cells (from 1.88 ± 0.14 to 7.16 ± 0.54 μM) following the addition of free cRGDfk. This finding suggests that the presence of free cRGDfk competes with the cRGDfk-modified metallacycles for binding to integrin receptors, reducing the uptake and effectiveness of metallacycles in tumor cells. Beyond the cRGDfk peptide, various other types of polypeptides have been explored as tumor cell targeting moieties. Casini *et al.*[169] developed the Pd_2L_2 metallacycle (where L = 3,5-bis(3-ethynylpyridine)phenyl) and modified it with an octapeptide on the SCCs, targeting the somatostatin-2 receptor (sst2R), which is pathologically overexpressed in various neuroendocrine tumors. This specific targeting approach aimed to achieve selective binding to tumor cells (Fig. 12e). Using peptides to modify metallacycles/metallacages is a strategic response to the unique endogenous characteristics of tumor cells. Such targeted designs are crucial for enhancing the active selectivity of SCCs towards tumor cells, which contributes to reducing their toxic side effects on healthy cells.

3.2. Reduce the potential toxicity and side effects of SCCs by changing the metal coordination centers

While various metals can be utilized to form coordination bonds, the assembly of SCCs predominantly employs heavy metals with strong coordination capabilities, such as Pt, Ru, Pd, and Ir. These heavy metals serve dual roles in assembled SCCs. They can act as chemotherapeutic agents, effectively killing tumor cells or bacteria. However, the excessive use of heavy metals poses significant health risks. They can potentially lead to DNA (deoxyribonucleic acid) mutations, autoimmune diseases, respiratory and hearing problems, and damage to vital organs, including the intestines, kidneys, and bone marrow.[211–213] The issue of heavy metal misuse due to drug resistance is a significant concern. For instance, organoplatinum, commonly used as a coordination center in the assembly of SCCs, exhibits effects similar to those of cisplatin. However, congenital and acquired resistance to platinum-based chemotherapy has been observed in patients over long-term clinical use,[214–218] significantly limiting the effectiveness of these drugs. Additionally, heavy metal misuse can stem from the instability of the assembled SCCs. If these complexes are not sufficiently stable, they may disassemble during transport within the body, leading to the unintended release of metal ions into non-diseased tissues. Altering the metal ion species at the coordination center is a viable option to reduce the potential toxicity of SCCs in biomedical applications. Opting for lighter metals that are essential to human health as coordination centers could be an ideal solution. However, the weaker coordination capabilities of these lighter metals compared to their heavy metal counterparts have led to their limited application in the SCC research in the biomedical field. For instance, Chan *et al.*[219] synthesized diverse heteroleptic metalla-

Table 4 Features of SCCs by changing the metal coordination centers. For dual metal ions, physicochemical properties and therapy outcomes are determined by comparison to a metal ligand

Topological structures	Metal ions	Physicochemical properties outcomes	Therapy outcomes	Ref.
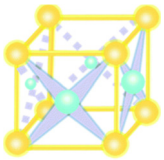	Ir(III)–Pd(II)	25.3-fold higher TPA; 1.3-fold higher $^1O_2$ quantum yield; brighter fluorescence image	Lower IC_{50}; 5-fold higher PDI; 28% tumor volume at 20 days of post-treatment	220
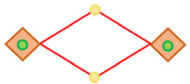	Ru(II)–Pt(II)	16.5-fold higher TPA; 1.1-fold higher $^1O_2$ quantum yield; brighter fluorescence image	Lower IC_{50}; 5–33-fold higher PDI for different cell lines	221
	Ru(II)–Pt(II)	33.9-fold higher TPA; 1.3-fold higher $^1O_2$ quantum yield; brighter fluorescence image	59% lower IC_{50}; 11.2-fold higher PDI	222
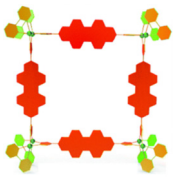	Pd(II)	Less than 8% change in the intensity of absorption spectra at pH = 7.4, 6.8, and 5.3	Imaging-guided PDT; no *in vivo* experiment	227
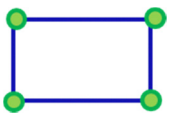	Ru(II)	Imidazole–Ru(II) coordination; no significant changes in the absorbance spectra from pH 4.5 to 8.0	Multimodal therapy; no *in vivo* experiment	228
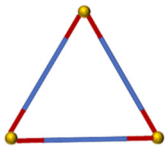	Pt(II)	Maintained for two days at pH 5.5 without obvious changes	Synergistic photochemotherapy; no *in vivo* experiment	229

supramolecules using cadmium-N coordination bonds. However, their work was primarily focused on the synthesis aspect, with no subsequent exploration of biomedical applications. Current research focuses on enhancing the efficacy of SCCs in killing cancer cells or bacteria and improving their stability to mitigate the potential toxicity and side effects. To provide a clearer understanding, the general characteristics of SCCs achieved by altering the metal coordination centers are summarized in Table 4.

3.2.1. Enhance the cancer/bacterial killing ability of individual SCCs by using a dual metal coordination center. As previously discussed, using monometallic ions in therapeutic applications can lead to drug resistance, and certain monometallic ions may be quickly inactivated or eliminated *in vivo*, limiting their therapeutic efficacy. To address these challenges, integrating heteronuclear bimetallic ions in the SCC assembly offers a promising alternative. This approach utilizes the synergistic effects of two different metal ions, potentially exhibiting higher biological activity and diverse antitumor/antibacterial mechanisms compared to monometallic complexes. Therefore, it is more challenging for target cells/bacteria to adapt to multiple distinct therapeutic mechanisms and reduce the risk of resistance development. However, employing heteronuclear bimetallic ions in SCCs poses certain challenges. Typically, the SCC assembly is driven by coordination bonds formed between the donor and acceptor molecules, mediated by the same metal ion. This homogeneous force is crucial for maintaining the geometric structure of SCCs, which is fundamental to their stability and functionality. Introducing the concept of assembling a metallacycle or metallacage using two or more acceptors, each with different species of metal ions, while retaining the same donor, is complex (Fig. 13a). To address this issue, researchers have adopted an innovative approach. They start by introducing a specific type of coordination metal ion into the organic donor. This initial metal-based coordination complex often possesses inherent therapeutic properties, such as PDT capabilities. This complex is then self-assembled with a receptor that has been modified with a different kind of metal ion, forming a metallacycle or metallacage that is effectively equipped with bimetallic ions (Fig. 13b). This method enhances the tumor- or bacteria-killing ability beyond that of individual SCCs.

Utilizing this concept, Su *et al.*[220] successfully assembled eight Ir(III)-based photosensitizers with four Pd(II)-based

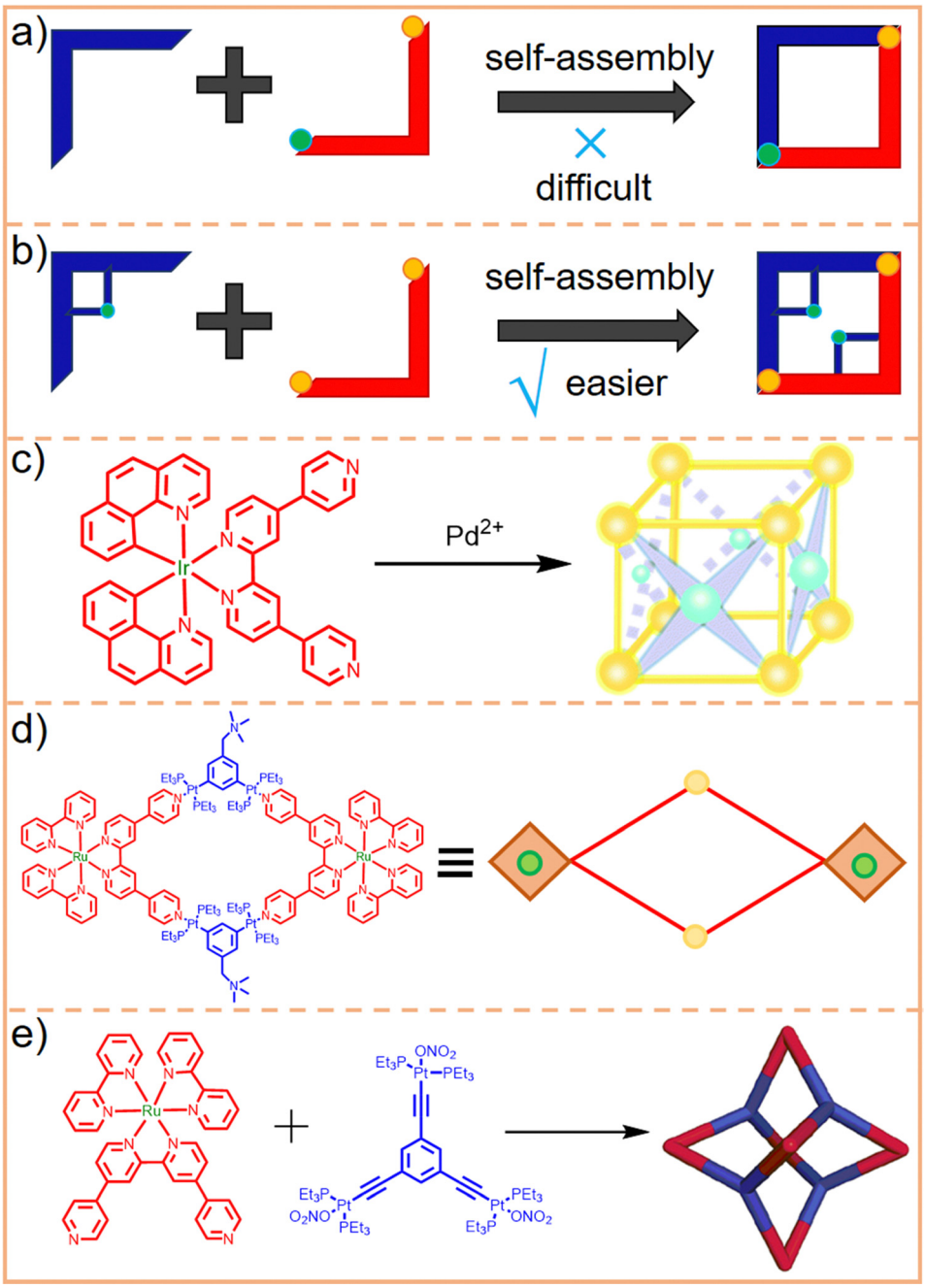

Fig. 13 Scheme of bimetallic SCCs assembled (a) by the donor and the acceptor with two species of metal ions and (b) by the donor with one metal ion and the acceptor with another metal ion. (c) Chemical structures of the Ir(III)–Pd(II) metallacage and the Ru(II)–Pt(II) metallacycle (d) and the metallacage (e).

receptors into a Pd_4Ir_8 metallacage (Fig. 13c). This structure demonstrated a maximum two-photon absorption (TPA) cross-section of 783 GM, while that of the Ir(III) ligand under the same experimental conditions peaked at 31 GM. This enhanced two-photon activation ability of the Pd_4Ir_8 metallacage facilitates two-photon PDT in tumor treatments and effectively increases the treatable depth of photosensitizers. Moreover, owing to an enlarged conjugation plane and efficient energy transfer facilitated by its highly ordered cubic cage structure, the singlet oxygen ($^1O_2$) quantum yield of the metallacage was higher than that of the Ir(III) ligand (0.84 *vs.* 0.67). Consequently, the bimetallic Pd_4Ir_8 metallacage demonstrated superior cell-killing ability and a higher PDI (the ratio of photocytotoxicities to dark cytotoxicities) compared to the monometallic Ir(III) ligand. Stang *et al.* designed heterometallic Ru(II)–Pt(II) metallacycles[221] and metallacages[222] (Fig. 13d and e, respectively). The metallacage exhibited the highest TPA and enhanced $^1O_2$ quantum yield compared to both the metallacycle and the Ru(II) ligand. This superior performance resulted in better therapeutic efficiency and a higher phototoxicity index

against tumor cells. These experimental results strongly suggest that incorporating bimetallic ions is a viable strategy for augmenting the therapeutic capabilities of SCCs.

3.2.2. Enhance the stability of individual SCCs' topological structure to avoid the leakage of heavy metal ions. In the context of Lewis acid–base theory, coordination reactions can typically be understood as acid–base interactions. In these reactions, the metal ion functions as a Lewis acid, offering an empty orbital, while the ligand acts as a Lewis base, providing an electron pair. Therefore, SCCs assembled through metal coordination bonds remain stable primarily in a neutral pH environment. Excessive acidity or alkalinity can disrupt these coordination bonds, leading to the disassembly of metallacycles or metallacages. The acidic nature of tumor tissues and intracellular lysosomes *in vivo*[223–226] presents a unique opportunity for the design of stimuli-responsive SCCs. In this approach, ligands and acceptors with different functionalities are self-assembled to form stable molecular structures. Once these SCCs reach the tumor site or lysosome, they respond to the pH change by disassembling, releasing each functional molecule at the target area. This release allows the individual components to function independently, enabling a synergistic therapeutic effect without altering the molecular structure or pharmacological activity. However, the complex physiological environment *in vivo* (a buffered solution system containing proteins, non-protein nitrogenous compounds, glucose, inorganic salts, oxygen, carbon dioxide, *etc.*) presents a significant challenge to the stability of SCCs. This complexity can lead to premature SCC disassembly due to protonation before reaching the target cells. Such early disassembly can result in the unintended release of metal ions, potentially causing uncontrollable side effects. Furthermore, even when SCCs successfully reach tumor tissues, their stability can be compromised by the slightly acidic environment that often surrounds tumors. This instability can prevent SCCs from effectively penetrating deep into the core of the tumor, where they are most needed. As a result, this limited penetration can significantly diminish the effectiveness of the treatment. In this context, maintaining the stability of the topological structures of SCCs across different environments could, to some extent, minimize their potential toxicity and side effects.

Moreover, imaging agents used for cellular imaging require structural stability in complex biological systems. This stability is crucial for maintaining the consistency and sustainability of signal intensity, making stable SCCs particularly advantageous for imaging-guided therapies. Chen *et al.*[227] designed a square metallacycle based on Pd–N coordination, named Pd_8L_4 (where L refers to *N*,*N*-3,5-dimethylpyrazole substituted perylene tetracarboxylic acid diimides) (Fig. 14a). This metallacycle demonstrated exceptional stability, with less than an 8% change in the intensity of absorption spectra under normal physiological conditions (pH = 7.4), in the slightly acidic microenvironment of tumor tissues (pH = 6.8, Fig. 14b) and in the more acidic environment of lysosomes (pH = 5.3, Fig. 14c). This robust stability makes Pd8L4 an ideal candidate for imaging-guided PDT of tumors. Sun *et al.*[228] designed imidazole ligands and

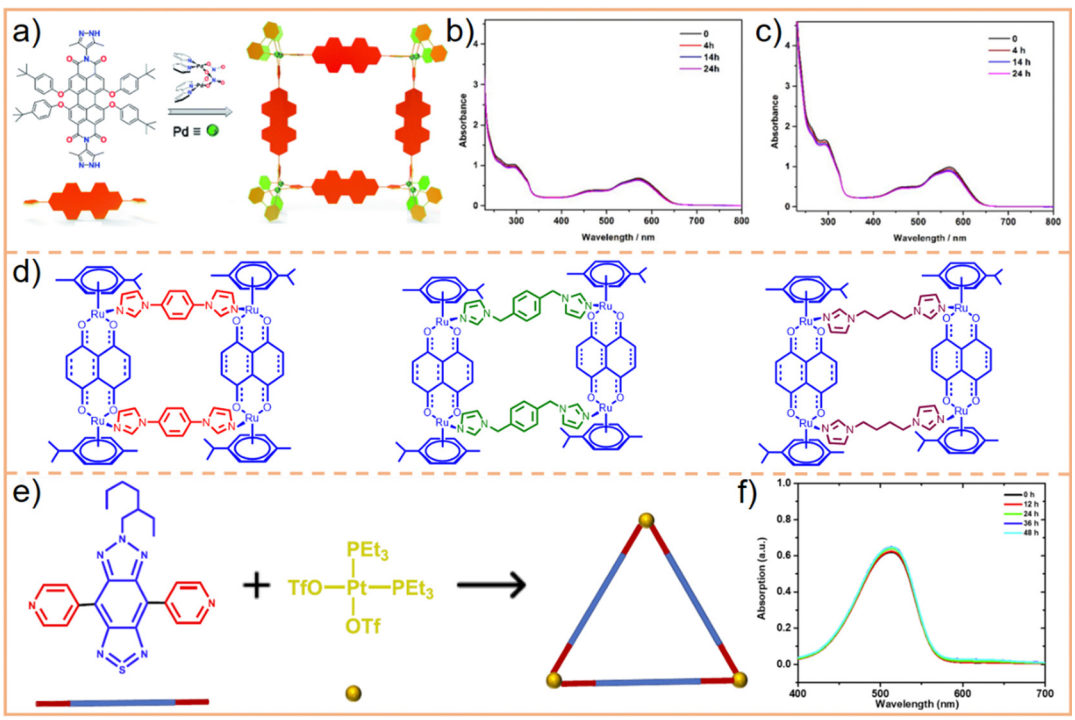

Fig. 14 (a) Construction of the Pd_8L_4 metallacycle and changes in the absorbance spectra of the metallacycle *versus* time in PBS buffer at (b) pH = 6.8 and (c) pH = 5.3. Figure adapted from ref. 227 with permission from the Royal Society of Chemistry, Copyright 2020. (d) The design and chemical structures of various Ru metallacycles. (e) Schematic representation of synthesis of the metallacycle and (f) absorption profiles of the metallacycle at pH = 5.5 at different times. Figure adapted from ref. 229 with permission from American Chemical Society, Copyright 2021.

coordinated them with Ru(II) to synthesize various tetragonal metallacycles (Fig. 14d). These metallacycles exhibited exceptional stability, with no significant changes observed in their absorbance spectra across a pH range from 4.5 to 8.0. Song *et al.*[229] developed a triangular metallacycle (Fig. 14e), demonstrating remarkable stability over two days in a slightly acidic environment at pH 5.5 (Fig. 14f). These studies provide valuable insights into the development of acid- and alkali-resistant SCCs, setting a precedent for future research aimed at creating SCCs with even greater stability and safety.

3.3. Reduce the potential toxicity and side effects of SCCs by monitoring their subcellular distribution for precision medicine

The subcellular distribution of drugs within eukaryotic cells plays a crucial role in determining their efficacy and toxicity. Studying this distribution is vital for drug targeting strategies and for minimizing toxic side effects, aligning with the fundamental principles of precision medicine.[230] Eukaryotic cells comprise various organelles, each with distinct biological characteristics and functions. These include the nucleus, mitochondria, lysosomes, endoplasmic reticulum, and Golgi apparatus, among others. Investigating how drugs are distributed across these different organelles can offer valuable insights into the specific sites and mechanisms of action of these drugs. For instance, mitochondria can release cytochrome *c* into the cytoplasm, which activates caspase 3, a key enzyme in the execution phase of apoptosis.[231–233] Drugs that target mitochondria and influence this pathway can effectively induce apoptosis in diseased cells, such as cancer cells. The Golgi plays a role in protein processing and trafficking, and its dysfunction can trigger cell death. Particularly, oxidative stress within the Golgi apparatus can initiate an apoptotic pathway.[234] Finally, DNA damage within the nucleus can directly lead to cell death. Currently, leveraging insights from studies on the chemical structure–localization relationship and organelle feature–localization relationship of small molecules,[235,236] the research into the subcellular distribution of SCCs is advancing. Inside the cell, SCCs typically accumulate in lysosomes and mitochondria,[237–242] except for certain metallacycles/metallacages that enter the nucleus.[243] For a more comprehensive understanding, the general features of SCCs with different subcellular locations are summarized in Table 5.

3.3.1. SCCs accumulate in lysosomes. Lysosomes are central in catabolic and anabolic processes within cells, as well as in mediating interactions with other organelles and the plasma membrane, acting as a platform for inter- and intracellular communication. Several substances phagocytosed by cells initially form endosomes, which subsequently fuse with lysosomes for digestion.[244–248] Consequently, larger SCCs are typically accumulated in lysosomes during the process of internalization. Furthermore, the acidic pH of the lysosomal cavity, typically maintained between 3.5 and 5.5, could provide an optimal environment for SCC disassembly and subsequent drug release. Furthermore, most soluble acid hydrolases in the lysosome and the inner surface of the lysosomal membrane carry negative charge.[249,250] Consequently, they can readily interact with positively charged SCCs, further promoting their

Table 5 Features of SCCs with different subcellular locations

Subcellular locations	Internalization pathways	Outcomes of distribution study	Outcomes of accumulation	Ref.
Lysosomes	—	Lysosome correlation coefficients were in the range of 0.73–0.89 for different cells	Lysosome-targeted cell imaging	239
Lysosomes	Energy-dependent clathrin-mediated and caveolae-mediated pathways	Lysosome correlation coefficient = 0.75; 78.5% of SCCs in lysosomes, 17.6% in mitochondria	Lysosomal damage; mitochondrial dysfunction; cell apoptosis	240
Lysosomes	Energy-dependent caveolae-mediated endocytic pathway	Lysosome correlation coefficient = 0.7; Ru content was 1.73-fold higher in lysosomes than that in mitochondria	Lysosomal and mitochondrial damage and dysfunction; cell cycle arrest at the G2/M phase; cell apoptosis	241
Mitochondria	—	62.5 ± 4.3% of Ru in the mitochondria	Mitochondrial membrane depolarization and superoxide generation; mitochondrial dysfunction; cell apoptosis	289
Mitochondria/ lysosomes	Energy-dependent endocytosis	55% **27** was in cytosolic fraction, and less in the mitochondria (37%); 58% **28** was in mitochondria, followed by the cytosolic (29%) fraction	Disruption of lysosomal integrity, mitochondrial membrane depolarization, perturbation of autophagy, necrotic cell death and cell apoptosis	238
Mitochondrial DNA	—	Mitochondrial correlation coefficient = 0.88 (**30**); higher mitochondrial DNA binding capacity with binding to the minor groove of DNA	The most efficient PDT efficacy with PDI > 33.3 and 97.5% total apoptotic ratio; cell apoptosis	237
Cell nucleus	—	Metallacycle target genes were located in chromosomal regions enriched with G4 structures and exhibited bright fluorescence in cell nucleus	Metallacycles interfere with the G4 epitope recognition by the quadruplex specific antibody BG4, replacing the latter to bind to G4 and kill tumor cells	243
Cell nucleus	Clathrin-mediated endocytosis pathway	Cytotoxic protein and genome-editing proteins were delivered into cell nucleus	Tumor cell death and specific protein expression	312
Cell nucleus	Caveolae/lipid raft-mediated endocytosis pathway	Higher protein delivery efficiency than commercial reagents; a majority of protein was released into cytosol and accumulated within nucleus after 18 h of delivery	Molecular chaperone was delivered into cell nucleus for neurodegenerative disease treatment	313

accumulation within the lysosome. When the SCCs' concentration inside the lysosome reaches a toxic threshold, the lysosomal membrane becomes unstable, permeability is enhanced, and membrane integrity is lost, a condition known as lysosomal membrane permeabilization (LMP). This results in the release of tissue proteases and hydrolases from the lysosomal cavity into the cytoplasm, causing cellular damage.[251–255] If LMP is not promptly repaired and lysosomal damage continues to escalate, the lysosome ruptures, releasing its entire contents into the cytoplasm. This event triggers a cascade of hydrolytic activity throughout the cytoplasm and extensive acidification, culminating in fatal cellular damage. The extent of lysosomal damage is pivotal for determining the cell death mode. Typically, moderate lysosomal damage, as characterized by LMP, triggers cell apoptosis,[256–259] while severe damage, such as lysosomal rupture, results in necrosis.[260–263] The accumulation of SCCs in lysosomes is often accompanied by their disassembly, where small-molecule constituents escape into the cytoplasm through the LMP process. These small molecules subsequently accumulate in other organelles, contributing to cell death through various pathways. Typically, SCC accumulation in lysosomes does not directly result in cell necrosis, but triggers lysosome-mediated cellular autophagy. This autophagy, in conjunction with the stimulation of other cell death pathways, collectively eliminates diseased cells.

Given the significance of lysosomes in mediating cell death, investigating the localization of SCCs within lysosomes is crucial and necessary. Sun *et al.*[240] assembled an Ru-based metallacycle (chemical **24**, Fig. 15a) for colocalization experiments. After 6 h of incubation, predominant metallacycle accumulation in lysosomes was observed (correlation coefficient = 0.75), while smaller amounts of these complexes were found in the mitochondria. Further analysis using laser ablation inductively coupled plasma mass spectrometry (LA-ICP-MS) revealed that 78.5% of metallacycles appeared in lysosomes, 17.6% in mitochondria, and almost none in the nucleus (Fig. 15b). On this basis, the internalization of metallacycles

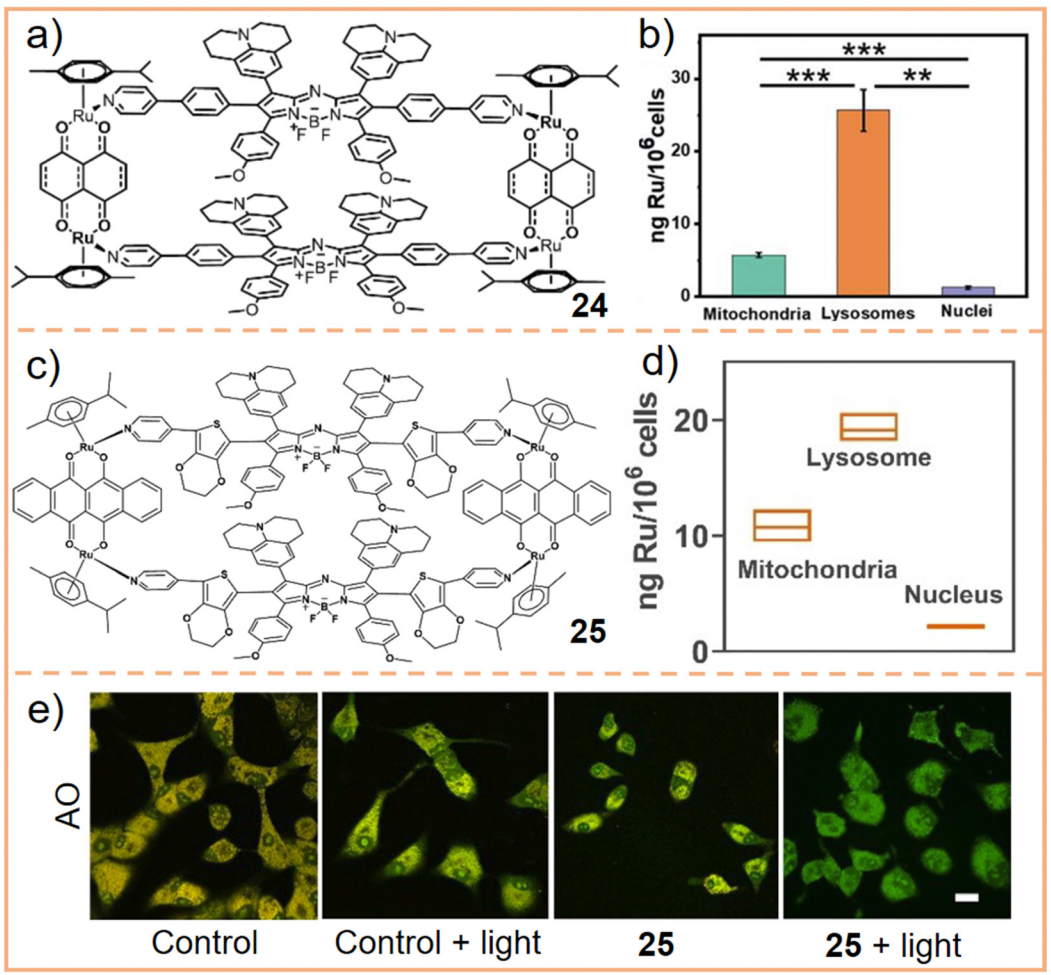

Fig. 15 (a) Chemical structure of an Ru(II)-based metallacycle **24**. (b) Subcellular distribution and quantification of Ru in A549 cells as inferred from ICP-MS studies. Figure adapted from ref. 240 with permission from the Royal Society of Chemistry, Copyright 2022. (c) Chemical structure of an Ru(II)-based metallacycle **25** and (d) Ru distribution in different organs with the incubation of the metallacycle for 6 h. (e) AO after incubation with the metallacycle or medium (control), followed by irradiation with or without laser illumination. Scale bar: 25 μm. Figure adapted from ref. 241 with permission from Wiley-VCH, Copyright 2023.

was confirmed to occur through the energy-dependent clathrin-mediated and caveolae-mediated pathways. Building on these findings, Sun *et al.* developed a π-expansive Ru receptor and a ligand with higher ROS yield. This was achieved using extended non-planar π-conjugation 3,4-ethylenedioxythiophene, which replaced the phenyl group to facilitate the intersystem crossing process.[241] The newly assembled metallacycle (chemical **25**, Fig. 15c) demonstrated a high localization coefficient (= 0.7) and high Ru content in lysosomes (Fig. 15d), indicating that it was primarily distributed within lysosomes. Moreover, an acridine orange (AO, a lysosomotropic dye that emits red fluorescence when localized within the acidic environment of lysosomes but shows green fluorescence in the cytosol) staining experiment was performed. This experiment revealed that, upon laser irradiation, the accumulation of **25** in lysosomes generated ROS, leading to the loss of lysosomal membrane integrity and lysosome dysfunction (Fig. 15e), eventually causing cell apoptosis. Fan *et al.*[239] utilized an assembled metallacycle encapsulating five kinds of dyes and conducted colocalization experiments in three cell types (with correlation coefficients ranging from 0.73 to 0.89), confirming that the metallacycle predominantly accumulates in lysosomes. These results corroborate that SCCs first accumulate in lysosomes and contribute to cell death through lysosomal damage.

The consistent observation of SCCs localizing primarily in lysosomes across different studies underscores the potential of targeting lysosomes in the development of SCC-based therapies. By exploiting the lysosome's role in cell metabolism and death, researchers can design SCCs that selectively activate cell death mechanisms in diseased cells, such as cancer cells, offering a promising strategy for targeted therapeutic interventions.

3.3.2. SCCs accumulate in mitochondria. Inside cells, mitochondria are crucial for energy production and induction of apoptosis.[264–267] There are significant structural and functional differences between the mitochondria of tumor cells and those of normal cells. Tumor cell mitochondria are more susceptible to damage due to more extensive mutations, such as a more fragile redox balance and unstable genome.[268–273] Moreover, compared to normal cells, tumor cells typically exhibit a higher mitochondrial membrane potential,[274–277] promoting the accumulation of positively charged SCCs in the mitochondria and selectively targeting tumor cells. Moreover, compared with other organelles, mitochondria have a higher oxygen concentration, leading to preferential SCC accumulation in the mitochondria during PDT. Conversely, only mitochondria and the nucleus contain DNA in human cells. The nucleus boasts multiple DNA damage repair mechanisms, including photorepair, excision repair, recombination repair, mismatch repair, and alkyl transfer repair.[278–283] Tumor cells often counteract drug-induced DNA damage by enhancing these specific DNA repair enzymes.[284] However, the mitochondrial DNA damage repair capacity is relatively limited compared to the nucleus. Targeting mitochondrial DNA damage can therefore bypass the drug resistance associated with DNA repair mechanisms in the nucleus. Additionally, research has indicated a functional connection between lysosomes and mitochondria, including direct contact.[285–288] Therefore, understanding the distribution of SCCs in lysosomes and their subsequent impact on mitochondrial function is crucial. This knowledge aids in comprehending therapy mechanisms from multiple perspectives, which is essential for the targeted treatment design.

Gou *et al.*[289] developed arene–Ru(II) supramolecular complexes (chemical **26**, Fig. 16a), capable of self-assembling into supramolecular vesicles through non-covalent interactions in water. Subcellular localization studies revealed that upon entering a cell, Ru predominantly accumulated in the mitochondria, accounting for 62.5 ± 4.3%. Conversely, only 3.5% appeared in the nucleus, with the rest 31.7% dispersed in other cellular fractions (Fig. 16b). Staining experiments using JC-1 and MitoSOX Red, which assess mitochondrial membrane potential and superoxide generation capacities respectively, demonstrated that chemical **26** causes mitochondrial membrane polarization and superoxide production when exposed to laser irradiation. This led to mitochondrial dysfunction, which was further linked to inducing apoptosis in tumor cells. These findings underscore that mitochondria are the primary targets of the arene–Ru(II) complex.

Building on the established connection between mitochondria and lysosomes, Che *et al.*[238] explored the physiological process of SCCs from lysosomal localization to mitochondrial release and their role in cell death. They created a planar Pt(II) terpyridyl scaffold linked to a glucose moiety (**27**), which undergoes cleavage by β-glucosidase, forming compound **28**. Their results demonstrated that **27** predominantly accumulated in lysosomes, leading to necrotic cell death, whereas **28** was more prevalent in mitochondria, causing late apoptosis. Necrosis resulted from lysosomal integrity disruption and autophagy perturbation. TEM analysis of cells treated with **27** revealed a significant increase in double-membrane cytosolic vesicles, indicative of autophagosomes. Based on these distribution patterns, they suggested an anticancer mechanism: Pt(II)-containing supramolecular structures accumulate in lysosomes and mitochondria, resulting in lysosomal integrity disruption, mitochondrial membrane depolarization, autophagy perturbation, and ultimately, cancer cell death (Fig. 16c).

Furthermore, given the distinct characteristics of mitochondrial DNA, several researchers have concentrated on strategies for localizing SCCs within mitochondrial DNA. Metallohelical supramolecular systems are particularly favored in this context due to their protein-like α-helical structure. This structural mimicry inherently enhances their DNA-targeting properties. However, Duan *et al.*[237] discovered that mesocate helical supramolecular systems exhibit a higher DNA-binding ability compared to traditional α-helices. They synthesized two mesocate supramolecules, labeled **29** and **30** (Fig. 17a), demonstrating impressive mitochondrial localization (with correlation coefficients of 0.91 and 0.88, respectively, Fig. 17b). Additionally, their DNA-binding capabilities were investigated through an ethidium bromide (EB) displacement assay using natural calf-thymus DNA (ct-DNA). Fig. 17c and d illustrate that the

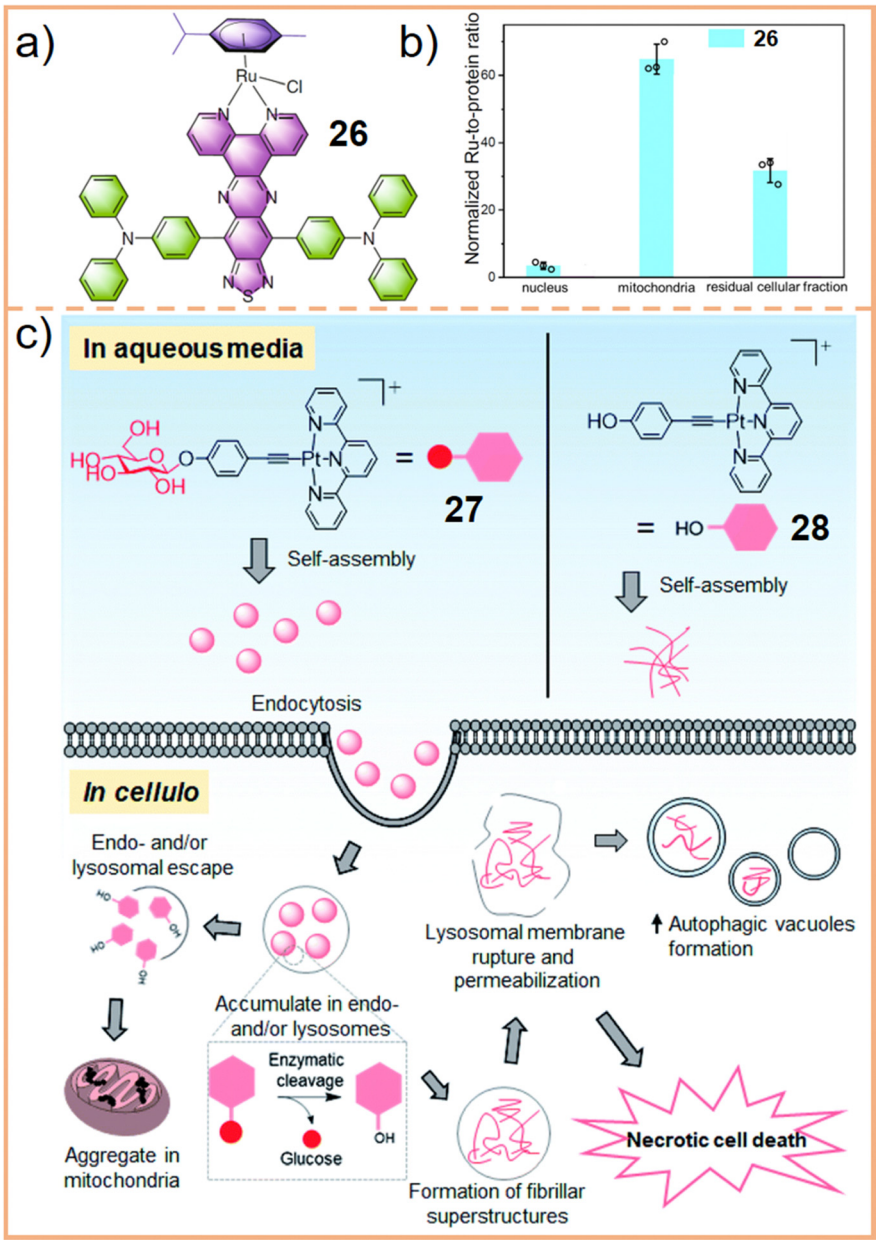

Fig. 16 (a) Chemical structure of the arene–Ru(II) complex (chemical **26**). (b) Ru uptake in the different cellular compartments of MDA-MB-231 cells treated with **26**. Figure adapted from ref. 289 with permission from Springer Nature, Copyright 2022; (c) schematic drawing of the proposed anti-cancer mechanisms of action of **27** and **28**. Figure adapted from ref. 238 with permission from the Royal Society of Chemistry, Copyright 2021.

fluorescence of EB-bound ct-DNA was effectively quenched following the addition of the mesocate complexes. The binding constants (K_{app}) were calculated at 0.67×10^7 M^{-1} for **29** and 1.12×10^7 M^{-1} for **30**. These results indicated that their inherent DNA-targeting ability, formed through noncovalent interactions, can be enhanced by extending the length of the diamine linkers (from **29** to **30**). Compared to metal ions in α-helical structures, exhibiting K_{app} values between 0.39×10^7 M^{-1} and 0.66×10^7 M^{-1}, mesocate supramolecular complexes demonstrate a considerably higher binding capacity. Molecular docking studies revealed distinct binding preferences: **29** predominantly binds in the major groove of DNA (Fig. 17e), with an average binding energy of -6.35 kcal mol^{-1}. Conversely, **30** favors the minor groove of DNA (Fig. 17f), indicated by a lower binding energy of -7.82 kcal mol^{-1} in the minor groove compared to -6.18 kcal mol^{-1} in the major groove. These findings suggest that the mesocate structure is critical for enhancing the interactions of supramolecular complexes with DNA. Consequently, **29** and **30** induced a higher rate of apoptosis in tumor cells, with rates of 88.9% and 97.5%, respectively. Overall, these studies significantly contribute to our understanding of the distribution of SCCs in cells, advancing research into the mechanisms of cell death caused by SCCs and aiding the development of precision medicine.

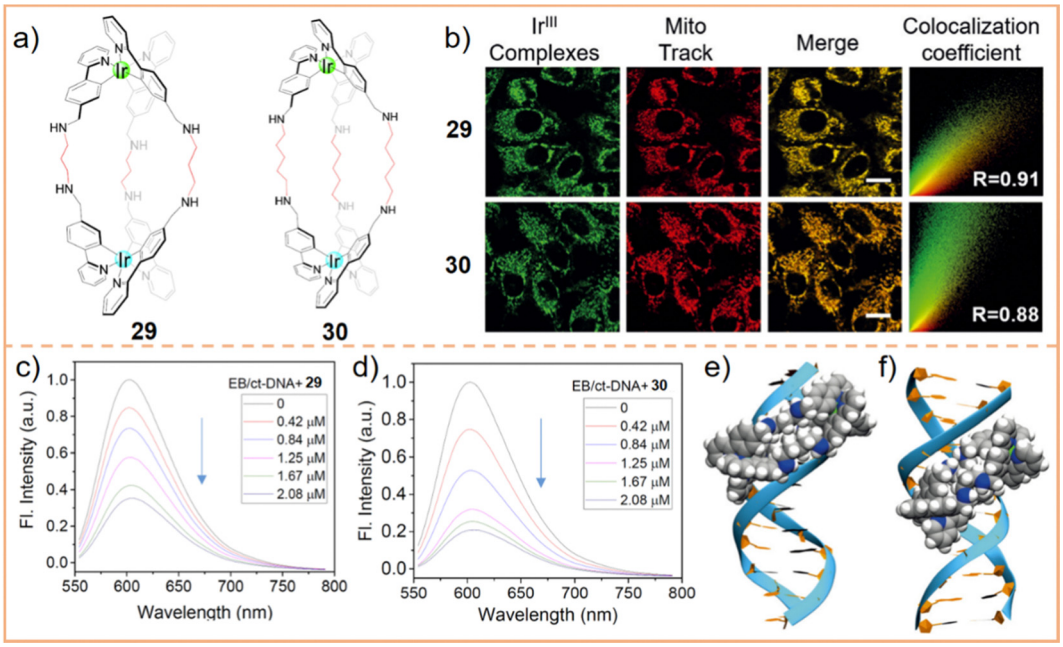

Fig. 17 (a) Chemical structures of **29** and **30**. (b) Determination of intercellular localization of **29** and **30**, and fluorescence quenching of the EB bound ct-DNA upon addition of **29** (c) and **30** (d). Scale bar: 20 μm. Molecular modeling for the interaction of **29** (e) and **30** (f) with DNA. Figure adapted from ref. 237 with permission from Wiley-VCH, Copyright 2020.

3.3.3. SCCs accumulate in the cell nucleus. Heavy metal ions in SCCs, serving as chemotherapeutic agents, are preferably bound to DNA to maximize therapeutic efficacy while minimizing toxic side effects. Therefore, understanding the DNA binding mechanism of SCCs is crucial. Historically, the development of SCCs, particularly Pt(II)-based ones, has often been benchmarked against the chemotherapeutic drug cisplatin. The prevailing belief is that organoplatinum compounds in SCCs can emulate cisplatin's role in eliminating diseased cells or bacteria *via* DNA damage. However, numerous experimental studies have demonstrated that several Pt(II)-based SCCs exhibit superior therapeutic effects compared to cisplatin. This can be partly attributed to their goal-oriented design. This involves early-stage adjustments to the molecular structure of SCCs to overcome cisplatin's limitations. Additionally, the difference in DNA damage mechanisms between SCCs and cisplatin plays a role. Cisplatin typically causes DNA damage through covalent binding with guanine on DNA after hydrolysis,[290–294] leading to cancer cell death. However, as previously mentioned, the existence of mechanisms like nucleotide excision repair,[295–297] base mismatch repair,[298–300] DNA double-strand break damage repair,[301–303] and trans-damage repair[304,305] contributes to a degree of nuclear DNA resistance to cisplatin. Contrastingly, Pt(II)-based SCCs often target noncanonical nucleic acid structures, such as the G-quadruplex (G4) structure in DNA.[306–311]

SCC accumulation in the cell nucleus has been intensively studied by Tereni *et al.*[243] They developed a hexagonal Pt(II) metallacycle (chemical **31**, Fig. 18a) and co-incubated it with cisplatin to test cell viability. The results indicated a slight antagonistic effect, implying that both might target nucleic acids but with different action modes. Gene set enrichment analysis revealed that **31** preferentially targets genes in chromosomal regions rich in G4 structures. Consequently, the metallacycle accumulates in the nucleus, exhibiting bright fluorescence upon entering the cell. However, when cells were also treated with pyridostatin, a known G4 stabilizer, the fluorescence intensity of **31** diminished. This suggests that the accumulation of **31** is linked to the presence of G4 structures. However, when cells were incubated with both **31** and cisplatin, the fluorescence intensity remained unaltered, indicating distinct DNA binding mechanisms for the two compounds. Further investigation through photobleaching experiments and immunofluorescence studies showed that **31** interferes with G4 epitope recognition by the quadruplex-specific antibody BG4. After entering the cell nucleus, **31** replaces BG4 to bind to G4, thereby killing tumor cells. While in-depth studies on the localization of SCCs in cell nuclei are less common compared to analyses of their presence in lysosomes and mitochondria, some innovative designs have been developed. For example, Wang *et al.* created discrete organometallic cages assembled into supramolecular nanoparticles, which were then fused with proteins carrying nuclear localization signals. These signals direct the intracellularly released protein to the nucleus. Through the clathrin-mediated endocytosis[312] or caveolae/lipid raft-mediated endocytosis pathway,[313] various proteins (*e.g.*, GFP, green fluorescence protein) and protein-based drugs are delivered into the nucleus (Fig. 18b). Such efforts significantly contribute to the advancement of precision medicine by elucidating the subcellular distribution of SCCs, whether through exploring their DNA

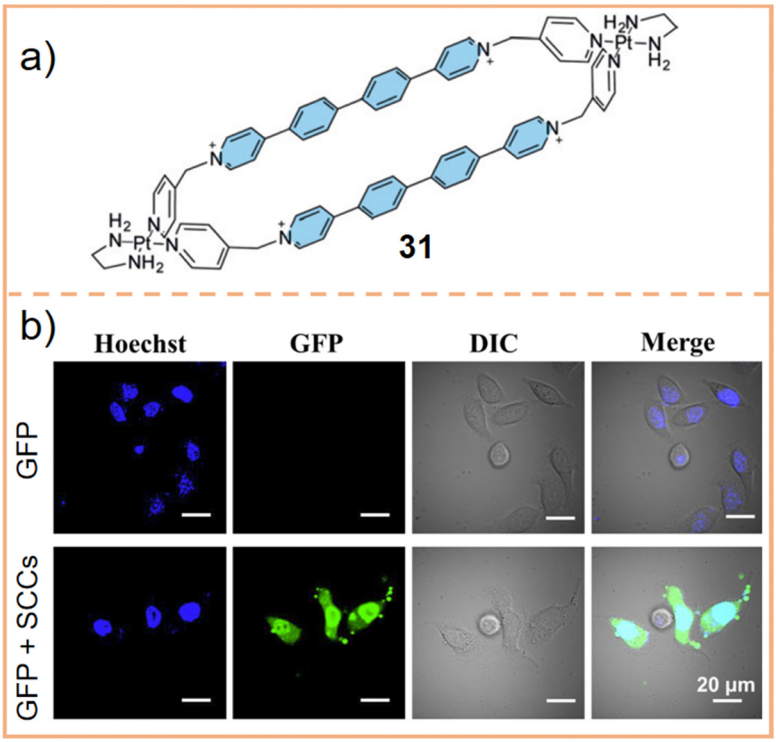

Fig. 18 (a) Chemical structure of a hexagonal Pt(II) metallacycle **31**. (b) Images of HeLa cells transfected with GFP alone and in GFP-SCC nanoparticles. Nuclei were stained with Hoechst 33342 (blue). Scale bar: 20 μm. Figure adapted from ref. 312 with permission from Wiley-VCH, Copyright 2021.

binding mechanisms or by achieving targeted release of cargoes within SCCs.

4. Conclusion and perspectives

In the biomedical realm, numerous treatment modalities, including theranostics,[314–316] imaging-guided therapy,[317–319] synergistic therapy,[320–322] and precision medicine, necessitate the involvement of various functional molecules. These molecules operate independently but synergistically contribute to achieving the ultimate therapeutic goal. During these treatments, it is essential to precisely control the dosage and location of different molecules to ensure targeted efficacy, a task challenging to accomplish through simple mixing of different components. In this context, the capability of SCCs to dynamically connect two or more molecules at a fixed ratio and angle offers them distinct advantages in these applications. To address the prevalent yet critical challenges associated with the use of SCCs, such as water solubility, biostability, and potential toxicity, significant progress has been made in recent years. This includes state-of-the-art research involving the use of DSPE–PEG-like liposomes and block copolymers like F127 as nanocarriers. These enhance the aqueous solubility and *in vivo* circulation stability of SCCs. Notably, the lengths and molecular weights of hydrophilic and hydrophobic segments in F127 block copolymers can be easily adjusted. Moreover, direct modification of hydrophilic small molecules, polypeptides, or PEG macromolecules on metallacycles/metallacages enables SCCs to self-assemble into carrier-free nanoparticles or vesicles. This approach improves water solubility and offers higher drug loading capacity. Additionally, targeted molecular modification allows SCCs to distinguish between diseased and normal cells. Altering the metal coordination centers can enhance the cancer/bacterial killing efficiency or prevent leakage of heavy metal ions from SCCs. Furthermore, colocalization experiments are being conducted to study the intracellular distribution of SCCs, aiming to elucidate their mechanism of action. These strategies are pivotal in reducing SCCs' side effects and focusing on precision medicine. Despite considerable progress, SCCs still face numerous challenges before clinical application, and many common issues across different systems must be addressed and resolved.

(1) SCCs are commonly administered intravenously, a method where the drugs must navigate several challenges before effectively targeting cells: circulation, accumulation, penetration, internalization, and drug release. Forming nanoparticles or vesicles with hydrophilic surfaces aids in maintaining the stability of SCCs in blood circulation, prolonging their presence. However, this hydrophilicity hinders their ability to cross the lipophilic outer cell membrane, posing challenges in cellular uptake and internalization. Conversely, injecting hydrophobic metallacycles/metallacages without hydrophilic chain modifications enhances cellular entry but compromises circulation stability under physiological conditions, risking premature disassembly before reaching the target. Hence, a delicate balance between circulation stability and cellular uptake efficiency of SCCs is essential, but studies in this area

are scarce. One potential approach is investigating the lipophilic/hydrophilic properties of various SCCs (before and after nanoparticle or vesicle formation). By comparing circulation stability and cellular uptake, a reasonable balance might be found. Although this endeavor demands extensive time and involves rigorous basic and comparative research, which can be tedious, the potential for yielding valuable, straightforward results makes it a promising avenue to explore.

(2) PEG has long been a cornerstone in DDSs, used extensively for encapsulating liposomes or block copolymers and modifying hydrophilic chains. As a versatile and enduring material in DDSs, PEG enhances drug stability, prevents adhesion by proteins in the bloodstream, and is highly biocompatible. However, research has shown that PEG can provoke the production of anti-PEG antibodies (being recognized by B cells as a foreign substance, leading to the generation of anti-PEG IgM and IgG),[323–325] which results in rapid clearance of PEG-containing drugs and compromises their therapeutic efficacy. Consequently, there is a pressing need to develop new materials. Replacing PEG with biological small molecules, peptides, or even proteins to provide a degree of hydrophilicity to SCCs could be a viable approach to mitigate the production of anti-PEG antibodies. The current challenge with these alternatives, compared to PEG, lies in their relatively weak hydrophilicity and flexibility. Adjusting their molecular weight, chain length, and hydrophilic force is challenging but represents a crucial area for future research and development. Addressing these issues could lead to more effective and less immunogenic drug delivery systems.

(3) Utilizing heavy metal ions in the self-assembly of SCCs presents both advantages and challenges. While the toxicity of these ions can be harnessed to kill targeted cells or bacteria, they can also harm normal cells, leading to severe side effects. Although constructing SCCs *via* light metal coordination-driven self-assembly is a known strategy, related research remains scarce. Current efforts are more focused on enhancing the targeting capability and individual treatment efficacy of SCCs, such as increasing the ROS yield for PDT, boosting photothermal conversion efficiency for PTT, and designing SCCs with dual-drug combinations or heteronuclear bimetallic ions. The goal is to achieve better therapeutic outcomes with lower doses of SCCs, reducing their toxic side effects. However, these design strategies often involve more complex donor/receptor structures or additional functional molecules, potentially increasing side effects while improving efficacy. Therefore, finding a balance between enhancing treatment effectiveness and minimizing side effects in SCC design is critical. This requires a multifaceted approach combining theoretical, experimental, simulation, and computational research to identify and assess key factors. These include the geometric structure, composition, and defects of SCCs, their pharmacokinetics, internalization mechanisms, and active sites of action. Such comprehensive evaluation can determine the overall performance of SCCs and indicate potential side effects, guiding the development of safer and more effective therapeutic solutions.

(4) Compared to healthy cells, tumor cells exhibit abnormalities in histology (angiogenesis,[326–328] lymphangiogenesis,[329–331] axonogenesis and neurogenesis[332–335]), cell types (fibroblast activation,[336–338] pericytes,[339–341] and adipocyte change[342–344]), biophysical status (hypoxia[345–347] and low pH[348–350]), and biochemical indices (up-regulation of the concentration of small molecules, such as glucose,[351–353] glutathione,[354–356] adenosine-5′-triphosphate,[357–359] guanosine-5′-triphosphate,[360–362] and large molecules, such as aminopeptidase N,[363–365] alkaline phosphatase,[366–368] cathepsin,[369–371] and matrix metallopeptidases[372–374]). Targeting these abnormalities can enhance treatment efficacy and reduce toxic side effects. However, the design of stimuli-responsive small molecule drugs has outpaced the development of SCCs. The requirement for angular and structural symmetry in the assembly of SCCs, typically from symmetrical ligands or acceptors, limits the variety of small molecular counterparts that can be used. Consequently, most SCCs currently target tumor cells through modifications with molecules like FA, biotin, and RGD or utilize the passive EPR effect. This approach falls short of meeting diverse clinical needs. A significant challenge for SCCs is broadening their stimulus responsiveness. Beyond synthesizing and structurally modifying ligands or acceptors, encapsulation post-assembly can impart additional functions. For instance, traditional amphiphilic polymer encapsulation of SCCs can be enhanced by coating them with various cell membranes, such as erythrocytes,[375–377] macrophages,[378–380] homologous tumor cells,[381–384] or hybrid membranes.[385–387] This method can improve blood circulation ability, reduce immunogenicity, and enhance internalization and invasion capabilities in tumor tissues. Such strategies can significantly expand the applications of SCCs in the biomedical field.

(5) In biomedical applications, designing treatments tailored to the specific characteristics of different tumor cells or bacteria is crucial. Numerous types of tumor cells exhibit consistent abnormalities in certain physiological parameters or biochemical indices. A common strategy involves exploiting these abnormalities, such as the high expression of FR and biotin receptors, to modify SCCs and enhance their targeting capabilities. However, the expression levels of these receptors can vary significantly among different types of cancer cells. For instance, certain lung, renal, colon, and breast cancer cell lines[388,389] overexpress the BR at higher levels than the FR. Therefore, carefully selecting targeting motifs is vital for achieving better targeting efficiency and therapeutic outcomes. Currently, most research on SCCs does not delve deeply into the issue of selectively targeting tumor cell characteristics. Instead, these studies often focus on demonstrating the therapeutic effects of SCCs on tumor cells, comparing the efficacy before and after modification with targeting motifs. To address this gap, future studies could involve a parallel comparison of different targeting motifs within the same cell line when examining the targeting efficiency of SCCs with a specific structure. Although this approach is not overly complex, it holds significant value in providing more comprehensive data for future designs.

(6) The acid cleavability of SCCs is advantageous as it ensures their disassembly at the tumor site, allowing for the independent release of ligands and receptors. This feature enables the assembly of two molecules with distinct functions into a single entity without altering their pharmacological activity and pharmacokinetics. However, to enhance the adaptability of SCCs to the complex *in vivo* physiological environment and maintain their stability during transportation, certain SCCs are designed to resist both acidic and alkaline conditions. This resistance prevents the leakage of small-molecule counterparts and metal ions, reducing potential toxicity and side effects. However, this acid–alkali resistance also means that these SCCs may lose their ability to disassemble at the tumor site or within lysosomes. This limitation adds to the research complexity, as it eliminates the possibility of independent ligand or receptor release. Consequently, researchers must consider SCCs as intact molecules and assess how changes in their molecular structure could impact their pharmacological activity and bioactivity. Balancing the stability of SCCs to prevent leakage of small-molecule counterparts or metal ions while ensuring their acid-responsive release at the tumor site is a critical aspect of their design. However, the relationship between the structure of SCCs and the leakage of metal ions, along with their potential toxic effects, has not been thoroughly and systematically explored. Studies on stability in acidic or alkaline environments have primarily been incidental, often using absorption or emission spectroscopy, without specific focus on the effects of SCC leakage or the comparative impacts of acid-cleavable *versus* non-cleavable SCCs on cellular/bacterial growth or systemic toxicity *in vivo*. This lack of targeted research means that the acid–alkali resistance of SCCs is more often a chance discovery rather than the result of intentional design. Given the known properties of some SCCs, follow-up research need not be overly complicated. Routine *in vitro* and *in vivo* experiments, such as ICP-MS, CLSM, flow cytometry, and MTT assays, can provide valuable insights. Based on these findings, researchers can undertake targeted designs starting from the molecular structure of SCCs. This approach will help clarify the optimal balance between stability and acid cleavability of SCCs in biomedical applications.

(7) Understanding the subcellular distribution of SCCs is crucial for deciphering their anticancer and antibacterial mechanisms. This knowledge facilitates the design of specific drug molecules that can minimize the side effects of SCCs, aligning with the core principles of precision medicine. Research has confirmed that SCCs predominantly localize within lysosomes, mitochondria, and nuclei. However, establishing a clear chemical structure–localization relationship and organelle feature–localization relationship akin to those for small molecule drugs remains a distant goal. To progress in this area, more data supporting the localization results of SCCs with varied structures are necessary. Additionally, exploring organelle-targeting motifs for localization in other organelles, such as the Golgi apparatus and endoplasmic reticulum, could provide more active sites and action mechanisms for SCCs. This would significantly enrich the study of their subcellular distribution. Given these challenges, while the potential of SCCs in the biomedical field is promising, there is still considerable work to be done.

Conflicts of interest

There are no conflicts to declare.

Acknowledgements

We are grateful for the financial support from the Natural Science Foundation of Zhejiang Province (grants LZ23B040001, and LY23E030003), the National Natural Science Foundation of China (grants 21971049, and 51903070), and ''Ten-thousand Talents Plan'' of Zhejiang Province (grant number 2019R52040), and the ''General scientific research project'' of Zhejiang Provincial Department of Education (grant Y202249956).

Notes and references

1 X. Z. Ai, C. J. H. Ho, J. Aw, A. B. E. Attia, J. Mu, Y. Wang, X. Y. Wang, Y. Wang, X. G. Liu, H. B. Chen, M. Y. Gao, X. Y. Chen, E. K. L. Yeow, G. Liu, M. Olivo and B. G. Xing, *Nat. Commun.*, 2016, **7**, 10432.
2 T. R. Cook, Y. R. Zheng and P. J. Stang, *Chem. Rev.*, 2013, **113**, 734–777.
3 Q. Guan, G. B. Wang, L. L. Zhou, W. Y. Li and Y. B. Dong, *Nanoscale Adv.*, 2020, **2**, 3656–3733.
4 P. Horcajada, R. Gref, T. Baati, P. K. Allan, G. Maurin, P. Couvreur, G. Ferey, R. E. Morris and C. Serre, *Chem. Rev.*, 2012, **112**, 1232–1268.
5 S. M. Li, J. Zou, L. F. Tan, Z. B. Huang, P. Liang and X. W. Meng, *Chem. Eng. J.*, 2022, **446**, 137148.
6 X. Zhang, X. Fan, G. Q. Zhu, Y. T. Wang, H. X. Ding, H. P. Lin, Y. Y. Li, Q. Li, J. Z. Gao, M. H. Pan and Q. M. Guo, *J. Phys. Chem. C*, 2020, **124**, 12589–12595.
7 A. S. Y. Law, L. C. C. Lee, K. K. W. Lo and V. W. W. Yam, *J. Am. Chem. Soc.*, 2021, **143**, 5396–5405.
8 K. D. M. Rao, M. Hossain, A. Roy, A. Ghosh, G. S. Kumar, P. Moitra, T. Kamitya, S. Acharya and S. Bhattacharya, *Nanoscale*, 2020, **12**, 11986–11996.
9 G. Tang, Y. Y. Tian, Y. H. Gao, Z. Y. Zhou, X. Chen, Y. Li, X. Y. Yu, H. C. Wang, X. Li and Y. S. Cao, *ACS Nano*, 2022, **16**, 4892–4904.
10 B. Chen, C. C. Chu, E. Ren, H. R. Lin, Y. Zhang, P. Y. Wang, H. Yao, A. L. Liu, G. Liu and X. H. Lin, *Front. Chem.*, 2022, **10**, 870769.
11 M. Dergham, S. M. Lin and J. Geng, *Angew. Chem., Int. Ed.*, 2022, **61**, e202114267.
12 S. Loescher and A. Walther, *Angew. Chem., Int. Ed.*, 2020, **59**, 5515–5520.
13 J. T. Xu, J. Wang, J. Ye, J. Jiao, Z. G. Liu, C. J. Zhao, B. Li and Y. J. Fu, *Adv. Sci.*, 2021, **8**, 21011101.
14 E. N. Salgado, R. J. Radford and F. A. Tezcan, *Acc. Chem. Res.*, 2010, **43**, 661–672.

15 C. B. He, D. M. Liu and W. B. Lin, *Chem. Rev.*, 2015, **115**, 11079–11108.
16 P. Stricklen and J. Verkade, *J. Am. Chem. Soc.*, 1983, **105**, 2494–2495.
17 P. Ballester, M. Fujita and J. Rebek, *Chem. Soc. Rev.*, 2015, **44**, 392–393.
18 M. Fujita, J. Yazaki and K. Ogura, *J. Am. Chem. Soc.*, 1990, **112**, 5645–5647.
19 R. Chakrabarty, P. S. Mukherjee and P. J. Stang, *Chem. Rev.*, 2011, **111**, 6810–6918.
20 T. R. Cook and P. J. Stang, *Chem. Rev.*, 2015, **115**, 7001–7045.
21 A. J. McConnell, C. S. Wood, P. P. Neelakandan and J. R. Nitschke, *Chem. Rev.*, 2015, **115**, 7729–7793.
22 D. Zhang, T. K. Ronson and J. R. Nitschke, *Acc. Chem. Res.*, 2018, **51**, 2423–2436.
23 S. Zarra, D. M. Wood, D. A. Roberts and J. R. Nitschke, *Chem. Soc. Rev.*, 2015, **44**, 419–432.
24 M. Fujita, M. Tominaga, A. Hori and B. Therrien, *Acc. Chem. Res.*, 2005, **38**, 369–378.
25 S. Chakraborty and G. R. Newkome, *Chem. Soc. Rev.*, 2018, **47**, 3991–4016.
26 M. D. Pluth and K. N. Raymond, *Chem. Soc. Rev.*, 2007, **36**, 161–171.
27 D. L. Caulder and K. N. Raymond, *Acc. Chem. Res.*, 1999, **32**, 975–982.
28 B. J. Holliday and C. A. Mirkin, *Angew. Chem., Int. Ed.*, 2001, **40**, 2022–2043.
29 A. M. Lifschitz, M. S. Rosen, C. M. McGuirk and C. A. Mirkin, *J. Am. Chem. Soc.*, 2015, **137**, 7252–7261.
30 X. Li, X. Zhao, W. Wang, Z. Shi, Y. Zhang, Q. Tian, Y. Yao, C. He and C. Duan, *Coord. Chem. Rev.*, 2023, **495**, 215366.
31 G. Yu, M. Jiang, F. Huang and X. Chen, *Curr. Opin. Chem. Biol.*, 2021, **61**, 19–31.
32 J. Zhou, L. Rao, G. Yu, T. R. Cook, X. Chen and F. Huang, *Chem. Soc. Rev.*, 2021, **50**, 2839–2891.
33 Y. Sun, C. Chen, J. Liu and P. J. Stang, *Chem. Soc. Rev.*, 2020, **49**, 3889–3919.
34 G. T. Williams, C. J. E. Haynes, M. Fares, C. Caltagirone, J. R. Hiscock and P. A. Gale, *Chem. Soc. Rev.*, 2021, **50**, 2737–2763.
35 H. Wang, S. Mumtaz, H. Li, J. Liu and F. Yang, *Future Gener. Comput. Syst.*, 2021, **117**, 145–154.
36 W. X. Gao, H. N. Zhang and G. X. Jin, *Coord. Chem. Rev.*, 2019, **386**, 69–84.
37 C. Guo, A. C. Sedgwick, T. Hirao and J. L. Sessler, *Coord. Chem. Rev.*, 2021, **427**, 213560.
38 H. Y. Lin, Y. T. Wang, X. Shi, H. B. Yang and L. Xu, *Chem. Soc. Rev.*, 2023, **52**, 1129–1154.
39 Y. Sun and P. J. Stang, *Aggregate*, 2021, **2**, e94.
40 C. Yin, J. Du, B. Olenyuk, P. J. Stang and Y. Sun, *Inorganics*, 2023, **11**, 54.
41 B. Li, T. He, Y. Fan, X. Yuan, H. Qiu and S. Yin, *Chem. Commun.*, 2019, **55**, 8036–8059.
42 Y. Xu, Y. Dou, Q. Li, H. Ye, Y. Li, S. Qiu, X. Xiong, J. Li and Y. Sun, *Coord. Chem. Rev.*, 2023, **493**, 215320.
43 W. Jogadi and Y. R. Zheng, *Curr. Opin. Chem. Biol.*, 2023, **73**, 102276.
44 V. Balzani, G. Bergamini, F. Marchioni and P. Ceroni, *Coord. Chem. Rev.*, 2006, **250**, 1254–1266.
45 I. Eryazici, C. N. Moorefield and G. R. Newkome, *Chem. Rev.*, 2008, **108**, 1834–1895.
46 D. Rota Martir and E. Zysman-Colman, *Chem. Commun.*, 2019, **55**, 139–158.
47 J. Wang, Q. Gong, L. Jiao and E. Hao, *Coord. Chem. Rev.*, 2023, **496**, 215367.
48 N. Kwon, H. Kim, X. Li and J. Yoon, *Chem. Sci.*, 2021, **12**, 7248–7268.
49 Q. Wu, Y. Zhu, X. Fang, X. Hao, L. Jiao, E. Hao and W. Zhang, *ACS Appl. Mater. Interfaces*, 2020, **12**, 47208–47219.
50 S. Bian, X. Zheng, W. Liu, J. Li, Z. Gao, H. Ren, W. Zhang, C. S. Lee and P. Wang, *Biomaterials*, 2023, **298**, 122130.
51 Y. Tian, H. Zhou, Q. Cheng, H. Dang, H. Qian, C. Teng, K. Xie and L. Yan, *J. Mater. Chem. B*, 2022, **10**, 707–716.
52 Y. Liu, Y. Li, S. Koo, Y. Sun, Y. Liu, X. Liu, Y. Pan, Z. Zhang, M. Du, S. Lu, X. Qiao, J. Gao, X. Wang, Z. Deng, X. Meng, Y. Xiao, J. S. Kim and X. Hong, *Chem. Rev.*, 2022, **122**, 209–268.
53 Z. Guo, J. Zhao, Y. Liu, G. Li, H. Wang, Y. Hou, M. Zhang, X. Li and X. Yan, *Chin. Chem. Lett.*, 2021, **32**, 1691–1695.
54 Y. Liu, Z. Guo, Y. Guo, G. Li, S. Yang, X. Yan, Y. Shen and J. Wang, *Chin. Chem. Lett.*, 2023, **34**, 108531.
55 C. Mu, Z. Zhang, Y. Hou, H. Liu, L. Ma, X. Li, S. Ling, G. He and M. Zhang, *Angew. Chem., Int. Ed.*, 2021, **60**, 12293–12297.
56 Y. Yin, Z. Chen, R.-H. Li, F. Yi, X. C. Liang, S. Q. Cheng, K. Wang, Y. Sun and Y. Liu, *Inorg. Chem.*, 2022, **61**, 2883–2891.
57 X. Yan, M. Wang, T. R. Cook, M. Zhang, M. L. Saha, Z. Zhou, X. Li, F. Huang and P. J. Stang, *J. Am. Chem. Soc.*, 2016, **138**, 4580–4588.
58 Z. Yin, X. Chang, J. Zang, S. Lin, Z. Zhou, T. Liu, L. Ding, H. Peng and Y. Fang, *J. Mater. Chem. C*, 2022, **10**, 10429–10438.
59 Y. Li, S. S. Rajasree, G. Y. Lee, J. Yu, J.-H. Tang, R. Ni, G. Li, K. N. Houk, P. Deria and P. J. Stang, *J. Am. Chem. Soc.*, 2021, **143**, 2908–2919.
60 H. Shen, C. Xu, F. Sun, M. Zhao, Q. Wu, J. Zhang, S. Li, J. Zhang, J. W. Y. Lam and B. Z. Tang, *ChemMedChem*, 2022, **17**, e202100578.
61 R. S. Gamage, J. L. Chasteen and B. D. Smith, *Bioconjugate Chem.*, 2023, **34**, 961–971.
62 Y. Sun, F. Ding, Z. Zhou, C. Li, M. Pu, Y. Xu, Y. Zhan, X. Lu, H. Li, G. Yang, Y. Sun and P. J. Stang, *Proc. Natl. Acad. Sci. U. S. A.*, 2019, **116**, 1968–1973.
63 C. Huang, T. Shi, J. Zhang, Y. Sun, T. Ma, W. Li, Y. Li, H. Qiu and S. Yin, *Dyes Pigm.*, 2023, **210**, 110932.
64 F. Chen, Y. Li, X. Lin, H. Qiu and S. Yin, *Polymers*, 2021, **13**, 370.
65 Y. Sun, F. Ding, Z. Chen, R. Zhang, C. Li, Y. Xu, Y. Zhang, R. Ni, X. Li, G. Yang, Y. Sun and P. J. Stang, *Proc. Natl. Acad. Sci. U. S. A.*, 2019, **116**, 16729–16735.

66 J. Zhang, M. Jiang, Y. Li, J. Yu, H. Qiu, M. Gu, Y. Li and S. Yin, *Dyes Pigm.*, 2022, **206**, 110679.
67 W. Chen, X. Li, C. Liu, J. He, M. Qi, Y. Sun, B. Shi, H. Sepehrpour, H. Li, W. Tian and P. J. Stang, *Proc. Natl. Acad. Sci. U. S. A.*, 2020, **117**, 30942–30948.
68 E. Villemin, Y. C. Ong, C. M. Thomas and G. Gasser, *Nat. Rev. Chem.*, 2019, **3**, 261–282.
69 V. P. Torchilin, *Adv. Drug Delivery Rev.*, 2012, **64**, 302–315.
70 S. Svenson, *Eur. J. Pharm. Biopharm.*, 2009, **71**, 445–462.
71 P. Huang, X. Wang, X. Liang, J. Yang, C. Zhang, D. Kong and W. Wang, *Acta Biomater.*, 2019, **85**, 1–26.
72 S. D. Li and L. Huang, *Mol. Pharmaceutics*, 2008, **5**, 496–504.
73 H. Maeda, *Adv. Enzyme Regul.*, 2001, **41**, 189–207.
74 H. Maeda, J. Wu, T. Sawa, Y. Matsumura and K. Hori, *J. Controlled Release*, 2000, **65**, 271–284.
75 Y. Matsumura and H. Maeda, *Cancer Res.*, 1986, **46**, 6387–6392.
76 R. Duncan, S. Dimitrijevic and E. Evagorou, *STP Pharma Sci.*, 1996, **6**, 237–263.
77 S. Wilhelm, A. J. Tavares, Q. Dai, S. Ohta, J. Audet, H. F. Dvorak and W. C. Chan, *Nat. Rev. Mater.*, 2016, **1**, 1–12.
78 K. K. Gill, A. Kaddoumi and S. Nazzal, *J. Drug Targeting*, 2015, **23**, 222–231.
79 N. Wauthoz and K. Amighi, *Eur. J. Lipid Sci. Technol.*, 2014, **116**, 1114–1128.
80 G. Khuller, M. Kapur and S. Sharma, *Curr. Pharm. Des.*, 2004, **10**, 3263–3274.
81 T. McPherson, A. Kidane, I. Szleifer and K. Park, *Langmuir*, 1998, **14**, 176–186.
82 A. Hucknall, S. Rangarajan and A. Chilkoti, *Adv. Mater.*, 2009, **21**, 2441–2446.
83 B. Huang, X. Liu, G. Yang, J. Tian, Z. Liu, Y. Zhu, X. Li, G. Yin, W. Zheng and L. Xu, *CCS Chem.*, 2022, **4**, 2090–2101.
84 G. Li, X. Zhang, W. Zhao, W. Zhao, F. Li, K. Xiao, Q. Yu, S. Liu and Q. Zhao, *ACS Appl. Mater. Interfaces*, 2020, **12**, 20180–20190.
85 X. Lin, F. Chen, X. Yu, H. Wang, H. Qiu, Y. Li, S. Yin and P. J. Stang, *Proc. Natl. Acad. Sci. U. S. A.*, 2022, **119**, e2203994119.
86 Y. Xu, C. Li, S. Lu, Z. Wang, S. Liu, X. Yu, X. Li and Y. Sun, *Nat. Commun.*, 2022, **13**, 2009.
87 Y. Xu, C. Li, X. Ma, W. Tuo, L. Tu, X. Li, Y. Sun, P. J. Stang and Y. Sun, *Proc. Natl. Acad. Sci. U. S. A.*, 2022, **119**, e2209904119.
88 K. C. de Castro, J. C. Coco, É. M. Dos Santos, J. A. Ataide, R. M. Martinez, M. H. M. do Nascimento, J. Prata, P. R. M. L. da Fonte, P. Severino and P. G. Mazzola, *J. Controlled Release*, 2023, **353**, 802–822.
89 L. Li, L. Mu and V. Torchilin, *J. Drug Delivery Sci. Technol.*, 2007, **17**, 389–392.
90 J. Yu, H. Qiu, S. Yin, H. Wang and Y. Li, *Molecules*, 2021, **26**, 3610.
91 M. Wang, B. Wu, J. D. Tucker, P. Lu and Q. Lu, *Drug Delivery*, 2016, **23**, 3224–3233.
92 P. Singla, O. Singh, S. Sharma, K. Betlem, V. K. Aswal, M. Peeters and R. K. Mahajan, *ACS Omega*, 2019, **4**, 11251–11262.
93 A. Pitto-Barry and N. P. Barry, *Polym. Chem.*, 2014, **5**, 3291–3297.
94 R. J. P J, O. S. Oluwafemi, S. Thomas and A. O. Oyedeji, *J. Drug Delivery Sci. Technol.*, 2022, **72**, 103390.
95 B. Shriky, A. Kelly, M. Isreb, M. Babenko, N. Mahmoudi, S. Rogers, O. Shebanova, T. Snow and T. Gough, *J. Colloid Interface Sci.*, 2020, **565**, 119–130.
96 G. Dumortier, J. L. Grossiord, F. Agnely and J. C. Chaumeil, *Pharm. Res.*, 2006, **23**, 2709–2728.
97 M. S. H. Akash and K. Rehman, *J. Controlled Release*, 2015, **209**, 120–138.
98 M. Kurahashi, K. Kanamori, K. Takeda, H. Kaji and K. Nakanishi, *RSC Adv.*, 2012, **2**, 7166–7173.
99 N. U. Khaliq, J. Lee, S. Kim, D. Sung and H. Kim, *Pharmaceutics*, 2023, **15**, 2102.
100 K. S. Patil, A. A. Hajare, A. S. Manjappa, H. N. More and J. I. Disouza, *J. Drug Delivery Sci. Technol.*, 2021, **65**, 102685.
101 J. Zhang, J. Yu, W. Li, Y. Fan, Y. Li, Y. Sun, S. Yin and P. J. Stang, *Inorganics*, 2022, **10**, 80.
102 J. Zhang, Y. Li, M. Jiang, H. Qiu, Y. Li, M. Gu and S. Yin, *ACS Biomater. Sci. Eng.*, 2023, **9**, 821–830.
103 H. Jia, T. Shi, T. He, Y. Li and S. Yin, *Dalton Trans.*, 2023, **52**, 4296–4302.
104 F. Ding, Z. Chen, W. Y. Kim, A. Sharma, C. Li, Q. Ouyang, H. Zhu, G. Yang, Y. Sun and J. S. Kim, *Chem. Sci.*, 2019, **10**, 7023–7028.
105 Y. Qin, X. Chen, Y. Gui, H. Wang, B. Z. Tang and D. Wang, *J. Am. Chem. Soc.*, 2022, **144**, 12825–12833.
106 H. Zhu, Q. Li, B. Shi, F. Ge, Y. Liu, Z. Mao, H. Zhu, S. Wang, G. Yu, F. Huang and P. J. Stang, *Angew. Chem., Int. Ed.*, 2020, **59**, 20208–20214.
107 X. Min, M. Li, W. Zhang, R. H. Li, Z. Zhang, P. Wang, W. Su, F. Li, Y. Sun and Y. Liu, *J. Mater. Chem. B*, 2023, **11**, 1090–1099.
108 C. Li, P. P. Jia, Y. L. Xu, F. Ding, W. C. Yang, Y. Sun, X. P. Li, G. Q. Yin, L. Xu and G. F. Yang, *Sci. China: Chem.*, 2021, **64**, 134–142.
109 K. Cai, X. He, Z. Song, Q. Yin, Y. Zhang, F. M. Uckun, C. Jiang and J. Cheng, *J. Am. Chem. Soc.*, 2015, **137**, 3458–3461.
110 J. Zhang, S. Li, F. F. An, J. Liu, S. Jin, J. C. Zhang, P. C. Wang, X. Zhang, C. S. Lee and X. J. Liang, *Nanoscale*, 2015, **7**, 13503–13510.
111 D. Landesman-Milo and D. Peer, *J. Controlled Release*, 2012, **161**, 600–608.
112 M. Longmire, P. L. Choyke and H. Kobayashi, *Nanomedicine*, 2008, **3**, 703–717.
113 J. M. Blonder, L. Baird, J. C. Fulfs and G. J. Rosenthal, *Life Sci.*, 1999, **65**, 261–266.
114 T. P. Johnston, L. B. Nguyen, W. A. Chu and S. Shefer, *Int. J. Pharm.*, 2001, **229**, 75–86.
115 E. Lepeltier, C. Bourgaux and P. Couvreur, *Adv. Drug Delivery Rev.*, 2014, **71**, 86–97.

116 W. S. Saad and R. K. Prud'homme, *Nano Today*, 2016, **11**, 212–227.
117 C. J. M. Rivas, M. Tarhini, W. Badri, K. Miladi, H. Greige-Gerges, Q. A. Nazari, S. A. G. Rodríguez, R. Á. Román, H. Fessi and A. Elaissari, *Int. J. Pharm.*, 2017, **532**, 66–81.
118 A. A. Date, N. Desai, R. Dixit and M. Nagarsenker, *Nanomedicine*, 2010, **5**, 1595–1616.
119 R. J. Wilson, Y. Li, G. Yang and C. X. Zhao, *Particuology*, 2022, **64**, 85–97.
120 K. B. Sutradhar and M. L. Amin, *Eur. J. Nanomed.*, 2013, **5**, 97–110.
121 H. Zhang, *Liposomes: Methods Protoc.*, 2017, pp. 17–22.
122 V. Ravalika and A. K. Sailaja, *Nano Biomed. Eng.*, 2017, **9**, 242–248.
123 S. Karki, H. Kim, S.-J. Na, D. Shin, K. Jo and J. Lee, *Asian J. Pharm. Sci.*, 2016, **11**, 559–574.
124 P. Huang, D. Wang, Y. Su, W. Huang, Y. Zhou, D. Cui, X. Zhu and D. Yan, *J. Am. Chem. Soc.*, 2014, **136**, 11748–11756.
125 W. Chen, J. He, H. Li, X. Li and W. Tian, *Supramol. Chem.*, 2020, **32**, 597–604.
126 A. G. Cheetham, P. Zhang, Y. A. Lin, L. L. Lock and H. Cui, *J. Am. Chem. Soc.*, 2013, **135**, 2907–2910.
127 N. Larson and H. Ghandehari, *Chem. Mater.*, 2012, **24**, 840–853.
128 Y. Li, X. Yuan, J. Yu, Y. Fan, T. He, S. Lu, X. Li, H. Qiu and S. Yin, *ACS Appl. Bio Mater.*, 2020, **3**, 8061–8068.
129 B. Woods, R. D. Silva, C. Schmidt, D. Wragg, M. Cavaco, V. Neves, V. F. Ferreira, L. Gano, T. S. Morais and F. Mendes, *Bioconjugate Chem.*, 2021, **32**, 1399–1408.
130 G. Tao, T. Ji, N. Wang, G. Yang, X. Lei, W. Zheng, R. Liu, X. Xu, L. Yang and G. Q. Yin, *ACS Macro Lett.*, 2019, **9**, 61–69.
131 Y. Fan, J. Zhang, Y. Li, Q. Chen, Z. Ni, H. Zhou, J. Yu, H. Qiu and S. Yin, *Mater. Chem. Front.*, 2022, **6**, 633–643.
132 Z. Wang, L. He, B. Liu, L. P. Zhou, L. X. Cai, S. J. Hu, X. Z. Li, Z. Li, T. Chen, X. Li and Q. F. Sun, *J. Am. Chem. Soc.*, 2020, **142**, 16409–16419.
133 J. Zhou, G. Yu, J. Yang, B. Shi, B. Ye, M. Wang, F. Huang and P. J. Stang, *Chem. Mater.*, 2020, **32**, 4564–4573.
134 J. Tian, B. Huang, S. Weng, W. Zheng and W. Zhang, *Mater. Today Adv.*, 2022, **14**, 100229.
135 E. Gammella, S. Recalcati and G. Cairo, *Oxid. Med. Cell. Longevity*, 2016, **2016**, 8629024.
136 Y. Qin, T. Guo, Z. Wang and Y. Zhao, *J. Mater. Chem. B*, 2021, **9**, 4793–4803.
137 A. Gabizon, H. Shmeeda and Y. Barenholz, *Clin. Pharmacokinet.*, 2003, **42**, 419–436.
138 D. Lorusso, A. Di Stefano, V. Carone, A. Fagotti, S. Pisconti and G. Scambia, *Ann. Oncol.*, 2007, **18**, 1159–1164.
139 Y. Barenholz, *J. Controlled Release*, 2012, **160**, 117–134.
140 R. Loomba, A. Rowley, R. Wesley, T. J. Liang, J. H. Hoofnagle, F. Pucino and G. Csako, *Ann. Intern. Med.*, 2008, **148**, 519–528.
141 R. Dillon, G. M. Hirschfield, M. E. D. Allison and K. P. Rege, *BMJ*, 2008, **337**, a423.
142 W. Yeo, K. C. Lam, B. Zee, P. S. K. Chan, F. K. F. Mo, W. M. Ho, W. L. Wong, T. W. T. Leung, A. T. C. Chan, B. Ma, T. S. K. Mok and P. J. Johnson, *Ann. Oncol.*, 2004, **15**, 1661–1666.
143 S. Gao, X. Yan, G. Xie, M. Zhu, X. Ju, P. J. Stang, Y. Tian and Z. Niu, *Proc. Natl. Acad. Sci. U. S. A.*, 2019, **116**, 23437–23443.
144 P. Jeyakkumar, Y. Liang, M. Guo, S. Lu, D. Xu, X. Li, B. Guo, G. He, D. Chu and M. Zhang, *Angew. Chem., Int. Ed.*, 2020, **59**, 15199–15203.
145 G. Y. Wu, X. Shi, H. Phan, H. Qu, Y. X. Hu, G. Q. Yin, X. L. Zhao, X. Li, L. Xu, Q. Yu and H. B. Yang, *Nat. Commun.*, 2020, **11**, 3178.
146 Z. Zhang, H. Ye, F. Cai and Y. Sun, *Dalton Trans.*, 2023, **52**, 15193–15202.
147 Y. Wang, C. Wang, R. Long, Y. Cao, D. Fan, M. Cen, L. Cao, Y. Chen and Y. Yao, *Chem. Commun.*, 2019, **55**, 5167–5170.
148 S. Datta, M. L. Saha and P. J. Stang, *Acc. Chem. Res.*, 2018, **51**, 2047–2063.
149 Y. Tian, X. Yan, M. L. Saha, Z. Niu and P. J. Stang, *J. Am. Chem. Soc.*, 2016, **138**, 12033–12036.
150 S. M. Kim, P. H. Faix and J. E. Schnitzer, *J. Controlled Release*, 2017, **267**, 15–30.
151 Y. Nakamura, A. Mochida, P. L. Choyke and H. Kobayashi, *Bioconjugate Chem.*, 2016, **27**, 2225–2238.
152 A. Nel, E. Ruoslahti and H. Meng, *ACS Nano*, 2017, **11**, 9567–9569.
153 E. Huynh and G. Zheng, *Nanomedicine*, 2015, **10**, 1993–1995.
154 H. Nakamura, F. Jun and H. Maeda, *Expert Opin. Drug Delivery*, 2015, **12**, 53–64.
155 D. Rosenblum, N. Joshi, W. Tao, J. M. Karp and D. Peer, *Nat. Commun.*, 2018, **9**, 1410.
156 W. C. W. Chan, *Acc. Chem. Res.*, 2017, **50**, 627–632.
157 F. Danhier, *J. Controlled Release*, 2016, **244**, 108–121.
158 S. Wilhelm, A. J. Tavares, Q. Dai, S. Ohta, J. Audet, H. F. Dvorak and W. C. W. Chan, *Nat. Rev. Mater.*, 2016, **1**, 16014.
159 J. W. Nichols and Y. H. Bae, *J. Controlled Release*, 2014, **190**, 451–464.
160 Q. Wang, Q. Liang, J. Dou, H. Zhou, C. Zeng, H. Pan, Y. Shen, Q. Li, Y. Liu, D. T. Leong, W. Jiang and Y. Wang, *Nat. Nanotechnol.*, 2024, **19**, 95–105.
161 S. Sindhwani, A. M. Syed, J. Ngai, B. R. Kingston, L. Maiorino, J. Rothschild, P. MacMillan, Y. Zhang, N. U. Rajesh, T. Hoang, J. L. Y. Wu, S. Wilhelm, A. Zilman, S. Gadde, A. Sulaiman, B. Ouyang, Z. Lin, L. Wang, M. Egeblad and W. C. W. Chan, *Nat. Mater.*, 2020, **19**, 566–575.
162 I. de Lázaro and D. J. Mooney, *Nat. Mater.*, 2020, **19**, 486–487.
163 Anonymous, *Nat. Mater.*, 2020, **19**, 477.
164 P. Zhang, Z. Zhou, W. Long, Y. Yan, Y. Li, T. Fu, Y. Liu, Z. Zhao, W. Tan and P. J. Stang, *Proc. Natl. Acad. Sci. U. S. A.*, 2022, **119**, e2202255119.
165 X. Wang, Q. Su, Z. Zhang, J. Yang, Y. Zhang and M. Zhang, *Chem. Commun.*, 2020, **56**, 8460–8463.

166 G. Yu, B. Zhu, L. Shao, J. Zhou, M. L. Saha, B. Shi, Z. Zhang, T. Hong, S. Li and X. Chen, *Proc. Natl. Acad. Sci. U. S. A.*, 2019, **116**, 6618–6623.
167 X. Jiang, Z. Zhou, H. Yang, C. Shan, H. Yu, L. Wojtas, M. Zhang, Z. Mao, M. Wang and P. J. Stang, *Inorg. Chem.*, 2020, **59**, 7380–7388.
168 G. Yu, S. Yu, M. L. Saha, J. Zhou, T. R. Cook, B. C. Yung, J. Chen, Z. Mao, F. Zhang and Z. Zhou, *Nat. Commun.*, 2018, **9**, 4335.
169 S. Deiser, M. Drexler, G. Moreno-Alcántar, M. Irl, C. Schmidt, T. Günther and A. Casini, *Inorg. Chem.*, 2023, **62**, 20710–20720.
170 A. C. Marques, P. J. Costa, S. Velho and M. H. Amaral, *J. Controlled Release*, 2020, **320**, 180–200.
171 S. Maiti and P. Paira, *Eur. J. Med. Chem.*, 2018, **145**, 206–223.
172 R. Kumar, W. S. Shin, K. Sunwoo, W. Y. Kim, S. Koo, S. Bhuniya and J. S. Kim, *Chem. Soc. Rev.*, 2015, **44**, 6670–6683.
173 P. S. Low and S. A. Kularatne, *Curr. Opin. Chem. Biol.*, 2009, **13**, 256–262.
174 P. Tagde, G. T. Kulkarni, D. K. Mishra and P. Kesharwani, *J. Drug Delivery Sci. Technol.*, 2020, **56**, 101613.
175 P. S. Low, W. A. Henne and D. D. Doorneweerd, *Acc. Chem. Res.*, 2008, **41**, 120–129.
176 E. J. Roy, U. Gawlick, B. A. Orr and D. M. Kranz, *Adv. Drug Delivery Rev.*, 2004, **56**, 1219–1231.
177 C. M. Paulos, M. J. Turk, G. J. Breur and P. S. Low, *Adv. Drug Delivery Rev.*, 2004, **56**, 1205–1217.
178 X. B. Zhao and R. J. Lee, *Adv. Drug Delivery Rev.*, 2004, **56**, 1193–1204.
179 D. N. Heo, D. H. Yang, H. J. Moon, J. B. Lee, M. S. Bae, S. C. Lee, W. J. Lee, I. C. Sun and I. K. Kwon, *Biomaterials*, 2012, **33**, 856–866.
180 H. Li, G. Bruce, N. Childerhouse, G. Keegan, G. Mantovani and S. Stolnik, *J. Controlled Release*, 2023, **357**, 333–341.
181 N. U. Deshpande and M. Jayakannan, *Biomacromolecules*, 2018, **19**, 3572–3585.
182 G. Yu, T. R. Cook, Y. Li, X. Yan, D. Wu, L. Shao, J. Shen, G. Tang, F. Huang, X. Chen and P. J. Stang, *Proc. Natl. Acad. Sci. U. S. A.*, 2016, **113**, 13720–13725.
183 X. Sun, Y. Li, T. Liu, Z. Li, X. Zhang and X. Chen, *Adv. Drug Delivery Rev.*, 2017, **110–111**, 38–51.
184 S. H. Wang and J. Yu, *Biomaterials*, 2018, **156**, 1–15.
185 B. M. Cooper, J. Iegre, D. H. O'Donovan, M. Ölwegård Halvarsson and D. R. Spring, *Chem. Soc. Rev.*, 2021, **50**, 1480–1494.
186 K. Kurrikoff, D. Aphkhazava and Ü. Langel, *Curr. Opin. Pharmacol.*, 2019, **47**, 27–32.
187 F. Araste, K. Abnous, M. Hashemi, S. M. Taghdisi, M. Ramezani and M. Alibolandi, *J. Controlled Release*, 2018, **292**, 141–162.
188 O. Larsson, A. Girnita and L. Girnita, *Br. J. Cancer*, 2005, **92**, 2097–2101.
189 S. Favelyukis, J. H. Till, S. R. Hubbard and W. T. Miller, *Nat. Struct. Biol.*, 2001, **8**, 1058–1063.
190 J. Zha and M. R. Lackner, *Clin. Cancer Res.*, 2010, **16**, 2512–2517.
191 H. Hamidi, M. Pietilä and J. Ivaska, *Br. J. Cancer*, 2016, **115**, 1017–1023.
192 P. H. Wu, A. E. Opadele, Y. Onodera and J. M. Nam, *Cancers*, 2019, **11**, 1783.
193 K. Ahmad, E. J. Lee, S. Shaikh, A. Kumar, K. M. Rao, S. Y. Park, J. O. Jin, S. S. Han and I. Choi, *Semin. Cancer Biol.*, 2021, **69**, 325–336.
194 S. L. Goodman and M. Picard, *Trends Pharmacol. Sci.*, 2012, **33**, 405–412.
195 K. Chen and X. Chen, *Theranostics*, 2011, **1**, 189–200.
196 F. Ciardiello and G. Tortora, *Clin. Cancer Res.*, 2001, **7**, 2958–2970.
197 J. Mendelsohn and J. Baselga, *Semin. Oncol.*, 2006, **33**, 369–385.
198 C. Yewale, D. Baradia, I. Vhora, S. Patil and A. Misra, *Biomaterials*, 2013, **34**, 8690–8707.
199 B. F. El-Rayes and P. M. LoRusso, *Br. J. Cancer*, 2004, **91**, 418–424.
200 F. Danhier, A. Le Breton and V. Préat, *Mol. Pharmaceutics*, 2012, **9**, 2961–2973.
201 L. Ge, X. You, K. Huang, Y. Kang, Y. Chen, Y. Zhu, Y. Ren, Y. Zhang, J. Wu and H. Qian, *Biomater. Sci.*, 2018, **6**, 125–135.
202 M. Nieberler, U. Reuning, F. Reichart, J. Notni, H. J. Wester, M. Schwaiger, M. Weinmüller, A. Räder, K. Steiger and H. Kessler, *Cancers*, 2017, **9**, 116.
203 S. Liu, *Mol. Pharmaceutics*, 2006, **3**, 472–487.
204 S. Liu, *Bioconjugate Chem.*, 2009, **20**, 2199–2213.
205 Z. Liu, F. Wang and X. Chen, *Drug Dev. Res.*, 2008, **69**, 329–339.
206 C. Adessi and C. Soto, *Curr. Med. Chem.*, 2002, **9**, 963–978.
207 G. Yu, S. Yu, M. L. Saha, J. Zhou, T. R. Cook, B. C. Yung, J. Chen, Z. Mao, F. Zhang, Z. Zhou, Y. Liu, L. Shao, S. Wang, C. Gao, F. Huang, P. J. Stang and X. Chen, *Nat. Commun.*, 2018, **9**, 4335.
208 G. Yu, B. Zhu, L. Shao, J. Zhou, M. L. Saha, B. Shi, Z. Zhang, T. Hong, S. Li, X. Chen and P. J. Stang, *Proc. Natl. Acad. Sci. U. S. A.*, 2019, **116**, 6618–6623.
209 B. Yang, H. Liu, H. Yang, W. Chen, J. Wu, X. Feng, R. Tong, H. Yu, Y. Chen, Z. Lv, W. Sun, B. He, J. Wu, G. Yu, Z. Mao and S. Zheng, *J. Mater. Chem. B*, 2019, **7**, 6476–6487.
210 Y. Ding, Z. Tong, L. Jin, B. Ye, J. Zhou, Z. Sun, H. Yang, L. Hong, F. Huang, W. Wang and Z. Mao, *Adv. Mater.*, 2022, **34**, 2106388.
211 A. J. Danford, D. Wang, Q. Wang, T. D. Tullius and S. J. Lippard, *Proc. Natl. Acad. Sci. U. S. A.*, 2005, **102**, 12311–12316.
212 E. Rudolph, S. Hann, G. Stingeder and C. Reiter, *Anal. Bioanal. Chem.*, 2005, **382**, 1500–1506.
213 J. H. Schiller and G. Bittner, *Clin. Cancer Res.*, 1999, **5**, 4287–4294.
214 B. Köberle, M. T. Tomicic, S. Usanova and B. Kaina, *Biochim. Biophys. Acta, Rev. Cancer*, 1806, **2010**, 172–182.

215 A.-M. Florea and D. Büsselberg, *Cancers*, 2011, **3**, 1351–1371.
216 L. Amable, *Pharmacol. Res.*, 2016, **106**, 27–36.
217 L. Galluzzi, I. Vitale, J. Michels, C. Brenner, G. Szabadkai, A. Harel-Bellan, M. Castedo and G. Kroemer, *Cell Death Dis.*, 2014, **5**, e1257.
218 L. Galluzzi, L. Senovilla, I. Vitale, J. Michels, I. Martins, O. Kepp, M. Castedo and G. Kroemer, *Oncogene*, 2012, **31**, 1869–1883.
219 S. C. Wang, K. Y. Cheng, J. H. Fu, Y. C. Cheng and Y. T. Chan, *J. Am. Chem. Soc.*, 2020, **142**, 16661–16667.
220 Y. Y. Liu, H. J. Yu, Y. P. Wang, C. J. Li, X. F. Wang, C. G. Ye, H. L. Yao, M. Pan and C. Y. Su, *Mater. Chem. Front.*, 2022, **6**, 948–955.
221 Z. Zhou, J. Liu, T. W. Rees, H. Wang, X. Li, H. Chao and P. J. Stang, *Proc. Natl. Acad. Sci. U. S. A.*, 2018, **115**, 5664–5669.
222 Z. Zhou, J. Liu, J. Huang, T. W. Rees, Y. Wang, H. Wang, X. Li, H. Chao and P. J. Stang, *Proc. Natl. Acad. Sci. U. S. A.*, 2019, **116**, 20296–20302.
223 E. L. Eskelinen, Y. Tanaka and P. Saftig, *Trends Cell Biol.*, 2003, **13**, 137–145.
224 J. A. Mindell, *Annu. Rev. Physiol.*, 2012, **74**, 69–86.
225 I. F. Tannock and D. Rotin, *Cancer Res.*, 1989, **49**, 4373–4384.
226 R. A. Gatenby, E. T. Gawlinski, A. F. Gmitro, B. Kaylor and R. J. Gillies, *Cancer Res.*, 2006, **66**, 5216–5223.
227 L. He, L. X. Cai, M. H. Li, G. L. Zhang, L. P. Zhou, T. Chen, M. J. Lin and Q. F. Sun, *Chem. Sci.*, 2020, **11**, 7940–7949.
228 L. Tu, C. Li, C. Liu, S. Bai, J. Yang, X. Zhang, L. Xu, X. Xiong and Y. Sun, *Chem. Commun.*, 2022, **58**, 9068–9071.
229 S. Lv, Y. Miao, D. Zheng, X. Li, D. Liu and F. Song, *Mol. Pharmaceutics*, 2021, **18**, 1229–1237.
230 K. Qiu, Y. Chen, T. W. Rees, L. Ji and H. Chao, *Coord. Chem. Rev.*, 2019, **378**, 66–86.
231 F. J. Bock and S. W. G. Tait, *Nat. Rev. Mol. Cell Biol.*, 2020, **21**, 85–100.
232 B. A. Carneiro and W. S. El-Deiry, *Nat. Rev. Clin. Oncol.*, 2020, **17**, 395–417.
233 S. Fulda and D. Vucic, *Nat. Rev. Drug Discovery*, 2012, **11**, 109–124.
234 Z. Jiang, Z. Hu, L. Zeng, W. Lu, H. Zhang, T. Li and H. Xiao, *Free Radical Biol. Med.*, 2011, **50**, 907–917.
235 Q. Li, T. Zhou, F. Wu, N. Li, R. Wang, Q. Zhao, Y.-M. Ma, J.-Q. Zhang and B.-L. Ma, *Drug Metab. Rev.*, 2018, **50**, 430–447.
236 N. Zheng, H. N. Tsai, X. Zhang, K. Shedden and G. R. Rosania, *Mol. Pharmaceutics*, 2011, **8**, 1611–1618.
237 X. Li, J. Wu, L. Wang, C. He, L. Chen, Y. Jiao and C. Duan, *Angew. Chem., Int. Ed.*, 2020, **59**, 6420–6427.
238 K.-C. Tong, P.-K. Wan, C.-N. Lok and C.-M. Che, *Chem. Sci.*, 2021, **12**, 15229–15238.
239 Q. Feng, T. Yang, L. Ma, X. Li, H. Yuan, M. Zhang, Y. Zhang and L. Fan, *ACS Appl. Mater. Interfaces*, 2022, **14**, 38594–38603.
240 C. Li, Y. Xu, L. Tu, M. Choi, Y. Fan, X. Chen, J. L. Sessler, J. S. Kim and Y. Sun, *Chem. Sci.*, 2022, **13**, 6541–6549.
241 L. Tu, C. Li, X. Xiong, J. Hyeon Kim, Q. Li, L. Mei, J. Li, S. Liu, J. Seung Kim and Y. Sun, *Angew. Chem., Int. Ed.*, 2023, **62**, e202301560.
242 Y. Xu, C. Li, S. Lu, Z. Wang, S. Liu, X. Yu, X. Li and Y. Sun, *Nat. Commun.*, 2022, **13**, 2009.
243 O. Domarco, C. Kieler, C. Pirker, C. Dinhof, B. Englinger, J. M. Reisecker, G. Timelthaler, M. D. García, C. Peinador, B. K. Keppler, W. Berger and A. Terenzi, *Angew. Chem., Int. Ed.*, 2019, **58**, 8007–8012.
244 C. Settembre, A. Fraldi, D. L. Medina and A. Ballabio, *Nat. Rev. Mol. Cell Biol.*, 2013, **14**, 283–296.
245 W. W. Y. Yim and N. Mizushima, *Cell Discovery*, 2020, **6**, 6.
246 J. P. Luzio, B. A. Rous, N. A. Bright, P. R. Pryor, B. M. Mullock and R. C. Piper, *J. Cell Sci.*, 2000, **113**, 1515–1524.
247 R. E. Lawrence and R. Zoncu, *Nat. Cell Biol.*, 2019, **21**, 133–142.
248 J. P. Luzio, M. D. J. Parkinson, S. R. Gray and N. A. Bright, *Biochem. Soc. Trans.*, 2009, **37**, 1019–1021.
249 P. Saftig and J. Klumperman, *Nat. Rev. Mol. Cell Biol.*, 2009, **10**, 623–635.
250 S. R. Bonam, F. Wang and S. Muller, *Nat. Rev. Drug Discovery*, 2019, **18**, 923–948.
251 A. Serrano-Puebla and P. Boya, *Ann. N. Y. Acad. Sci.*, 2016, **1371**, 30–44.
252 Ana M. Villamil Giraldo, H. Appelqvist, T. Ederth and K. Öllinger, *Biochem. Soc. Trans.*, 2014, **42**, 1460–1464.
253 Y. Chen, Z. Yang, S. Wang, Q. Ma, L. Li, X. Wu, Q. Guo, L. Tao and X. Shen, *Adv. Healthcare Mater.*, 2023, **12**, 2202150.
254 P. Boya and G. Kroemer, *Oncogene*, 2008, **27**, 6434–6451.
255 A. Serrano-Puebla and P. Boya, *Biochem. Soc. Trans.*, 2018, **46**, 207–215.
256 C. Oberle, J. Huai, T. Reinheckel, M. Tacke, M. Rassner, P. G. Ekert, J. Buellesbach and C. Borner, *Cell Death Differ.*, 2010, **17**, 1167–1178.
257 H. Erdal, M. Berndtsson, J. Castro, U. Brunk, M. C. Shoshan and S. Linder, *Proc. Natl. Acad. Sci. U. S. A.*, 2005, **102**, 192–197.
258 F. Wang, R. Gómez-Sintes and P. Boya, *Traffic*, 2018, **19**, 918–931.
259 U. Repnik, M. Hafner Česen and B. Turk, *Mitochondrion*, 2014, **19**, 49–57.
260 M. F. Chung, K. J. Chen, H. F. Liang, Z. X. Liao, W. T. Chia, Y. Xia and H.-W. Sung, *Angew. Chem., Int. Ed.*, 2012, **51**, 10089–10093.
261 Z. Liu, Y. Xiao, W. Chen, Y. Wang, B. Wang, G. Wang, X. Xu and R. Tang, *J. Mater. Chem. B*, 2014, **2**, 3480–3489.
262 H. Lima Jr, L. Jacobson, M. Goldberg, K. Chandran, F. Diaz-Griffero, M. P. Lisanti and J. Brojatsch, *Cell Cycle*, 2013, **12**, 1868–1878.
263 T. Yamashima and S. Oikawa, *Prog. Neurobiol.*, 2009, **89**, 343–358.
264 E. Gulbins, S. Dreschers and J. Bock, *Exp. Physiol.*, 2003, **88**, 85–90.
265 S. Desagher and J.-C. Martinou, *Trends Cell Biol.*, 2000, **10**, 369–377.

266 D. R. Green and J. C. Reed, *Science*, 1998, **281**, 1309–1312.
267 C. Wang and R. J. Youle, *Annu. Rev. Genet.*, 2009, **43**, 95–118.
268 H. Kong and N. S. Chandel, *J. Biol. Chem.*, 2018, **293**, 7499–7507.
269 S. M. Richard, G. Bailliet, G. L. Páez, M. S. Bianchi, P. I. Peltomäki and N. S. O. Bianchi, *Cancer Res.*, 2000, **60**, 4231–4237.
270 G. D. Dakubo, R. L. Parr, L. C. Costello, R. B. Franklin and R. E. Thayer, *J. Clin. Pathol.*, 2006, **59**, 10–16.
271 N. O. Bianchi, M. S. Bianchi and S. M. Richard, *Mutat. Res., Rev. Mutat. Res.*, 2001, **488**, 9–23.
272 F. Ciccarese and V. Ciminale, *Front. Oncol.*, 2017, **7**, 117.
273 S. Mani, G. Swargiary and S. J. Ralph, *Mitochondrion*, 2022, **62**, 50–73.
274 C.-H. Ni, C.-S. Yu, H.-F. Lu, J.-S. Yang, H.-Y. Huang, P.-Y. Chen, S.-H. Wu, S.-W. Ip, S.-Y. Chiang, J.-G. Lin and J.-G. Chung, *Environ. Toxicol.*, 2014, **29**, 740–749.
275 B. G. Heerdt, M. A. Houston and L. H. Augenlicht, *Cancer Res.*, 2005, **65**, 9861–9867.
276 L. D. Zorova, V. A. Popkov, E. Y. Plotnikov, D. N. Silachev, I. B. Pevzner, S. S. Jankauskas, V. A. Babenko, S. D. Zorov, A. V. Balakireva, M. Juhaszova, S. J. Sollott and D. B. Zorov, *Anal. Biochem.*, 2018, **552**, 50–59.
277 E. N. Maldonado, J. Patnaik, M. R. Mullins and J. J. Lemasters, *Cancer Res.*, 2010, **70**, 10192–10201.
278 N. J. Haradhvala, P. Polak, P. Stojanov, K. R. Covington, E. Shinbrot, J. M. Hess, E. Rheinbay, J. Kim, Y. E. Maruvka, L. Z. Braunstein, A. Kamburov, P. C. Hanawalt, D. A. Wheeler, A. Koren, M. S. Lawrence and G. Getz, *Cell*, 2016, **164**, 538–549.
279 M. Ljungman, *Chem. Rev.*, 2009, **109**, 2929–2950.
280 A. Torgovnick and B. Schumacher, *Front. Genet.*, 2015, **6**, 157.
281 A. Marnef and G. Legube, *Curr. Opin. Cell Biol.*, 2017, **46**, 1–8.
282 N. Chatterjee and G. C. Walker, *Environ. Mol. Mutagen.*, 2017, **58**, 235–263.
283 M. Saki and A. Prakash, *Free Radical Biol. Med.*, 2017, **107**, 216–227.
284 K. V. Ferry, T. C. Hamilton and S. W. Johnson, *Biochem. Pharmacol.*, 2000, **60**, 1305–1313.
285 U. Repnik and B. Turk, *Mitochondrion*, 2010, **10**, 662–669.
286 F. Guerra, G. Girolimetti, R. Beli, M. Mitruccio, C. Pacelli, A. Ferretta, G. Gasparre, T. Cocco and C. Bucci, *Cells*, 2019, **8**, 452.
287 L. F. Burbulla, P. Song, J. R. Mazzulli, E. Zampese, Y. C. Wong, S. Jeon, D. P. Santos, J. Blanz, C. D. Obermaier, C. Strojny, J. N. Savas, E. Kiskinis, X. Zhuang, R. Krüger, D. J. Surmeier and D. Krainc, *Science*, 2017, **357**, 1255–1261.
288 Y. C. Wong, D. Ysselstein and D. Krainc, *Nature*, 2018, **554**, 382–386.
289 G. Xu, C. Li, C. Chi, L. Wu, Y. Sun, J. Zhao, X. H. Xia and S. Gou, *Nat. Commun.*, 2022, **13**, 3064.
290 D. S. Goodsell, *Stem Cells*, 2006, **24**, 514–515.
291 J. Raber, C. Zhu and L. A. Eriksson, *J. Phys. Chem. B*, 2005, **109**, 11006–11015.
292 I. L. Zilberberg, V. I. Avdeev and G. M. Zhidomirov, *THEOCHEM*, 1997, **418**, 73–81.
293 D. S. Eric, M. B. James and B. H. Stephen, *Mol. Pharmacol.*, 1999, **56**, 633.
294 M.-H. Baik, R. A. Friesner and S. J. Lippard, *J. Am. Chem. Soc.*, 2003, **125**, 14082–14092.
295 J. R. Mitchell, J. H. J. Hoeijmakers and L. J. Niedernhofer, *Curr. Opin. Cell Biol.*, 2003, **15**, 232–240.
296 E. C. Friedberg, *Nat. Rev. Cancer*, 2001, **1**, 22–33.
297 J. A. Marteijn, H. Lans, W. Vermeulen and J. H. J. Hoeijmakers, *Nat. Rev. Mol. Cell Biol.*, 2014, **15**, 465–481.
298 M. Baretti and D. T. Le, *Pharmacol. Ther.*, 2018, **189**, 45–62.
299 D. C. Chung and A. K. Rustgi, *Gastroenterology*, 1995, **109**, 1685–1699.
300 P. Modrich, *Science*, 1994, **266**, 1959–1960.
301 T. Aparicio, R. Baer and J. Gautier, *DNA Repair*, 2014, **19**, 169–175.
302 T. Helleday, J. Lo, D. C. van Gent and B. P. Engelward, *DNA Repair*, 2007, **6**, 923–935.
303 K. K. Khanna and S. P. Jackson, *Nat. Genet.*, 2001, **27**, 247–254.
304 M. Nechay, D. Wang and R. E. Kleiner, *Cell Chem. Biol.*, 2023, **30**, 906–919.
305 H. Hu, B. Li, J. Wang, Y. Tan, M. Xu, W. Xu and H. Lu, *Biomed. Pharmacother.*, 2023, **163**, 114778.
306 Q. Cao, Y. Li, E. Freisinger, P. Z. Qin, R. K. O. Sigel and Z.-W. Mao, *Inorg. Chem. Front.*, 2017, **4**, 10–32.
307 W. Liu, Y. F. Zhong, L. Y. Liu, C. T. Shen, W. Zeng, F. Wang, D. Yang and Z. W. Mao, *Nat. Commun.*, 2018, **9**, 3496.
308 E. Palma, J. Carvalho, C. Cruz and A. Paulo, *Pharmaceuticals*, 2021, **14**, 605.
309 I. Alessandrini, M. Recagni, N. Zaffaroni and M. Folini, *Int. J. Mol. Sci.*, 2021, **22**, 5947.
310 R. Hänsel-Hertsch, A. Simeone, A. Shea, W. W. I. Hui, K. G. Zyner, G. Marsico, O. M. Rueda, A. Bruna, A. Martin, X. Zhang, S. Adhikari, D. Tannahill, C. Caldas and S. Balasubramanian, *Nat. Genet.*, 2020, **52**, 878–883.
311 X. H. Zheng, Y. F. Zhong, C. P. Tan, L. N. Ji and Z. W. Mao, *Dalton Trans.*, 2012, **41**, 11807–11812.
312 J. Liu, T. Luo, Y. Xue, L. Mao, P. J. Stang and M. Wang, *Angew. Chem., Int. Ed.*, 2021, **60**, 5429–5435.
313 J. Liu, J. Sheng, L. Shao, Q. Zheng, W. Li, X. Chen, L. Mao and M. Wang, *Angew. Chem., Int. Ed.*, 2021, **60**, 26740–26746.
314 S. Jeelani, R. J. Reddy, T. Maheswaran, G. Asokan, A. Dany and B. Anand, *J. Pharm. BioAllied Sci.*, 2014, **6**, S6.
315 E.-K. Lim, T. Kim, S. Paik, S. Haam, Y.-M. Huh and K. Lee, *Chem. Rev.*, 2015, **115**, 327–394.
316 G. Chen, H. Qiu, P. N. Prasad and X. Chen, *Chem. Rev.*, 2014, **114**, 5161–5214.
317 L. Xing, B. Thorndyke, E. Schreibmann, Y. Yang, T. F. Li, G. Y. Kim, G. Luxton and A. Koong, *Med. Dosim.*, 2006, **31**, 91–112.
318 H. Y. Yoon, S. Jeon, D. G. You, J. H. Park, I. C. Kwon, H. Koo and K. Kim, *Bioconjugate Chem.*, 2017, **28**, 124–134.

319 Y. Huang, S. He, W. Cao, K. Cai and X.-J. Liang, *Nanoscale*, 2012, **4**, 6135–6149.
320 J. Huo, Q. Jia, H. Huang, J. Zhang, P. Li, X. Dong and W. Huang, *Chem. Soc. Rev.*, 2021, **50**, 8762–8789.
321 C. He, Z. Tang, H. Tian and X. Chen, *Adv. Drug Delivery Rev.*, 2016, **98**, 64–76.
322 W. Fan, B. Yung, P. Huang and X. Chen, *Chem. Rev.*, 2017, **117**, 13566–13638.
323 J. J. Verhoef, J. F. Carpenter, T. J. Anchordoquy and H. Schellekens, *Drug Discovery Today*, 2014, **19**, 1945–1952.
324 G. T. Kozma, T. Shimizu, T. Ishida and J. Szebeni, *Adv. Drug Delivery Rev.*, 2020, **154**, 163–175.
325 P. Zhang, F. Sun, S. Liu and S. Jiang, *J. Controlled Release*, 2016, **244**, 184–193.
326 D. Huang, H. Lan, F. Liu, S. Wang, X. Chen, K. Jin and X. Mou, *Int. J. Clin. Exp. Med.*, 2015, **8**, 8369–8376.
327 P. Carmeliet and R. K. Jain, *Nat. Rev. Drug Discovery*, 2011, **10**, 417–427.
328 R. K. Jain, *Science*, 2005, **307**, 58–62.
329 J. Hagendoorn, R. Tong, D. Fukumura, Q. Lin, J. Lobo, T. P. Padera, L. Xu, R. Kucherlapati and R. K. Jain, *Cancer Res.*, 2006, **66**, 3360–3364.
330 A. Alitalo and M. Detmar, *Oncogene*, 2012, **31**, 4499–4508.
331 R. P. Kataru, C. L. Ly, J. Shin, H. J. Park, J. E. Baik, S. Rehal, S. Ortega, D. Lyden and B. J. Mehrara, *Cancer Immunol. Res.*, 2019, **7**, 1345–1358.
332 M. Madeo, P. L. Colbert, D. W. Vermeer, C. T. Lucido, J. T. Cain, E. G. Vichaya, A. J. Grossberg, D. Muirhead, A. P. Rickel, Z. Hong, J. Zhao, J. M. Weimer, W. C. Spanos, J. H. Lee, R. Dantzer and P. D. Vermeer, *Nat. Commun.*, 2018, **9**, 4284.
333 G. E. Ayala, H. Dai, M. Powell, R. Li, Y. Ding, T. M. Wheeler, D. Shine, D. Kadmon, T. Thompson, B. J. Miles, M. M. Ittmann and D. Rowley, *Clin. Cancer Res.*, 2008, **14**, 7593–7603.
334 D. Hanahan and M. Monje, *Cancer Cell*, 2023, **41**, 573–580.
335 F. Winkler, H. S. Venkatesh, M. Amit, T. Batchelor, I. E. Demir, B. Deneen, D. H. Gutmann, S. Hervey-Jumper, T. Kuner, D. Mabbott, M. Platten, A. Rolls, E. K. Sloan, T. C. Wang, W. Wick, V. Venkataramani and M. Monje, *Cell*, 2023, **186**, 1689–1707.
336 G. Biffi and D. A. Tuveson, *Physiol. Rev.*, 2021, **101**, 147–176.
337 N. I. Nissen, M. Karsdal and N. Willumsen, *J. Exp. Clin. Cancer Res.*, 2019, **38**, 115.
338 A. Arina, C. Idel, E. M. Hyjek, M.-L. Alegre, Y. Wang, V. P. Bindokas, R. R. Weichselbaum and H. Schreiber, *Proc. Natl. Acad. Sci. U. S. A.*, 2016, **113**, 7551–7556.
339 G. Bergers, S. Song, N. Meyer-Morse, E. Bergsland and D. Hanahan, *J. Clin. Invest.*, 2003, **111**, 1287–1295.
340 V. G. Cooke, V. S. LeBleu, D. Keskin, Z. Khan, J. T. O'Connell, Y. Teng, M. B. Duncan, L. Xie, G. Maeda, S. Vong, H. Sugimoto, R. M. Rocha, A. Damascena, R. R. Brentani and R. Kalluri, *Cancer Cell*, 2012, **21**, 66–81.
341 A. L. Ribeiro and O. K. Okamoto, *Stem Cells Int.*, 2015, **2015**, 868475.
342 K. M. Nieman, I. L. Romero, B. Van Houten and E. Lengyel, *Biochim. Biophys. Acta, Mol. Cell Biol. Lipids*, 1831, **2013**, 1533–1541.
343 Q. Wu, B. Li, J. Li, S. Sun, J. Yuan and S. Sun, *Biomark. Res.*, 2021, **9**, 1–21.
344 Q. Wu, B. Li, Z. Li, J. Li, S. Sun and S. Sun, *J. Hematol. Oncol.*, 2019, **12**, 95.
345 M. S. Nakazawa, B. Keith and M. C. Simon, *Nat. Rev. Cancer*, 2016, **16**, 663–673.
346 J. M. Brown and W. R. Wilson, *Nat. Rev. Cancer*, 2004, **4**, 437–447.
347 S. R. McKeown, *Br. J. Radiol.*, 2014, **87**, 20130676.
348 L. E. Gerweck and K. Seetharaman, *Cancer Res.*, 1996, **56**, 1194–1198.
349 M. Stubbs, P. M. J. McSheehy, J. R. Griffiths and C. L. Bashford, *Mol. Med. Today*, 2000, **6**, 15–19.
350 A. J. Thistlethwaite, D. B. Leeper, D. J. Moylan, III and R. E. Nerlinger, *Int. J. Radiat. Oncol., Biol., Phys.*, 1985, **11**, 1647–1652.
351 L. Szablewski, *Biochim. Biophys. Acta, Rev. Cancer*, 2013, **1835**, 164–169.
352 R. A. S. Nascimento, R. E. Özel, W. H. Mak, M. Mulato, B. Singaram and N. Pourmand, *Nano Lett.*, 2016, **16**, 1194–1200.
353 N. Hay, *Nat. Rev. Cancer*, 2016, **16**, 635–649.
354 B. J. Altman, Z. E. Stine and C. V. Dang, *Nat. Rev. Cancer*, 2016, **16**, 619–634.
355 D. R. Wise and C. B. Thompson, *Trends Biochem. Sci.*, 2010, **35**, 427–433.
356 A. A. Cluntun, M. J. Lukey, R. A. Cerione and J. W. Locasale, *Trends Cancer*, 2017, **3**, 169–180.
357 S. Trabanelli, D. Očadlíková, S. Gulinelli, A. Curti, V. Salvestrini, R. de Paula Vieira, M. Idzko, F. Di Virgilio, D. Ferrari and R. M. Lemoli, *J. Immunol.*, 2012, **189**, 1303–1310.
358 P. Pellegatti, L. Raffaghello, G. Bianchi, F. Piccardi, V. Pistoia and F. Di Virgilio, *PLoS One*, 2008, **3**, e2599.
359 V. Vultaggio-Poma, A. C. Sarti and F. Di Virgilio, *Cells*, 2020, **9**, 2496.
360 P. A. Smethurst and M. Griffin, *Biochem. J.*, 1996, **313**, 803–808.
361 T. Inaoka and K. Ochi, *J. Bacteriol.*, 2002, **184**, 3923–3930.
362 A. Meshkini, *Cell Biochem. Biophys.*, 2014, **70**, 27–32.
363 T. Tokuhara, N. Hattori, H. Ishida, T. Hirai, M. Higashiyama, K. Kodama and M. Miyake, *Clin. Cancer Res.*, 2006, **12**, 3971–3978.
364 R. Pasqualini, E. Koivunen, R. Kain, J. Lahdenranta, M. Sakamoto, A. Stryhn, R. A. Ashmun, L. H. Shapiro, W. Arap and E. Ruoslahti, *Cancer Res.*, 2000, **60**, 722–727.
365 A. Kehlen, U. Lendeckel, H. Dralle, J. Langner and C. Hoang-Vu, *Cancer Res.*, 2003, **63**, 8500–8506.
366 J. Zhou, X. Du and B. Xu, *Angew. Chem., Int. Ed.*, 2016, **55**, 5770–5775.
367 M. Uhlén, L. Fagerberg, B. M. Hallström, C. Lindskog, P. Oksvold, A. Mardinoglu, Å. Sivertsson, C. Kampf, E. Sjöstedt, A. Asplund, I. Olsson, K. Edlund, E. Lundberg,

S. Navani, C. A.-K. Szigyarto, J. Odeberg, D. Djureinovic, J. O. Takanen, S. Hober, T. Alm, P.-H. Edqvist, H. Berling, H. Tegel, J. Mulder, J. Rockberg, P. Nilsson, J. M. Schwenk, M. Hamsten, K. von Feilitzen, M. Forsberg, L. Persson, F. Johansson, M. Zwahlen, G. von Heijne, J. Nielsen and F. Pontén, *Science*, 2015, **347**, 1260419.

368 F. J. Benham, J. Fogh and H. Harris, *Int. J. Cancer*, 1981, **27**, 637–644.

369 I. Podgorski and B. F. Sloane, *Biochem. Soc. Symp.*, 2003, **70**, 263–276.

370 M. H. Abdulla, M. A. Valli Mohammed, K. Al Khayal, A. Al Shkieh, A. Zubaidi, R. Ahmad, K. Al Saleh, O. Al Obeed and J. McKerrow, *Oncol. Rep.*, 2017, **37**, 3175–3180.

371 C. S. Gondi and J. S. Rao, *Expert Opin. Ther. Targets*, 2013, **17**, 281–291.

372 L. Zhang, J. Shi, J. Feng, H. Klocker, C. Lee and J. Zhang, *Prostate Cancer Prostatic Dis.*, 2004, **7**, 327–332.

373 L. M. Coussens, B. Fingleton and L. M. Matrisian, *Science*, 2002, **295**, 2387–2392.

374 R. E. Vandenbroucke and C. Libert, *Nat. Rev. Drug Discovery*, 2014, **13**, 904–927.

375 L. Rao, Q. F. Meng, L. L. Bu, B. Cai, Q. Huang, Z. J. Sun, W. F. Zhang, A. Li, S. S. Guo, W. Liu, T. H. Wang and X. Z. Zhao, *ACS Appl. Mater. Interfaces*, 2017, **9**, 2159–2168.

376 M. Gao, C. Liang, X. Song, Q. Chen, Q. Jin, C. Wang and Z. Liu, *Adv. Mater.*, 2017, **29**, 1701429.

377 L. Rao, B. Cai, L. L. Bu, Q. Q. Liao, S. S. Guo, X. Z. Zhao, W. F. Dong and W. Liu, *ACS Nano*, 2017, **11**, 3496–3505.

378 Y. Xia, L. Rao, H. Yao, Z. Wang, P. Ning and X. Chen, *Adv. Mater.*, 2020, **32**, 2002054.

379 Y. Zhang, K. Cai, C. Li, Q. Guo, Q. Chen, X. He, L. Liu, Y. Zhang, Y. Lu, X. Chen, T. Sun, Y. Huang, J. Cheng and C. Jiang, *Nano Lett.*, 2018, **18**, 1908–1915.

380 H. Cao, Z. Dan, X. He, Z. Zhang, H. Yu, Q. Yin and Y. Li, *ACS Nano*, 2016, **10**, 7738–7748.

381 Z. Chen, P. Zhao, Z. Luo, M. Zheng, H. Tian, P. Gong, G. Gao, H. Pan, L. Liu, A. Ma, H. Cui, Y. Ma and L. Cai, *ACS Nano*, 2016, **10**, 10049–10057.

382 J. Y. Zhu, D. W. Zheng, M. K. Zhang, W. Y. Yu, W. X. Qiu, J. J. Hu, J. Feng and X. Z. Zhang, *Nano Lett.*, 2016, **16**, 5895–5901.

383 Q. Hu, W. Sun, J. Wang, H. Ruan, X. Zhang, Y. Ye, S. Shen, C. Wang, W. Lu, K. Cheng, G. Dotti, J. F. Zeidner, J. Wang and Z. Gu, *Nat. Biomed. Eng.*, 2018, **2**, 831–840.

384 H. Sun, J. Su, Q. Meng, Q. Yin, L. Chen, W. Gu, P. Zhang, Z. Zhang, H. Yu, S. Wang and Y. Li, *Adv. Mater.*, 2016, **28**, 9581–9588.

385 Q. Jiang, Y. Liu, R. Guo, X. Yao, S. Sung, Z. Pang and W. Yang, *Biomaterials*, 2019, **192**, 292–308.

386 S. Rezaei, R. F. de Araújo Júnior, I. L. G. da Silva, T. Schomann, C. Eich and L. J. Cruz, *Biomater. Adv.*, 2023, **151**, 213456.

387 H. Y. Chen, J. Deng, Y. Wang, C. Q. Wu, X. Li and H.-W. Dai, *Acta Biomater.*, 2020, **112**, 1–13.

388 G. Russell-Jones, K. McTavish, J. McEwan, J. Rice and D. Nowotnik, *J. Inorg. Biochem.*, 2004, **98**, 1625–1633.

389 A. Raza, A. Singh, S. Amin, J. E. Spallholz and A. K. Sharma, *Chem. – Biol. Interact.*, 2022, **365**, 110071.

